

Neutrino Mixing

With the possible exceptions of "short-baseline anomalies," such as LSND, all neutrino data can be described within the framework of a 3×3 mixing matrix between the mass eigenstates ν_1 , ν_2 , and ν_3 , leading to the flavor eigenstates ν_e , ν_μ , and ν_τ , as described in the review "*Neutrino masses, mixing and oscillations.*"

The Listings are divided in the following sections:

(A) Neutrino fluxes and event ratios: shows measurements which correspond to various oscillation tests for Accelerator, Reactor, Atmospheric, and Solar neutrino experiments. Typically, ratios involve a measurement in a realm sensitive to oscillations compared to one for which no oscillation effect is expected.

(B) Neutrino mixing parameters: shows measurements of $\sin^2(\theta_{12})$, $\sin^2(\theta_{23})$, $\sin^2(\theta_{13})$, Δm_{21}^2 , Δm_{32}^2 , and δ_{CP} as extracted from the measured data in the quoted publications in the frame of the three-neutrino mixing scheme. The quoted averages are not the result of a global fit, as in the review "*Neutrino masses, mixing, and oscillations,*" and, as a consequence, might slightly differ from them. In some cases, measurements depend on the mass order (normal when $\Delta m_{32}^2 > 0$ or inverted when $\Delta m_{32}^2 < 0$) or octant of θ_{23} (lower when $\theta_{23} < 45^\circ$ or upper when $\theta_{23} > 45^\circ$).

(C) Other neutrino mixing results:

The LSND anomaly [AGUILAR 01], reported a signal which is consistent with $\bar{\nu}_\mu \rightarrow \bar{\nu}_e$ oscillations. In a three neutrino framework, this would be a measurement of θ_{12} and Δm_{21}^2 . This does not appear to be consistent with the interpretation of other neutrino data. It has been interpreted as evidence for a 4th "sterile" neutrino. The following listings include results

which might be relevant towards understanding this observation. They include searches for $\nu_\mu \rightarrow \nu_e$, $\bar{\nu}_\mu \rightarrow \bar{\nu}_e$, sterile neutrino oscillations, and others.

(A) Neutrino fluxes and event ratios

Events (observed/expected) from accelerator ν_μ experiments.

Some neutrino oscillation experiments compare the flux in two or more detectors. This is usually quoted as the ratio of the event rate in the far detector to the expected rate based on an extrapolation from the near detector in the absence of oscillations.

<u>VALUE</u>	<u>DOCUMENT ID</u>	<u>TECN</u>	<u>COMMENT</u>
● ● ● We do not use the following data for averages, fits, limits, etc. ● ● ●			
1.01 ± 0.10	¹ ABE	14B T2K	ν_e rate in T2K near detect.
0.71 ± 0.08	² AHN	06A K2K	K2K to Super-K
0.64 ± 0.05	³ MICHAEL	06 MINS	All charged current events
$0.71^{+0.08}_{-0.09}$	⁴ ALIU	05 K2K	KEK to Super-K
$0.70^{+0.10}_{-0.11}$	⁵ AHN	03 K2K	KEK to Super-K

¹ The rate of ν_e from μ decay was measured to be 0.68 ± 0.30 compared to the predicted flux. From K decay 1.10 ± 0.14 compared to the predicted flux.

² Based on the observation of 112 events when $158.1^{+9.2}_{-8.6}$ were expected without oscillations. Including not only the number of events but also the shape of the energy distribution, the evidence for oscillation is at the level of about 4.3σ . Supersedes ALIU 05.

³ This ratio is based on the observation of 215 events compared to an expectation of 336 ± 14 without oscillations. See also ADAMSON 08.

⁴ This ratio is based on the observation of 107 events at the far detector 250 km away from KEK, and an expectation of 151^{+12}_{-10} .

⁵ This ratio is based on the observation of 56 events with an expectation of $80.1^{+6.2}_{-5.4}$.

Events (observed/expected) from reactor $\bar{\nu}_e$ experiments.

The quoted values are the ratios of the measured reactor $\bar{\nu}_e$ event rate at the quoted distances, and the rate expected without oscillations. The expected rate is based on the experimental data for the most significant reactor fuels (^{235}U , ^{239}Pu , ^{241}Pu) and on calculations for ^{238}U .

A recent re-evaluation of the spectral conversion of electron to $\bar{\nu}_e$ in MUELLER 11 results in an upward shift of the reactor $\bar{\nu}_e$ spectrum by 3% and, thus, might require revisions to the ratios listed in this table.

<u>VALUE</u>	<u>DOCUMENT ID</u>	<u>TECN</u>	<u>COMMENT</u>
● ● ● We do not use the following data for averages, fits, limits, etc. ● ● ●			
$0.948 \pm 0.008 \pm 0.033$	¹ ALMAZAN	20 RHF	RHF reactor at ILL
0.952 ± 0.027	² ADEY	19 DAYA	DayaBay, Ling Ao/Ao II reactors
	³ AN	16 DAYA	DayaBay, Ling Ao/Ao II reactors
$1.08 \pm 0.21 \pm 0.16$	⁴ DENIZ	10 TEXO	Kuo-Sheng reactor, 28 m
$0.658 \pm 0.044 \pm 0.047$	⁵ ARAKI	05 KLND	Japanese react. ~ 180 km
$0.611 \pm 0.085 \pm 0.041$	⁶ EGUCHI	03 KLND	Japanese react. ~ 180 km
$1.01 \pm 0.024 \pm 0.053$	⁷ BOEHM	01	Palo Verde react. 0.75–0.89 km

1.01 ± 0.028 ± 0.027	⁸ APOLLONIO 99	CHOZ	Chooz reactors 1 km
0.987 ± 0.006 ± 0.037	⁹ GREENWOOD 96		Savannah River, 18.2 m
0.988 ± 0.004 ± 0.05	ACHKAR 95	CNTR	Bugey reactor, 15 m
0.994 ± 0.010 ± 0.05	ACHKAR 95	CNTR	Bugey reactor, 40 m
0.915 ± 0.132 ± 0.05	ACHKAR 95	CNTR	Bugey reactor, 95 m
0.987 ± 0.014 ± 0.027	¹⁰ DECLAIS 94	CNTR	Bugey reactor, 15 m
0.985 ± 0.018 ± 0.034	KUVSHINN... 91	CNTR	Rovno reactor
1.05 ± 0.02 ± 0.05	VUILLEUMIER 82		Gösgen reactor
0.955 ± 0.035 ± 0.110	¹¹ KWON 81		$\bar{\nu}_e p \rightarrow e^+ n$
0.89 ± 0.15	¹¹ BOEHM 80		$\bar{\nu}_e p \rightarrow e^+ n$

- ¹ ALMAZAN 20 use the RHF research reactor at ILL to compare their measured anti-neutrino event rate to the calculation by HUBER 11. Reported $0.948 \pm 0.008 \pm 0.023 \pm 0.023$ measurement with uncertainties from statistics, systematic, and model. Note that this result is obtained for highly enriched ^{235}U reactor fuel while most other reactor experiments utilize a low-enrichment mix of fissile nuclides.
- ² ADEY 19 present a re-analysis of 1230 days of Daya Bay near detector data with reduced systematic uncertainties on the neutron detection efficiency. Note that ADEY 19 report the measured to predicted antineutrino ratio using the reactor model of MUELLER 11 (Huber-Mueller model). The ratio using the older ILL-Vogel model is $1.001 \pm 0.015 \pm 0.027$.
- ³ AN 16 use 217 days of data (338k events) to determine the neutrino flux ratio relative to the prediction of Mueller-Huber and ILL-Vogel models (see AN 16 for details). The reported flux ratios were corrected for θ_{13} oscillation effect. The flux measurement is consistent with results from previous short-baseline reactor experiments. The measured inverse beta decay yield is $(1.55 \pm 0.04) \times 10^{-18} \text{ cm}^2/(\text{GW day})$ or $\sigma_f = (5.92 \pm 0.14) \times 10^{-43} \text{ cm}^2/\text{fission}$. About 4σ excess of events was observed in the 4–6 MeV prompt energy region.
- ⁴ DENIZ 10 observe reactor $\bar{\nu}_e e$ scattering with recoil kinetic energies 3–8 MeV using CsI(Tl) detectors. The observed rate is consistent with the Standard Model prediction, leading to a constraint on $\sin^2\theta_{WW} = 0.251 \pm 0.031(\text{stat}) \pm 0.024(\text{sys})$.
- ⁵ Updated result of KamLAND, including the data used in EGUCHI 03. Note that the survival probabilities for different periods are not directly comparable because the effective baseline varies with power output of the reactor sources involved, and there were large variations in the reactor power production in Japan in 2003.
- ⁶ EGUCHI 03 observe reactor neutrino disappearance at ~ 180 km baseline to various Japanese nuclear power reactors.
- ⁷ BOEHM 01 search for neutrino oscillations at 0.75 and 0.89 km distance from the Palo Verde reactors.
- ⁸ APOLLONIO 99, APOLLONIO 98 search for neutrino oscillations at 1.1 km fixed distance from Chooz reactors. They use $\bar{\nu}_e p \rightarrow e^+ n$ in Gd-loaded scintillator target. APOLLONIO 99 supersedes APOLLONIO 98. See also APOLLONIO 03 for detailed description.
- ⁹ GREENWOOD 96 search for neutrino oscillations at 18 m and 24 m from the reactor at Savannah River.
- ¹⁰ DECLAIS 94 result based on integral measurement of neutrons only. Result is ratio of measured cross section to that expected in standard V-A theory. Replaced by ACHKAR 95.
- ¹¹ KWON 81 represents an analysis of a larger set of data from the same experiment as BOEHM 80.

————— Atmospheric neutrinos —————

Neutrinos and antineutrinos produced in the atmosphere induce μ -like and e -like events in underground detectors. The ratio of the numbers of the two kinds of events is defined as μ/e . It has the advantage that systematic effects, such as flux uncertainty, tend to cancel, for both experimental and theoretical values of the ratio. The “ratio of the ratios” of experimental to theoretical μ/e , $R(\mu/e)$, or that of experimental to theoretical μ/total , $R(\mu/\text{total})$ with $\text{total} = \mu + e$, is reported below. If the actual value is not unity, the value obtained in a given experiment may depend on the experimental conditions. In addition, the measured “up-down asymmetry” for μ ($N_{up}(\mu)/N_{down}(\mu)$) or e ($N_{up}(e)/N_{down}(e)$) is reported. The expected “up-down asymmetry” is nearly unity if there is no neutrino oscillation.

$R(\mu/e) = (\text{Measured Ratio } \mu/e) / (\text{Expected Ratio } \mu/e)$

VALUE	DOCUMENT ID	TECN	COMMENT
• • • We do not use the following data for averages, fits, limits, etc. • • •			
$0.658 \pm 0.016 \pm 0.035$	¹ ASHIE	05	SKAM sub-GeV
$0.702^{+0.032}_{-0.030} \pm 0.101$	² ASHIE	05	SKAM multi-GeV
$0.69 \pm 0.10 \pm 0.06$	³ SANCHEZ	03	SOU2 Calorimeter raw data
	⁴ FUKUDA	96B	KAMI Water Cherenkov
$1.00 \pm 0.15 \pm 0.08$	⁵ DAUM	95	FREJ Calorimeter
$0.60^{+0.06}_{-0.05} \pm 0.05$	⁶ FUKUDA	94	KAMI sub-GeV
$0.57^{+0.08}_{-0.07} \pm 0.07$	⁷ FUKUDA	94	KAMI multi-GeV
	⁸ BECKER-SZ...	92B	IMB Water Cherenkov

¹ ASHIE 05 results are based on an exposure of 92 kton yr during the complete Super-Kamiokande I running period. The analyzed data sample consists of fully-contained single-ring e -like events with $0.1 \text{ GeV}/c < p_e$ and μ -like events $0.2 \text{ GeV}/c < p_\mu$, both having a visible energy $< 1.33 \text{ GeV}$. These criteria match the definition used by FUKUDA 94.

² ASHIE 05 results are based on an exposure of 92 kton yr during the complete Super-Kamiokande I running period. The analyzed data sample consists of fully-contained single-ring events with visible energy $> 1.33 \text{ GeV}$ and partially-contained events. All partially-contained events are classified as μ -like.

³ SANCHEZ 03 result is based on an exposure of 5.9 kton yr, and updates ALLISON 99 result. The analyzed data sample consists of fully-contained e -flavor and μ -flavor events having lepton momentum $> 0.3 \text{ GeV}/c$.

⁴ FUKUDA 96B studied neutron background in the atmospheric neutrino sample observed in the Kamiokande detector. No evidence for the background contamination was found.

⁵ DAUM 95 results are based on an exposure of 2.0 kton yr which includes the data used by BERGER 90B. This ratio is for the contained and semicontained events. DAUM 95 also report $R(\mu/e) = 0.99 \pm 0.13 \pm 0.08$ for the total neutrino induced data sample which includes upward going stopping muons and horizontal muons in addition to the contained and semicontained events.

⁶ FUKUDA 94 result is based on an exposure of 7.7 kton yr and updates the HIRATA 92 result. The analyzed data sample consists of fully-contained e -like events with $0.1 < p_e < 1.33 \text{ GeV}/c$ and fully-contained μ -like events with $0.2 < p_\mu < 1.5 \text{ GeV}/c$.

⁷ FUKUDA 94 analyzed the data sample consisting of fully contained events with visible energy $> 1.33 \text{ GeV}$ and partially contained μ -like events.

⁸ BECKER-SZENDY 92B reports the fraction of nonshowering events (mostly muons from atmospheric neutrinos) as $0.36 \pm 0.02 \pm 0.02$, as compared with expected fraction $0.51 \pm$

0.01 ± 0.05 . After cutting the energy range to the Kamiokande limits, BEIER 92 finds $R(\mu/e)$ very close to the Kamiokande value.

$R(\nu_\mu) = (\text{Measured Flux of } \nu_\mu) / (\text{Expected Flux of } \nu_\mu)$

<u>VALUE</u>	<u>DOCUMENT ID</u>	<u>TECN</u>	<u>COMMENT</u>
● ● ● We do not use the following data for averages, fits, limits, etc. ● ● ●			
0.84 ± 0.12	¹ ADAMSON	06	MINS MINOS atmospheric
$0.72 \pm 0.026 \pm 0.13$	² AMBROSIO	01	MCRO upward through-going
$0.57 \pm 0.05 \pm 0.15$	³ AMBROSIO	00	MCRO upgoing partially contained
$0.71 \pm 0.05 \pm 0.19$	⁴ AMBROSIO	00	MCRO downgoing partially contained + upgoing stopping
$0.74 \pm 0.036 \pm 0.046$	⁵ AMBROSIO	98	MCRO Streamer tubes
	⁶ CASPER	91	IMB Water Cherenkov
	⁷ AGLIETTA	89	NUSX
0.95 ± 0.22	⁸ BOLIEV	81	Baksan
0.62 ± 0.17	CROUCH	78	Case Western/UCI

¹ ADAMSON 06 uses a measurement of 107 total neutrinos compared to an expected rate of 127 ± 13 without oscillations.

² AMBROSIO 01 result is based on the upward through-going muon tracks with $E_\mu > 1$ GeV. The data came from three different detector configurations, but the statistics is largely dominated by the full detector run, from May 1994 to December 2000. The total live time, normalized to the full detector configuration, is 6.17 years. The first error is the statistical error, the second is the systematic error, dominated by the theoretical error in the predicted flux.

³ AMBROSIO 00 result is based on the upgoing partially contained event sample. It came from 4.1 live years of data taking with the full detector, from April 1994 to February 1999. The average energy of atmospheric muon neutrinos corresponding to this sample is 4 GeV. The first error is statistical, the second is the systematic error, dominated by the 25% theoretical error in the rate (20% in the flux and 15% in the cross section, added in quadrature). Within statistics, the observed deficit is uniform over the zenith angle.

⁴ AMBROSIO 00 result is based on the combined samples of downgoing partially contained events and upgoing stopping events. These two subsamples could not be distinguished due to the lack of timing information. The result came from 4.1 live years of data taking with the full detector, from April 1994 to February 1999. The average energy of atmospheric muon neutrinos corresponding to this sample is 4 GeV. The first error is statistical, the second is the systematic error, dominated by the 25% theoretical error in the rate (20% in the flux and 15% in the cross section, added in quadrature). Within statistics, the observed deficit is uniform over the zenith angle.

⁵ AMBROSIO 98 result is for all nadir angles and updates AHLEN 95 result. The lower cutoff on the muon energy is 1 GeV. In addition to the statistical and systematic errors, there is a Monte Carlo flux error (theoretical error) of ± 0.13 . With a neutrino oscillation hypothesis, the fit either to the flux or zenith distribution independently yields $\sin^2 2\theta = 1.0$ and $\Delta(m^2) \sim$ a few times 10^{-3} eV^2 . However, the fit to the observed zenith distribution gives a maximum probability for χ^2 of only 5% for the best oscillation hypothesis.

⁶ CASPER 91 correlates showering/nonshowering signature of single-ring events with parent atmospheric-neutrino flavor. They find nonshowering ($\approx \nu_\mu$ induced) fraction is $0.41 \pm 0.03 \pm 0.02$, as compared with expected 0.51 ± 0.05 (syst).

⁷ AGLIETTA 89 finds no evidence for any anomaly in the neutrino flux. They define $\rho = (\text{measured number of } \nu_e \text{'s}) / (\text{measured number of } \nu_\mu \text{'s})$. They report $\rho(\text{measured}) = \rho(\text{expected}) = 0.96^{+0.32}_{-0.28}$.

⁸ From this data BOLIEV 81 obtain the limit $\Delta(m^2) \leq 6 \times 10^{-3} \text{ eV}^2$ for maximal mixing, $\nu_\mu \nleftrightarrow \nu_\mu$ type oscillation.

$R(\mu/\text{total}) = (\text{Measured Ratio } \mu/\text{total}) / (\text{Expected Ratio } \mu/\text{total})$

<u>VALUE</u>	<u>DOCUMENT ID</u>	<u>TECN</u>	<u>COMMENT</u>
--------------	--------------------	-------------	----------------

• • • We do not use the following data for averages, fits, limits, etc. • • •

$1.1^{+0.07}_{-0.12} \pm 0.11$	¹ CLARK	97	IMB multi-GeV
--------------------------------	--------------------	----	---------------

¹ CLARK 97 obtained this result by an analysis of fully contained and partially contained events in the IMB water-Cherenkov detector with visible energy > 0.95 GeV.

$N_{\text{up}}(\mu)/N_{\text{down}}(\mu)$

<u>VALUE</u>	<u>DOCUMENT ID</u>	<u>TECN</u>	<u>COMMENT</u>
--------------	--------------------	-------------	----------------

• • • We do not use the following data for averages, fits, limits, etc. • • •

0.71 ± 0.06	¹ ADAMSON	12B	MINS contained-vertex muons
$0.551^{+0.035}_{-0.033} \pm 0.004$	² ASHIE	05	SKAM multi-GeV

¹ ADAMSON 12B reports the atmospheric neutrino results obtained with MINOS far detector in 2,553 live days (an exposure of 37.9 kton·yr). This result is obtained with a sample of high resolution contained-vertex muons. The quoted error is statistical only.

² ASHIE 05 results are based on an exposure of 92 kton yr during the complete Super-Kamiokande I running period. The analyzed data sample consists of fully-contained single-ring μ -like events with visible energy > 1.33 GeV and partially-contained events. All partially-contained events are classified as μ -like. Upward-going events are those with $-1 < \cos(\text{zenith angle}) < -0.2$ and downward-going events are those with $0.2 < \cos(\text{zenith angle}) < 1$. The μ -like up-down ratio for the multi-GeV data deviates from 1 (the expectation for no atmospheric ν_{μ} oscillations) by more than 12 standard deviations.

$N_{\text{up}}(e)/N_{\text{down}}(e)$

<u>VALUE</u>	<u>DOCUMENT ID</u>	<u>TECN</u>	<u>COMMENT</u>
--------------	--------------------	-------------	----------------

• • • We do not use the following data for averages, fits, limits, etc. • • •

$0.961^{+0.086}_{-0.079} \pm 0.016$	¹ ASHIE	05	SKAM multi-GeV
-------------------------------------	--------------------	----	----------------

¹ ASHIE 05 results are based on an exposure of 92 kton yr during the complete Super-Kamiokande I running period. The analyzed data sample consists of fully-contained single-ring e -like events with visible energy > 1.33 GeV. Upward-going events are those with $-1 < \cos(\text{zenith angle}) < -0.2$ and downward-going events are those with $0.2 < \cos(\text{zenith angle}) < 1$. The e -like up-down ratio for the multi-GeV data is consistent with 1 (the expectation for no atmospheric ν_e oscillations).

$R(\text{up/down}; \mu) = (\text{Measured up/down}; \mu) / (\text{Expected up/down}; \mu)$

<u>VALUE</u>	<u>DOCUMENT ID</u>	<u>TECN</u>	<u>COMMENT</u>
--------------	--------------------	-------------	----------------

• • • We do not use the following data for averages, fits, limits, etc. • • •

$0.62 \pm 0.05 \pm 0.02$	¹ ADAMSON	12B	MINS contained-vertex muons
$0.62^{+0.19}_{-0.14} \pm 0.02$	² ADAMSON	06	MINS atmospheric ν with far detector

¹ ADAMSON 12B reports the atmospheric neutrino results obtained with MINOS far detector in 2,553 live days (an exposure of 37.9 kton·yr). This result is obtained with a sample of high resolution contained-vertex muons. The expected ratio is calculated with no neutrino oscillation.

² ADAMSON 06 result is obtained with the MINOS far detector with an exposure of 4.54 kton yr. The expected ratio is calculated with no neutrino oscillation.

$N(\mu^+)/N(\mu^-)$

<u>VALUE</u>	<u>DOCUMENT ID</u>	<u>TECN</u>	<u>COMMENT</u>
● ● ● We do not use the following data for averages, fits, limits, etc. ● ● ●			
$0.46^{+0.05}_{-0.04}$	1,2 ADAMSON	12B MINS	contained-vertex muons
$0.63^{+0.09}_{-0.08}$	1,3 ADAMSON	12B MINS	ν -induced rock-muons

¹ ADAMSON 12B reports the atmospheric neutrino results obtained with MINOS far detector in 2,553 live days (an exposure of 37.9 kton·yr). The muon charge ratio $N(\mu^+)/N(\mu^-)$ represents the $\bar{\nu}_\mu/\nu_\mu$ ratio.

² This result is obtained with a charge-separated sample of high resolution contained-vertex muons. The quoted error is statistical only.

³ This result is obtained with a charge-separated sample of high resolution neutrino-induced rock-muons. The quoted error is statistical only.

$R(\mu^+/\mu^-) = (\text{Measured } N(\mu^+)/N(\mu^-)) / (\text{Expected } N(\mu^+)/N(\mu^-))$

<u>VALUE</u>	<u>DOCUMENT ID</u>	<u>TECN</u>	<u>COMMENT</u>
● ● ● We do not use the following data for averages, fits, limits, etc. ● ● ●			
$0.93 \pm 0.09 \pm 0.09$	1,2 ADAMSON	12B MINS	contained-vertex muons
$1.29^{+0.19}_{-0.17} \pm 0.16$	1,3 ADAMSON	12B MINS	ν -induced rock-muons
$1.03 \pm 0.08 \pm 0.08$	1,4 ADAMSON	12B MINS	contained
$1.39^{+0.35+0.08}_{-0.46-0.14}$	5 ADAMSON	07 MINS	Upward and horizontal μ with far detector
$0.96^{+0.38}_{-0.27} \pm 0.15$	6 ADAMSON	06 MINS	atmospheric ν with far detector

¹ ADAMSON 12B reports the atmospheric neutrino results obtained with MINOS far detector in 2,553 live days (an exposure of 37.9 kton·yr). The muon charge ratio $N(\mu^+)/N(\mu^-)$ represents the $\bar{\nu}_\mu/\nu_\mu$ ratio. As far as the same oscillation parameters are used for ν s and $\bar{\nu}$ s, the expected $\bar{\nu}_\mu/\nu_\mu$ ratio is almost entirely independent of any input oscillations.

² This result is obtained with a charge-separated sample of high resolution contained-vertex muons.

³ This result is obtained with a charge-separated sample of high resolution neutrino-induced rock-muons.

⁴ The charge-separated samples of high resolution contained-vertex muons and neutrino-induced rock-muons are combined to obtain this result which is consistent with unity.

⁵ ADAMSON 07 result is obtained with the MINOS far detector in 854.24 live days, based on neutrino-induced upward-going and horizontal muons. This result is consistent with *CPT* conservation.

⁶ ADAMSON 06 result is obtained with the MINOS far detector with an exposure of 4.54 kton yr, based on contained events. The expected ratio is calculated by assuming the same oscillation parameters for neutrinos and antineutrinos.

————— Solar neutrinos —————

Solar neutrinos are produced by thermonuclear fusion reactions in the Sun. Radiochemical experiments measure particular combinations of fluxes from various neutrino-producing reactions, whereas water-Cherenkov experiments mainly measure a flux of neutrinos from decay of ^8B . Solar neutrino fluxes are composed of all active neutrino species, ν_e , ν_μ , and ν_τ . In addition, some other mechanisms may cause antineutrino components in solar neutrino fluxes. Each measurement method is sensitive to a particular component or a combination of components of solar neutrino fluxes.

ν_e Capture Rates from Radiochemical Experiments

1 SNU (Solar Neutrino Unit) = 10^{-36} captures per atom per second.

VALUE (SNU)	DOCUMENT ID	TECN	COMMENT
73.4 $\begin{smallmatrix} +6.1 & +3.7 \\ -6.0 & -4.1 \end{smallmatrix}$	1 KAETHER	10	GALX reanalysis
67.6 $\pm 4.0 \pm 3.2$	2 KAETHER	10	GNO+GALX reanalysis combined
65.4 $\begin{smallmatrix} +3.1 & +2.6 \\ -3.0 & -2.8 \end{smallmatrix}$	3 ABDURASHI...	09 SAGE	$^{71}\text{Ga} \rightarrow ^{71}\text{Ge}$
62.9 $\begin{smallmatrix} +5.5 & \pm 2.5 \\ -5.3 & \end{smallmatrix}$	4 ALTMANN	05 GNO	$^{71}\text{Ga} \rightarrow ^{71}\text{Ge}$
69.3 $\pm 4.1 \pm 3.6$	5 ALTMANN	05 GNO	GNO + GALX combined
77.5 $\begin{smallmatrix} \pm 6.2 & +4.3 \\ & -4.7 \end{smallmatrix}$	6 HAMPEL	99 GALX	$^{71}\text{Ga} \rightarrow ^{71}\text{Ge}$
2.56 $\pm 0.16 \pm 0.16$	7 CLEVELAND	98 HOME	$^{37}\text{Cl} \rightarrow ^{37}\text{Ar}$

• • • We do not use the following data for averages, fits, limits, etc. • • •

¹ KAETHER 10 reports the reanalysis results of a complete GALLEX data (GALLEX I+II+III+IV, reported in HAMPEL 99) based on the event selection with a new pulse shape analysis, which provides a better background reduction than the rise time analysis adopted in HAMPEL 99.

² Combined result of GALLEX I+II+III+IV reanalysis and GNO I+II+III (ALTMANN 05).

³ ABDURASHITOV 09 reports a combined analysis of 168 extractions of the SAGE solar neutrino experiment during the period January 1990 through December 2007, and updates the ABDURASHITOV 02 result. The data are consistent with the assumption that the solar neutrino production rate is constant in time. Note that a $\sim 15\%$ systematic uncertainty in the overall normalization may be added to the ABDURASHITOV 09 result, because calibration experiments for gallium solar neutrino measurements using intense ^{51}Cr (twice by GALLEX and once by SAGE) and ^{37}Ar (by SAGE) result in an average ratio of 0.87 ± 0.05 of the observed to calculated rates.

⁴ ALTMANN 05 reports the complete result from the GNO solar neutrino experiment (GNO I+II+III), which is the successor project of GALLEX. Experimental technique of GNO is essentially the same as that of GALLEX. The run data cover the period 20 May 1998 through 9 April 2003.

⁵ Combined result of GALLEX I+II+III+IV (HAMPEL 99) and GNO I+II+III.

⁶ HAMPEL 99 report the combined result for GALLEX I+II+III+IV (65 runs in total), which update the HAMPEL 96 result. The GALLEX IV result (12 runs) is $118.4 \pm 17.8 \pm 6.6$ SNU. (HAMPEL 99 discuss the consistency of partial results with the mean.) The GALLEX experimental program has been completed with these runs. The total run data cover the period 14 May 1991 through 23 January 1997. A total of 300 ^{71}Ge events were observed. Note that a $\sim 15\%$ systematic uncertainty in the overall normalization may be added to the HAMPEL 99 result, because calibration experiments for gallium solar neutrino measurements using intense ^{51}Cr (twice by GALLEX and once by SAGE) and ^{37}Ar (by SAGE) result in an average ratio of 0.87 ± 0.05 of the observed to calculated rates.

⁷ CLEVELAND 98 is a detailed report of the ^{37}Cl experiment at the Homestake Mine. The average solar neutrino-induced ^{37}Ar production rate from 108 runs between 1970 and 1994 updates the DAVIS 89 result.

$\phi_{ES} (^8\text{B})$

^8B solar-neutrino flux measured via ν_e elastic scattering. This process is sensitive to all active neutrino flavors, but with reduced sensitivity to ν_μ, ν_τ due to the cross-section difference, $\sigma(\nu_{\mu,\tau} e) \sim 0.16\sigma(\nu_e e)$. If the ^8B solar-neutrino flux involves nonelectron flavor active neutrinos, their contribution to the flux is ~ 0.16 times of ν_e .

<u>VALUE ($10^6 \text{ cm}^{-2}\text{s}^{-1}$)</u>	<u>DOCUMENT ID</u>	<u>TECN</u>	<u>COMMENT</u>
● ● ● We do not use the following data for averages, fits, limits, etc. ● ● ●			
2.57 $\begin{smallmatrix} +0.17 \\ -0.18 \end{smallmatrix}$ $\begin{smallmatrix} +0.07 \\ -0.07 \end{smallmatrix}$	1 AGOSTINI	20A BORX	average flux
2.53 $\begin{smallmatrix} +0.31 \\ -0.28 \end{smallmatrix}$ $\begin{smallmatrix} +0.13 \\ -0.10 \end{smallmatrix}$	2 ANDERSON	19 SNO+	Water phase; average flux
2.57 $\begin{smallmatrix} +0.17 \\ -0.18 \end{smallmatrix}$ $\begin{smallmatrix} +0.07 \\ -0.07 \end{smallmatrix}$	3 AGOSTINI	18B BORX	average flux
2.345 $\pm 0.014 \pm 0.036$	4 ABE	16C SKAM	SK-I+II+III+IV average flux
2.308 $\pm 0.020 \begin{smallmatrix} +0.039 \\ -0.040 \end{smallmatrix}$	5 ABE	16C SKAM	SK-IV average flux
2.250 $\begin{smallmatrix} +0.030 \\ -0.029 \end{smallmatrix} \pm 0.038$	5 ABE	16C SKAM	SK-IV day flux
2.364 $\pm 0.029 \pm 0.040$	5 ABE	16C SKAM	SK-IV night flux
2.404 $\pm 0.039 \pm 0.053$	6 ABE	16C SKAM	SK-III average flux
2.41 $\pm 0.05 \begin{smallmatrix} +0.16 \\ -0.15 \end{smallmatrix}$	7 ABE	11 SKAM	SK-II average flux
2.38 $\pm 0.02 \pm 0.08$	8 ABE	11 SKAM	SK-I average flux
2.77 $\pm 0.26 \pm 0.32$	9 ABE	11B KLND	average flux
2.4 $\pm 0.4 \pm 0.1$	10 BELLINI	10A BORX	average flux
1.77 $\begin{smallmatrix} +0.24 \\ -0.21 \end{smallmatrix} \begin{smallmatrix} +0.09 \\ -0.10 \end{smallmatrix}$	11 AHARMIM	08 SNO	Phase III
2.38 $\pm 0.05 \begin{smallmatrix} +0.16 \\ -0.15 \end{smallmatrix}$	12 CRAVENS	08 SKAM	average flux
2.35 $\pm 0.02 \pm 0.08$	13 HOSAKA	06 SKAM	average flux
2.35 $\pm 0.22 \pm 0.15$	14 AHARMIM	05A SNO	Salty D_2O ; 8B shape not constrained
2.34 $\pm 0.23 \begin{smallmatrix} +0.15 \\ -0.14 \end{smallmatrix}$	14 AHARMIM	05A SNO	Salty D_2O ; 8B shape constrained
2.39 $\begin{smallmatrix} +0.24 \\ -0.23 \end{smallmatrix} \pm 0.12$	15 AHMAD	02 SNO	average flux
2.39 $\pm 0.34 \begin{smallmatrix} +0.16 \\ -0.14 \end{smallmatrix}$	16 AHMAD	01 SNO	average flux
2.80 $\pm 0.19 \pm 0.33$	17 FUKUDA	96 KAMI	average flux
2.70 ± 0.27	17 FUKUDA	96 KAMI	day flux
2.87 $\begin{smallmatrix} +0.27 \\ -0.26 \end{smallmatrix}$	17 FUKUDA	96 KAMI	night flux

¹ AGOSTINI 20A obtained this result from the $\nu_e e$ elastic scattering rate over the period between January 2008 and December 2016. Uses the same data as AGOSTINI 18B, but the analysis technique is significantly improved.

² ANDERSON 19 reports this result from the $\nu_e e$ elastic scattering rate using a 69.2 kton-day (or 114.7 days) of exposure from May through December, 2017 during the SNO+ detector's water commissioning phase. The events over the reconstructed electron kinetic energy range of 5–15 MeV were analyzed.

³ AGOSTINI 18B obtained this result from the $\nu_e e$ elastic scattering rate over the period between January 2008 and December 2016.

⁴ ABE 16C reports the combined results of the four phases of the Super-Kamiokande average flux measurements. Here the revised Super-Kamiokande-III result is used.

⁵ ABE 16C reports the Super-Kamiokande-IV results for 1664 live days from September 2008 to February 2014. The analysis threshold is total electron energy of 4.0 MeV.

⁶ ABE 16C revised the Super-Kamiokande-III average flux value reported in ABE 11. Super-Kamiokande-III results are for 548 live days from August 4, 2006 to August 18, 2008. The analysis threshold is 5.0 MeV, but the event sample in the 5.0–6.5 MeV total electron energy range has a total live time of 298 days.

- 7 ABE 11 recalculated the Super-Kamiokande-II results using ^8B spectrum of WINTER 06A.
- 8 ABE 11 recalculated the Super-Kamiokande-I results using ^8B spectrum of WINTER 06A.
- 9 ABE 11B use a 123 kton-day exposure of the KamLAND liquid scintillation detector to measure the ^8B solar neutrino flux. They utilize $\nu - e$ elastic scattering above a reconstructed-energy threshold of 5.5 MeV, corresponding to 5 MeV electron recoil energy. 299 electron recoil candidate events are reported, of which 157 ± 23.6 are assigned to background.
- 10 BELLINI 10A reports the Borexino result with 3 MeV energy threshold for scattered electrons. The data correspond to 345.3 live days with a target mass of 100 t, between July 15, 2007 and August 23, 2009.
- 11 AHARMIM 08 reports the results from SNO Phase III measurement using an array of ^3He proportional counters to measure the rate of NC interactions in heavy water, over the period between November 27, 2004 and November 28, 2006, corresponding to 385.17 live days. A simultaneous fit was made for the number of NC events detected by the proportional counters and the numbers of NC, CC, and ES events detected by the PMTs, where the spectral distributions of the ES and CC events were not constrained to the ^8B shape.
- 12 CRAVENS 08 reports the Super-Kamiokande-II results for 791 live days from December 2002 to October 2005. The photocathode coverage of the detector is 19% (reduced from 40% of that of Super-Kamiokande-I due to an accident in 2001). The analysis threshold for the average flux is 7 MeV.
- 13 HOSAKA 06 reports the final results for 1496 live days with Super-Kamiokande-I between May 31, 1996 and July 15, 2001, and replace FUKUDA 02 results. The analysis threshold is 5 MeV except for the first 280 live days (6.5 MeV).
- 14 AHARMIM 05A measurements were made with dissolved NaCl (0.195% by weight) in heavy water over the period between July 26, 2001 and August 28, 2003, corresponding to 391.4 live days, and update AHMED 04A. The CC, ES, and NC events were statistically separated. In one method, the ^8B energy spectrum was not constrained. In the other method, the constraint of an undistorted ^8B energy spectrum was added for comparison with AHMAD 02 results.
- 15 AHMAD 02 reports the ^8B solar-neutrino flux measured via νe elastic scattering above the kinetic energy threshold of 5 MeV. The data correspond to 306.4 live days with SNO between November 2, 1999 and May 28, 2001, and updates AHMAD 01 results.
- 16 AHMAD 01 reports the ^8B solar-neutrino flux measured via νe elastic scattering above the kinetic energy threshold of 6.75 MeV. The data correspond to 241 live days with SNO between November 2, 1999 and January 15, 2001.
- 17 FUKUDA 96 results are for a total of 2079 live days with Kamiokande II and III from January 1987 through February 1995, covering the entire solar cycle 22, with threshold $E_e > 9.3$ MeV (first 449 days), > 7.5 MeV (middle 794 days), and > 7.0 MeV (last 836 days). These results update the HIRATA 90 result for the average ^8B solar-neutrino flux and HIRATA 91 result for the day-night variation in the ^8B solar-neutrino flux. The total data sample was also analyzed for short-term variations: within experimental errors, no strong correlation of the solar-neutrino flux with the sunspot numbers was found.

$\phi_{CC} (^8\text{B})$

^8B solar-neutrino flux measured with charged-current reaction which is sensitive exclusively to ν_e .

<u>VALUE ($10^6 \text{ cm}^{-2} \text{ s}^{-1}$)</u>	<u>DOCUMENT ID</u>	<u>TECN</u>	<u>COMMENT</u>
• • • We do not use the following data for averages, fits, limits, etc. • • •			
$1.67^{+0.05}_{-0.04} +^{0.07}_{-0.08}$	1 AHARMIM	08 SNO	Phase III
$1.68 \pm 0.06^{+0.08}_{-0.09}$	2 AHARMIM	05A SNO	Salty D_2O ; ^8B shape not const.

$1.72 \pm 0.05 \pm 0.11$	² AHARMIM	05A	SNO	Salty D ₂ O; ⁸ B shape constrained
$1.76^{+0.06}_{-0.05} \pm 0.09$	³ AHMAD	02	SNO	average flux
$1.75 \pm 0.07^{+0.12}_{-0.11} \pm 0.05$	⁴ AHMAD	01	SNO	average flux

¹ AHARMIM 08 reports the results from SNO Phase III measurement using an array of ³He proportional counters to measure the rate of NC interactions in heavy water, over the period between November 27, 2004 and November 28, 2006, corresponding to 385.17 live days. A simultaneous fit was made for the number of NC events detected by the proportional counters and the numbers of NC, CC, and ES events detected by the PMTs, where the spectral distributions of the ES and CC events were not constrained to the ⁸B shape.

² AHARMIM 05A measurements were made with dissolved NaCl (0.195% by weight) in heavy water over the period between July 26, 2001 and August 28, 2003, corresponding to 391.4 live days, and update AHMED 04A. The CC, ES, and NC events were statistically separated. In one method, the ⁸B energy spectrum was not constrained. In the other method, the constraint of an undistorted ⁸B energy spectrum was added for comparison with AHMAD 02 results.

³ AHMAD 02 reports the SNO result of the ⁸B solar-neutrino flux measured with charged-current reaction on deuterium, $\nu_e d \rightarrow ppe^-$, above the kinetic energy threshold of 5 MeV. The data correspond to 306.4 live days with SNO between November 2, 1999 and May 28, 2001, and updates AHMAD 01 results. The complete description of the SNO Phase I data set is given in AHARMIM 07.

⁴ AHMAD 01 reports the first SNO result of the ⁸B solar-neutrino flux measured with the charged-current reaction on deuterium, $\nu_e d \rightarrow ppe^-$, above the kinetic energy threshold of 6.75 MeV. The data correspond to 241 live days with SNO between November 2, 1999 and January 15, 2001.

$\phi_{NC} (^8B)$

⁸B solar neutrino flux measured with neutral-current reaction, which is equally sensitive to ν_e , ν_μ , and ν_τ .

<u>VALUE ($10^6 \text{ cm}^{-2} \text{ s}^{-1}$)</u>	<u>DOCUMENT ID</u>	<u>TECN</u>	<u>COMMENT</u>
● ● ● We do not use the following data for averages, fits, limits, etc. ● ● ●			
$5.25 \pm 0.16^{+0.11}_{-0.13}$	¹ AHARMIM	13	SNO All three phases combined
$5.140^{+0.160+0.132}_{-0.158-0.117}$	² AHARMIM	10	SNO Phase I+II, low threshold
$5.54^{+0.33+0.36}_{-0.31-0.34}$	³ AHARMIM	08	SNO Phase III, prop. counter + PMT
$4.94 \pm 0.21^{+0.38}_{-0.34}$	⁴ AHARMIM	05A	SNO Salty D ₂ O; ⁸ B shape not const.
$4.81 \pm 0.19^{+0.28}_{-0.27}$	⁴ AHARMIM	05A	SNO Salty D ₂ O; ⁸ B shape constrained
$5.09^{+0.44+0.46}_{-0.43-0.43}$	⁵ AHMAD	02	SNO average flux; ⁸ B shape const.
$6.42 \pm 1.57^{+0.55}_{-0.58}$	⁵ AHMAD	02	SNO average flux; ⁸ B shape not const.

¹ AHARMIM 13 obtained this result from a combined analysis of the data from all three phases, SNO-I, II, and III. The measurement of the ⁸B flux mostly comes from the NC signal, however, CC contribution is included in the fit.

² AHARMIM 10 reports this result from a joint analysis of SNO Phase I+II data with the "effective electron kinetic energy" threshold of 3.5 MeV. This result is obtained with a "binned-histogram unconstrained fit" where binned probability distribution functions of the neutrino signal observables were used without any model constraints on the shape of the neutrino spectrum.

³ AHARMIM 08 reports the results from SNO Phase III measurement using an array of ³He proportional counters to measure the rate of NC interactions in heavy water, over the period between November 27, 2004 and November 28, 2006, corresponding to 385.17 live days. A simultaneous fit was made for the number of NC events detected by the proportional counters and the numbers of NC, CC, and ES events detected by the PMTs, where the spectral distributions of the ES and CC events were not constrained to the ⁸B shape.

⁴ AHARMIM 05A measurements were made with dissolved NaCl (0.195% by weight) in heavy water over the period between July 26, 2001 and August 28, 2003, corresponding to 391.4 live days, and update AHMED 04A. The CC, ES, and NC events were statistically separated. In one method, the ⁸B energy spectrum was not constrained. In the other method, the constraint of an undistorted ⁸B energy spectrum was added for comparison with AHMAD 02 results.

⁵ AHMAD 02 reports the first SNO result of the ⁸B solar-neutrino flux measured with the neutral-current reaction on deuterium, $\nu_\ell d \rightarrow n p \nu_\ell$, above the neutral-current reaction threshold of 2.2 MeV. The data correspond to 306.4 live days with SNO between November 2, 1999 and May 28, 2001. The complete description of the SNO Phase I data set is given in AHARMIM 07.

$\phi_{\nu_\mu + \nu_\tau}$ (⁸B)

Nonelectron-flavor active neutrino component (ν_μ and ν_τ) in the ⁸B solar-neutrino flux.

VALUE ($10^6 \text{ cm}^{-2} \text{ s}^{-1}$)	DOCUMENT ID	TECN	COMMENT
• • • We do not use the following data for averages, fits, limits, etc. • • •			
$3.26 \pm 0.25^{+0.40}_{-0.35}$	¹ AHARMIM	05A SNO	From ϕ_{NC} , ϕ_{CC} , and ϕ_{ES} ; ⁸ B shape not const.
$3.09 \pm 0.22^{+0.30}_{-0.27}$	¹ AHARMIM	05A SNO	From ϕ_{NC} , ϕ_{CC} , and ϕ_{ES} ; ⁸ B shape constrained
$3.41 \pm 0.45^{+0.48}_{-0.45}$	² AHMAD	02 SNO	From ϕ_{NC} , ϕ_{CC} , and ϕ_{ES}
3.69 ± 1.13	³ AHMAD	01	Derived from SNO+SuperKam, water Cherenkov

¹ AHARMIM 05A measurements were made with dissolved NaCl (0.195% by weight) in heavy water over the period between July 26, 2001 and August 28, 2003, corresponding to 391.4 live days, and update AHMED 04A. The CC, ES, and NC events were statistically separated. In one method, the ⁸B energy spectrum was not constrained. In the other method, the constraint of an undistorted ⁸B energy spectrum was added for comparison with AHMAD 02 results.

² AHMAD 02 deduced the nonelectron-flavor active neutrino component (ν_μ and ν_τ) in the ⁸B solar-neutrino flux, by combining the charged-current result, the νe elastic-scattering result and the neutral-current result. The complete description of the SNO Phase I data set is given in AHARMIM 07.

³ AHMAD 01 deduced the nonelectron-flavor active neutrino component (ν_μ and ν_τ) in the ⁸B solar-neutrino flux, by combining the SNO charged-current result (AHMAD 01) and the Super-Kamiokande νe elastic-scattering result (FUKUDA 01).

Total Flux of Active pp Solar Neutrinos

Total flux of active neutrinos (ν_e, ν_μ, ν_τ).

VALUE ($10^{10} \text{ cm}^{-2}\text{s}^{-1}$)	DOCUMENT ID	TECN	COMMENT
--	-------------	------	---------

• • • We do not use the following data for averages, fits, limits, etc. • • •

$6.1 \pm 0.5^{+0.3}_{-0.5}$	¹ AGOSTINI	18B	BORX $\nu_e e$ scattering rate
-----------------------------	-----------------------	-----	--------------------------------

¹ AGOSTINI 18B obtained this result from the measured $\nu_e e$ elastic scattering rate over the period between December 2011 and May 2016, assuming the MSW-LMA oscillation parameters derived by ESTEBAN 17. Assuming a high-metallicity standard solar model, the electron neutrino survival probability for the pp solar neutrino is calculated to be 0.57 ± 0.09 .

Total Flux of Active ${}^7\text{Be}$ Solar Neutrinos

Total flux of active neutrinos (ν_e, ν_μ, ν_τ).

VALUE ($10^9 \text{ cm}^{-2}\text{s}^{-1}$)	DOCUMENT ID	TECN	COMMENT
---	-------------	------	---------

• • • We do not use the following data for averages, fits, limits, etc. • • •

$4.99 \pm 0.11^{+0.06}_{-0.08}$	¹ AGOSTINI	18B	BORX $\nu_e e$ scattering rate
---------------------------------	-----------------------	-----	--------------------------------

¹ AGOSTINI 18B obtained this result from the measured $\nu_e e$ elastic scattering rate over the period between December 2011 and May 2016, assuming the MSW-LMA oscillation parameters derived by ESTEBAN 17. Assuming a high-metallicity standard solar model, the electron neutrino survival probability for the ${}^7\text{Be}$ solar neutrino is calculated to be 0.53 ± 0.05 .

Total Flux of Active pep Solar Neutrinos

Total flux of active neutrinos (ν_e, ν_μ, ν_τ).

VALUE ($10^8 \text{ cm}^{-2}\text{s}^{-1}$)	DOCUMENT ID	TECN	COMMENT
---	-------------	------	---------

• • • We do not use the following data for averages, fits, limits, etc. • • •

$1.27 \pm 0.19^{+0.08}_{-0.12}$	¹ AGOSTINI	18B	BORX $\nu_e e$ scattering rate
---------------------------------	-----------------------	-----	--------------------------------

¹ AGOSTINI 18B obtained this result from the measured $\nu_e e$ elastic scattering rate over the period between December 2011 and May 2016, assuming the MSW-LMA oscillation parameters derived by ESTEBAN 17 and a high-metallicity standard solar model. The electron neutrino survival probability for the pep solar neutrino is calculated to be 0.43 ± 0.11 .

Total Flux of Active ${}^8\text{B}$ Solar Neutrinos

Total flux of active neutrinos (ν_e, ν_μ , and ν_τ).

VALUE ($10^6 \text{ cm}^{-2}\text{s}^{-1}$)	DOCUMENT ID	TECN	COMMENT
---	-------------	------	---------

• • • We do not use the following data for averages, fits, limits, etc. • • •

$5.95^{+0.75}_{-0.71}^{+0.28}_{-0.30}$	¹ ANDERSON	19	SNO+ Water phase; $\nu_e e$ scattering rate
$5.68^{+0.39}_{-0.41}^{+0.03}_{-0.03}$	² AGOSTINI	18B	BORX From $\nu_e e$ scattering rate
$5.25 \pm 0.16^{+0.11}_{-0.13}$	³ AHARMIM	13	SNO All three phases combined
$5.046^{+0.159}_{-0.152}^{+0.107}_{-0.123}$	⁴ AHARMIM	10	SNO From ϕ_{NC} in Phase I+II, low threshold
$5.54^{+0.33}_{-0.31}^{+0.36}_{-0.34}$	⁵ AHARMIM	08	SNO ϕ_{NC} in Phase III

4.94 ±0.21	$\begin{matrix} +0.38 \\ -0.34 \end{matrix}$	⁶ AHARMIM	05A	SNO	From ϕ_{NC} ; ⁸ B shape not const.
4.81 ±0.19	$\begin{matrix} +0.28 \\ -0.27 \end{matrix}$	⁶ AHARMIM	05A	SNO	From ϕ_{NC} ; ⁸ B shape constrained
5.09	$\begin{matrix} +0.44 \\ -0.43 \end{matrix}$	⁷ AHMAD	02	SNO	Direct measurement from ϕ_{NC}
5.44 ±0.99		⁸ AHMAD	01		Derived from SNO+SuperKam, water Cherenkov

¹ ANDERSON 19 reports this result from the measured $\nu_e e$ elastic scattering rate using a 69.2 kton-day (or 114.7 days) of exposure from May through December, 2017 during the SNO+ detector's water commissioning phase, assuming the neutrino mixing parameters given in PDG 16 and a standard solar model given in BAHCALL 05.

² AGOSTINI 18B obtained this result from the measured $\nu_e e$ elastic scattering rate over the period between January 2008 and December 2016, assuming the MSW-LMA oscillation parameters derived by ESTEBAN 17. Assuming a high-metallicity standard solar model, the electron neutrino survival probability for the ⁸B solar neutrino is calculated to be 0.37 ± 0.08 .

³ AHARMIM 13 obtained this result from a combined analysis of the data from all three phases, SNO-I, II, and III. The measurement of the ⁸B flux mostly comes from the NC signal, however, CC contribution is included in the fit.

⁴ AHARMIM 10 reports this result from a joint analysis of SNO Phase I+II data with the "effective electron kinetic energy" threshold of 3.5 MeV. This result is obtained with the assumption of unitarity, which relates the NC, CC, and ES rates. The data were fit with the free parameters directly describing the total ⁸B neutrino flux and the energy-dependent ν_e survival probability.

⁵ AHARMIM 08 reports the results from SNO Phase III measurement using an array of ³He proportional counters to measure the rate of NC interactions in heavy water, over the period between November 27, 2004 and November 28, 2006, corresponding to 385.17 live days. A simultaneous fit was made for the number of NC events detected by the proportional counters and the numbers of NC, CC, and ES events detected by the PMTs, where the spectral distributions of the ES and CC events were not constrained to the ⁸B shape.

⁶ AHARMIM 05A measurements were made with dissolved NaCl (0.195% by weight) in heavy water over the period between July 26, 2001 and August 28, 2003, corresponding to 391.4 live days, and update AHMED 04A. The CC, ES, and NC events were statistically separated. In one method, the ⁸B energy spectrum was not constrained. In the other method, the constraint of an undistorted ⁸B energy spectrum was added for comparison with AHMAD 02 results.

⁷ AHMAD 02 determined the total flux of active ⁸B solar neutrinos by directly measuring the neutral-current reaction, $\nu_\ell d \rightarrow n p \nu_\ell$, which is equally sensitive to ν_e , ν_μ , and ν_τ . The complete description of the SNO Phase I data set is given in AHARMIM 07.

⁸ AHMAD 01 deduced the total flux of active ⁸B solar neutrinos by combining the SNO charged-current result (AHMAD 01) and the Super-Kamiokande νe elastic-scattering result (FUKUDA 01).

Total Flux of Active CNO Solar Neutrinos

Total flux of active neutrinos (ν_e, ν_μ, ν_τ).

<u>VALUE ($10^8 \text{ cm}^{-2} \text{ s}^{-1}$)</u>	<u>CL%</u>	<u>DOCUMENT ID</u>	<u>TECN</u>	<u>COMMENT</u>
---	------------	--------------------	-------------	----------------

• • • We do not use the following data for averages, fits, limits, etc. • • •

6.6 $\begin{matrix} +2.0 \\ -0.9 \end{matrix}$		¹ APPEL	22	BORX $\nu_e e$ scattering rate
--	--	--------------------	----	--------------------------------

$7.0^{+3.0}_{-2.0}$		² AGOSTINI	20D	BORX	$\nu_e e$ scattering rate
<7.9	95	³ AGOSTINI	18B	BORX	$\nu_e e$ scattering rate

¹ APPEL 22 obtained this result from the measured $\nu_e e$ elastic scattering rate over the period between January 2017 and October 2021, assuming the MSW-LMA oscillation parameters derived by ESTEBAN 20A. The exposure corresponding to this data is 1431.6 days \times 71.3 tons.

² AGOSTINI 20D obtained this result from the measured $\nu_e e$ elastic scattering rate over the period between July 2016 to February 2020, assuming the MSW-LMA oscillation parameters derived by CAPOZZI 18.

³ AGOSTINI 18B obtained this result from an upper limit of the $\nu_e e$ elastic scattering rate for the CNO neutrinos over the period between December 2011 and May 2016, assuming the MSW-LMA oscillation parameters derived by ESTEBAN 17.

Total Flux of Active hep Solar Neutrinos

Total flux of active neutrinos (ν_e, ν_μ, ν_τ).

VALUE ($10^5 \text{ cm}^{-2} \text{ s}^{-1}$)	CL%	DOCUMENT ID	TECN	COMMENT
---	-----	-------------	------	---------

• • • We do not use the following data for averages, fits, limits, etc. • • •

<1.8	90	¹ AGOSTINI	20A	BORX	$\nu_e e$ scattering and $^{12}\text{C}(\nu, \nu')^{12}\text{C}^*$
<0.3	90	² AHARMIM	20	SNO	CC, NC, $\nu_e e$ scattering
<2.2	90	³ AGOSTINI	18B	BORX	$\nu_e e$ scattering rate

¹ AGOSTINI 20A obtained this result from an upper limit of the $\nu_e e$ elastic scattering rate and NC-mediated inelastic scattering on carbon nuclei with 15.1 MeV deexcitation γ -ray for the hep neutrino. The dataset corresponds to an effective exposure of 0.745 kt-yr from November 2009 to October 2017. A FADC DAQ system, optimized for the acquisition of high-energy events was used for data collection. The MSW-LMA oscillation parameters derived by ESTEBAN 17 were assumed.

² AHARMIM 20 uses the entire SNO dataset, corresponding to 2.47 kton-yr of exposure after fiducialization. With the D_2O target, SNO was sensitive to charged current, neutral current, and elastic scattering channels.

³ AGOSTINI 18B obtained this result from an upper limit of the $\nu_e e$ elastic scattering rate for the hep neutrino using the dataset corresponding to an exposure of 0.8 kt-yr and assuming the MSW-LMA oscillation parameters derived by ESTEBAN 17.

Day-Night Asymmetry (^8B)

$$A = (\phi_{\text{night}} - \phi_{\text{day}}) / \phi_{\text{average}}$$

VALUE	DOCUMENT ID	TECN	COMMENT
$0.033 \pm 0.010 \pm 0.005$	¹ ABE	16C	SKAM SK combined; Based on ϕ_{ES}

• • • We do not use the following data for averages, fits, limits, etc. • • •

$0.036 \pm 0.016 \pm 0.006$	² ABE	16C	SKAM SK-IV; Based on ϕ_{ES}
$0.032 \pm 0.011 \pm 0.005$	³ RENSHAW	14	SKAM Based on ϕ_{ES}
$0.063 \pm 0.042 \pm 0.037$	⁴ CRAVENS	08	SKAM Based on ϕ_{ES}
$0.021 \pm 0.020^{+0.012}_{-0.013}$	⁵ HOSAKA	06	SKAM Based on ϕ_{ES}
$0.017 \pm 0.016^{+0.012}_{-0.013}$	⁶ HOSAKA	06	SKAM Fitted in the LMA region
$-0.056 \pm 0.074 \pm 0.053$	⁷ AHARMIM	05A	SNO From salty SNO ϕ_{CC}
$-0.037 \pm 0.063 \pm 0.032$	⁷ AHARMIM	05A	SNO From salty SNO ϕ_{CC} ; const. of no ϕ_{NC} asymmetry

$0.14 \pm 0.063^{+0.015}_{-0.014}$	⁸ AHMAD	02B	SNO	Derived from SNO ϕ_{CC}
$0.07 \pm 0.049^{+0.013}_{-0.012}$	⁹ AHMAD	02B	SNO	Const. of no ϕ_{NC} asymmetry

¹ ABE 16C reports the combined day-night flux asymmetry results of the four phases of the Super-Kamiokande measurements. Amplitude fit method is used. See footnote to RENSHAW 14.

² ABE 16C reports the Super-Kamiokande-IV results for 1664 live days from September 2008 to February 2014. The analysis threshold for day-night flux asymmetry is recoil electron energy of 4.49 MeV (total electron energy of 5.0 MeV). Amplitude fit method is used. See footnote to RENSHAW 14.

³ RENSHAW 14 obtains this result by using the "amplitude fit" introduced in SMY 04. The data from the Super-Kamiokande(SK)-I, -II, -III, and 1306 live days of the SK-IV measurements are used. The analysis threshold is recoil-electron kinetic energy of 4.5 MeV for SK-III, and SK-IV except for 250 live days in SK-III (6.0 MeV). The analysis threshold for SK-I and SK-II is the same as in the previous reports. (Note that in the previous SK solar-neutrino results, the analysis threshold is quoted as recoil-electron total energy.) This day-night asymmetry result is consistent with neutrino oscillations for $4 \times 10^{-5} \text{ eV}^2 < \Delta m_{21}^2 < 7 \times 10^{-5} \text{ eV}^2$ and large mixing values of θ_{12} at the 68% CL.

⁴ CRAVENS 08 reports the Super-Kamiokande-II results for 791 live days from December 2002 to October 2005. The photocathode coverage of the detector is 19% (reduced from 40% of that of Super-Kamiokande-I due to an accident in 2001). The analysis threshold for the day and night fluxes is 7.5 MeV except for the first 159 live days (8.0 MeV).

⁵ HOSAKA 06 reports the final results for 1496 live days with Super-Kamiokande-I between May 31, 1996 and July 15, 2001, and replace FUKUDA 02 results. The analysis threshold is 5 MeV except for the first 280 live days (6.5 MeV).

⁶ This result with reduced statistical uncertainty is obtained by assuming two-neutrino oscillations within the LMA (large mixing angle) region and by fitting the time variation of the solar neutrino flux measured via ν_e elastic scattering to the variations expected from neutrino oscillations. For details, see SMY 04. There is an additional small systematic error of ± 0.0004 coming from uncertainty of oscillation parameters.

⁷ AHARMIM 05A measurements were made with dissolved NaCl (0.195% by weight) in heavy water over the period between July 26, 2001 and August 28, 2003, with 176.5 days of the live time recorded during the day and 214.9 days during the night. This result is obtained with the spectral distribution of the CC events not constrained to the ⁸B shape.

⁸ AHMAD 02B results are based on the charged-current interactions recorded between November 2, 1999 and May 28, 2001, with the day and night live times of 128.5 and 177.9 days, respectively. The complete description of the SNO Phase I data set is given in AHARMIM 07.

⁹ AHMAD 02B results are derived from the charged-current interactions, neutral-current interactions, and νe elastic scattering, with the total flux of active neutrinos constrained to have no asymmetry. The data were recorded between November 2, 1999 and May 28, 2001, with the day and night live times of 128.5 and 177.9 days, respectively. The complete description of the SNO Phase I data set is given in AHARMIM 07.

$\phi_{ES} (^7\text{Be})$

⁷Be solar-neutrino flux measured via ν_e elastic scattering. This process is sensitive to all active neutrino flavors, but with reduced sensitivity to ν_μ, ν_τ due to the cross-section difference, $\sigma(\nu_{\mu,\tau} e) \sim 0.2 \sigma(\nu_e e)$. If the ⁷Be solar-neutrino flux involves nonelectron flavor active neutrinos, their contribution to the flux is ~ 0.2 times that of ν_e .

<u>VALUE ($10^9 \text{ cm}^{-2} \text{ s}^{-1}$)</u>	<u>DOCUMENT ID</u>	<u>TECN</u>	<u>COMMENT</u>
---	--------------------	-------------	----------------

• • • We do not use the following data for averages, fits, limits, etc. • • •

3.26 ± 0.52	¹ GANDO	15	KLND	average flux
3.10 ± 0.15	² BELLINI	11A	BORX	average flux

¹ GANDO 15 uses 165.4 kton-day exposure of the KamLAND liquid scintillator detector to measure the 862 keV ⁷Be solar neutrino flux via $\nu - e$ elastic scattering

² BELLINI 11A reports the ⁷Be solar neutrino flux measured via $\nu - e$ elastic scattering. The data correspond to 740.7 live days between May 16, 2007 and May 8, 2010, and also correspond to 153.6 ton-year fiducial exposure. BELLINI 11A measured the 862 keV ⁷Be solar neutrino flux, which is an 89.6% branch of the ⁷Be solar neutrino flux, to be $(2.78 \pm 0.13) \times 10^9 \text{ cm}^{-2} \text{ s}^{-1}$. Supercedes ARPESELLA 08A.

$\phi_{ES}(pep)$

pep solar-neutrino flux measured via ν_e elastic scattering. This process is sensitive to all active neutrino flavors, but with reduced sensitivity to ν_μ, ν_τ due to the cross section difference, $\sigma(\nu_{\mu,\tau} e) \sim 0.2 \sigma(\nu_e e)$. If the pep solar-neutrino flux involves non-electron flavor active neutrinos, their contribution to the flux is ~ 0.2 times that of ν_e .

<u>VALUE ($10^8 \text{ cm}^{-2} \text{ s}^{-1}$)</u>	<u>DOCUMENT ID</u>	<u>TECN</u>	<u>COMMENT</u>
---	--------------------	-------------	----------------

• • • We do not use the following data for averages, fits, limits, etc. • • •

1.0 ± 0.2	¹ BELLINI	12A	BORX	average flux
---------------	----------------------	-----	------	--------------

¹ BELLINI 12A reports 1.44 MeV pep solar-neutrino flux measured via ν_e elastic scattering. The data were collected between January 13, 2008 and May 9, 2010, corresponding to 20,4009 ton-day fiducial exposure. The listed flux value is calculated from the observed rate of pep solar neutrino interactions in Borexino ($3.1 \pm 0.6 \pm 0.3$ counts/(day·100 ton)) and the corresponding rate expected for no neutrino flavor oscillations (4.47 ± 0.05 counts/(day·100 ton)), using the SSM prediction for the pep solar neutrino flux of $(1.441 \pm 0.012) \times 10^8 \text{ cm}^{-2} \text{ s}^{-1}$.

$\phi_{ES}(CNO)$

CNO solar-neutrino flux measured via ν_e elastic scattering. This process is sensitive to all active neutrino flavors, but with reduced sensitivity to ν_μ, ν_τ due to the cross section difference, $\sigma(\nu_{\mu,\tau} e) \sim 0.2 \sigma(\nu_e e)$. If the CNO solar-neutrino flux involves non-electron flavor active neutrinos, their contribution to the flux is ~ 0.2 times that of ν_e .

<u>VALUE ($10^8 \text{ cm}^{-2} \text{ s}^{-1}$)</u>	<u>CL%</u>	<u>DOCUMENT ID</u>	<u>TECN</u>	<u>COMMENT</u>
---	------------	--------------------	-------------	----------------

• • • We do not use the following data for averages, fits, limits, etc. • • •

<7.7	90	¹ BELLINI	12A	BORX MSW-LMA solution assumed
--------	----	----------------------	-----	-------------------------------

¹ BELLINI 12A reports an upper limit of the CNO solar neutrino flux measured via ν_e elastic scattering. The data were collected between January 13, 2008 and May 9, 2010, corresponding to 20,409 ton-day fiducial exposure.

$\phi_{ES}(pp)$

pp solar-neutrino flux measured via νe elastic scattering. This process is sensitive to all active neutrino flavors, but with reduced sensitivity to ν_μ, ν_τ due to the cross section difference, $\sigma(\nu_{\mu,\tau} e) \sim 0.3 \sigma(\nu_e e)$. If the pp solar-neutrino flux involves nonelectron flavor active neutrinos, their contribution to the flux is ~ 0.3 times of ν_e .

<u>VALUE ($10^{10} \text{ cm}^{-2} \text{ s}^{-1}$)</u>	<u>DOCUMENT ID</u>	<u>TECN</u>	<u>COMMENT</u>
--	--------------------	-------------	----------------

• • • We do not use the following data for averages, fits, limits, etc. • • •

4.4 ± 0.5	¹ BELLINI	14A	BORX	average flux
---------------	----------------------	-----	------	--------------

¹ BELLINI 14A reports pp solar-neutrino flux measured via νe elastic scattering. The data were collected between January 2012 and May 2013, corresponding to 408 days of

data. The pp neutrino interaction rate in Borexino is measured to be $144 \pm 13 \pm 10$ counts/(day·100 ton) by fitting the measured energy spectrum of events in the 165–590 keV recoil electron kinetic energy window with the expected signal + background spectrum. The listed flux value $\phi_{ES}(pp)$ is calculated from the observed rate and the number of $(3.307 \pm 0.003) \times 10^{31}$ electrons for 100 tons of the Borexino scintillator, and the $\nu_e e$ integrated cross section over the pp neutrino spectrum, $\sigma(\nu_e e) = 11.38 \times 10^{-46} \text{ cm}^2$.

$\phi_{CC}(pp)$

pp solar-neutrino flux measured with charged-current reaction which is sensitive exclusively to ν_e .

VALUE ($10^{10} \text{ cm}^{-2} \text{ s}^{-1}$)	DOCUMENT ID	TECN	COMMENT
--	-------------	------	---------

• • • We do not use the following data for averages, fits, limits, etc. • • •

3.38 ± 0.47	¹ ABDURASHI... 09	FIT	Fit existing solar- ν data
-----------------	------------------------------	-----	--------------------------------

¹ ABDURASHITOV 09 reports the pp solar-neutrino flux derived from the Ga solar neutrino capture rate by subtracting contributions from ^8B , ^7Be , $p e p$ and CNO solar neutrino fluxes determined by other solar neutrino experiments as well as neutrino oscillation parameters determined from available world neutrino oscillation data.

$\phi_{ES}(\text{hep})$

hep solar-neutrino flux measured via νe elastic scattering. This process is sensitive to all active neutrino flavors, but with reduced sensitivity to ν_μ, ν_τ due to the cross-section difference, $\sigma(\nu_{\mu,\tau} e) \sim 0.16\sigma(\nu_e e)$. If the hep solar-neutrino flux involves nonelectron flavor active neutrinos, their contribution to the flux is ~ 0.16 times of ν_e .

VALUE ($10^3 \text{ cm}^{-2} \text{ s}^{-1}$)	CL%	DOCUMENT ID	TECN
---	-----	-------------	------

• • • We do not use the following data for averages, fits, limits, etc. • • •

< 73	90	¹ HOSAKA	06 SKAM
--------	----	---------------------	---------

¹ HOSAKA 06 result is obtained from the recoil electron energy window of 18–21 MeV, and updates FUKUDA 01 result.

$\phi_{\bar{\nu}_e} (^8\text{B})$

Searches are made for electron antineutrino flux from the Sun. Flux limits listed here are derived relative to the BS05(OP) Standard Solar Model ^8B solar neutrino flux ($5.69 \times 10^6 \text{ cm}^{-2} \text{ s}^{-1}$), with an assumption that solar $\bar{\nu}_e$ s follow an unoscillated ^8B neutrino spectrum.

VALUE (%)	CL%	DOCUMENT ID	TECN	COMMENT
-----------	-----	-------------	------	---------

• • • We do not use the following data for averages, fits, limits, etc. • • •

< 0.0072	90	¹ AGOSTINI	21 BORX	$E_{\bar{\nu}_e} > 1.8 \text{ MeV}$
< 0.013	90	² BELLINI	11 BORX	$E_{\bar{\nu}_e} > 1.8 \text{ MeV}$
< 1.9	90	³ BALATA	06 CNTR	$1.8 < E_{\bar{\nu}_e} < 20.0 \text{ MeV}$
< 0.72	90	AHARMIM	04 SNO	$4.0 < E_{\bar{\nu}_e} < 14.8 \text{ MeV}$
< 0.022	90	EGUCHI	04 KLND	$8.3 < E_{\bar{\nu}_e} < 14.8 \text{ MeV}$
< 0.7	90	GANDO	03 SKAM	$8.0 < E_{\bar{\nu}_e} < 20.0 \text{ MeV}$
< 1.7	90	AGLIETTA	96 LSD	$7 < E_{\bar{\nu}_e} < 17 \text{ MeV}$

¹ AGOSTINI 21 derived this result relative to the Standard Solar Model ^8B solar neutrino flux, under an assumption of high solar metallicity, of $5.46 (1 \pm 0.12) \times 10^6 \text{ cm}^{-2} \text{ s}^{-1}$ (see VINYOLES 17).

² Superseded by AGOSTINI 21.

³BALATA 06 obtained this result from the search for $\bar{\nu}_e$ interactions with Counting Test Facility (the prototype of the Borexino detector).

(B) Three-neutrino mixing parameters

$\sin^2(\theta_{12})$

If an experiment reports $\sin^2(2\theta_{12})$ we convert the value to $\sin^2(\theta_{12})$.

VALUE	DOCUMENT ID	TECN	COMMENT
$0.307^{+0.013}_{-0.012}$	¹ ABE	16C FIT	KamLAND+global solar; 3ν
● ● ● We do not use the following data for averages, fits, limits, etc. ● ● ●			
0.318 ± 0.016	² SALAS	21 FIT	global fit
0.304 ± 0.012	³ ESTEBAN	20A FIT	Global fit
$0.320^{+0.020}_{-0.016}$	DE-SALAS	18 FIT	Global fit
0.310 ± 0.014	⁴ ABE	16C FIT	SKAM+SNO; 3ν
$0.334^{+0.027}_{-0.023}$	⁵ ABE	16C FIT	SK-I+II+III+IV; 3ν
$0.327^{+0.026}_{-0.031}$	⁶ ABE	16C FIT	SK-IV; 3ν
0.323 ± 0.016	⁷ FORERO	14 FIT	3ν
$0.304^{+0.013}_{-0.012}$	⁸ GONZALEZ...	14 FIT	Either mass ordering; global fit
$0.299^{+0.014}_{-0.014}$	^{9,10} AHARMIM	13 FIT	global solar: 2ν
$0.307^{+0.016}_{-0.013}$	^{10,11} AHARMIM	13 FIT	global solar: 3ν
$0.304^{+0.022}_{-0.018}$	^{10,12} AHARMIM	13 FIT	KamLAND + global solar: 3ν
$0.304^{+0.014}_{-0.013}$	¹³ GANDO	13 FIT	KamLAND + global solar + SBL + accelerator: 3ν
$0.304^{+0.014}_{-0.013}$	¹⁴ GANDO	13 FIT	KamLAND + global solar: 3ν
$0.325^{+0.039}_{-0.039}$	¹⁵ GANDO	13 FIT	KamLAND: 3ν
$0.30^{+0.02}_{-0.01}$	¹⁶ ABE	11 FIT	KamLAND + global solar: 2ν
$0.30^{+0.02}_{-0.01}$	¹⁷ ABE	11 FIT	global solar: 2ν
$0.31^{+0.03}_{-0.02}$	¹⁸ ABE	11 FIT	KamLAND + global solar: 3ν
$0.31^{+0.03}_{-0.03}$	¹⁹ ABE	11 FIT	global solar: 3ν
$0.314^{+0.015}_{-0.012}$	²⁰ BELLINI	11A FIT	KamLAND + global solar: 2ν
$0.319^{+0.017}_{-0.015}$	²¹ BELLINI	11A FIT	global solar: 2ν
$0.311^{+0.016}_{-0.016}$	²² GANDO	11 FIT	KamLAND + solar: 3ν
$0.304^{+0.046}_{-0.042}$	²³ GANDO	11 FIT	KamLAND: 3ν
$0.314^{+0.018}_{-0.014}$	^{24,25} AHARMIM	10 FIT	KamLAND + global solar: 2ν
$0.314^{+0.017}_{-0.020}$	^{24,26} AHARMIM	10 FIT	global solar: 2ν

$0.319^{+0.019}_{-0.016}$	24,27	AHARMIM	10	FIT	KamLAND + global solar: 3ν
$0.319^{+0.023}_{-0.024}$	24,28	AHARMIM	10	FIT	global solar: 3ν
$0.36^{+0.05}_{-0.04}$	29	ABE	08A	FIT	KamLAND
0.32 ± 0.03	30	ABE	08A	FIT	KamLAND + global fit
0.32 ± 0.02	31	AHARMIM	08	FIT	KamLAND + global solar
$0.31^{+0.04}_{-0.04}$	32	HOSAKA	06	FIT	KamLAND + global solar
$0.31^{+0.04}_{-0.03}$	33	HOSAKA	06	FIT	SKAM+SNO+KamLAND
$0.31^{+0.03}_{-0.04}$	34	HOSAKA	06	FIT	SKAM+SNO
$0.31^{+0.02}_{-0.03}$	35	AHARMIM	05A	FIT	KamLAND + global solar
0.25–0.39	36	AHARMIM	05A	FIT	global solar
0.29 ± 0.03	37	ARAKI	05	FIT	KamLAND + global solar
$0.29^{+0.03}_{-0.02}$	38	AHMED	04A	FIT	KamLAND + global solar
0.23–0.37	39	AHMED	04A	FIT	global solar
$0.31^{+0.04}_{-0.04}$	40	SMY	04	FIT	KamLAND + global solar
$0.29^{+0.04}_{-0.04}$	41	SMY	04	FIT	global solar
$0.32^{+0.06}_{-0.05}$	42	SMY	04	FIT	SKAM + SNO
0.19–0.33	43	AHMAD	02B	FIT	global solar
0.19–0.39	44	FUKUDA	02	FIT	global solar

¹ ABE 16C obtained this result by a three-neutrino oscillation analysis, with a constraint of $\sin^2(\theta_{13}) = 0.0219 \pm 0.0014$ coming from reactor neutrino experiments, using all solar data and KamLAND data. *CPT* invariance is assumed.

² SALAS 21 reports results of a global fit to neutrino oscillation data available at the time of the Neutrino 2020 conference.

³ ESTEBAN 20A reports results of a global fit to neutrino oscillation data available at the time of the Neutrino2020 conference.

⁴ ABE 16C obtained this result by a three-neutrino oscillation analysis, with a constraint of $\sin^2(\theta_{13}) = 0.0219 \pm 0.0014$ coming from reactor neutrino experiments, using Super-Kamiokande (I+II+III+IV) and SNO data.

⁵ ABE 16C obtained this result by a three-neutrino oscillation analysis, with a constraint of $\sin^2(\theta_{13}) = 0.0219 \pm 0.0014$ coming from reactor neutrino experiments, by combining the four phases of the Super-Kamiokande solar data.

⁶ ABE 16C obtained this result by a three-neutrino oscillation analysis, with a constraint of $\sin^2(\theta_{13}) = 0.0219 \pm 0.0014$ coming from reactor neutrino experiments, using the Super-Kamiokande-IV data.

⁷ FORERO 14 performs a global fit to neutrino oscillations using solar, reactor, long-baseline accelerator, and atmospheric neutrino data.

⁸ GONZALEZ-GARCIA 14 result comes from a frequentist global fit. The corresponding Bayesian global fit to the same data results are reported in BERGSTROM 15 as $0.304^{+0.013}_{-0.012}$ for normal and $0.305^{+0.012}_{-0.013}$ for inverted mass ordering.

⁹ AHARMIM 13 obtained this result by a two-neutrino oscillation analysis using global solar neutrino data.

¹⁰ AHARMIM 13 global solar neutrino data include SNO's all-phases-combined analysis results on the total active ^8B neutrino flux and energy-dependent ν_e survival probability parameters, measurements of Cl (CLEVELAND 98), Ga (ABDURASHITOV 09 which contains combined analysis with GNO (ALTMANN 05 and Ph.D. thesis of F. Kaether)),

- and ${}^7\text{Be}$ (BELLINI 11A) rates, and ${}^8\text{B}$ solar-neutrino recoil electron measurements of SK-I (HOSAKA 06) zenith, SK-II (CRAVENS 08) and SK-III (ABE 11) day/night spectra, and Borexino (BELLINI 10A) spectra.
- 11 AHARMIM 13 obtained this result by a three-neutrino oscillation analysis with the value of Δm_{32}^2 fixed to $2.45 \times 10^{-3} \text{ eV}^2$, using global solar neutrino data.
 - 12 AHARMIM 13 obtained this result by a three-neutrino oscillation analysis with the value of Δm_{32}^2 fixed to $2.45 \times 10^{-3} \text{ eV}^2$, using global solar neutrino and KamLAND (GANDO 11) data. *CPT* invariance is assumed.
 - 13 GANDO 13 obtained this result by a three-neutrino oscillation analysis using KamLAND, global solar neutrino, short-baseline (SBL) reactor, and accelerator data, assuming *CPT* invariance. Supersedes GANDO 11.
 - 14 GANDO 13 obtained this result by a three-neutrino oscillation analysis using KamLAND and global solar neutrino data, assuming *CPT* invariance. Supersedes GANDO 11.
 - 15 GANDO 13 obtained this result by a three-neutrino oscillation analysis using KamLAND data. Supersedes GANDO 11.
 - 16 ABE 11 obtained this result by a two-neutrino oscillation analysis using solar neutrino data including Super-Kamiokande, SNO, Borexino (ARPESELLA 08A), Homestake, GALLEX/GNO, SAGE, and KamLAND data. *CPT* invariance is assumed.
 - 17 ABE 11 obtained this result by a two-neutrino oscillation analysis using solar neutrino data including Super-Kamiokande, SNO, Borexino (ARPESELLA 08A), Homestake, GALLEX/GNO, and SAGE data.
 - 18 ABE 11 obtained this result by a three-neutrino oscillation analysis with the value of Δm_{32}^2 fixed to $2.4 \times 10^{-3} \text{ eV}^2$, using solar neutrino data including Super-Kamiokande, SNO, Borexino (ARPESELLA 08A), Homestake, GALLEX/GNO, SAGE, and KamLAND data. The normal neutrino mass ordering and *CPT* invariance are assumed.
 - 19 ABE 11 obtained this result by a three-neutrino oscillation analysis with the value of Δm_{32}^2 fixed to $2.4 \times 10^{-3} \text{ eV}^2$, using solar neutrino data including Super-Kamiokande, SNO, Borexino (ARPESELLA 08A), Homestake, and GALLEX/GNO data. The normal neutrino mass ordering is assumed.
 - 20 BELLINI 11A obtained this result by a two-neutrino oscillation analysis using KamLAND, Homestake, SAGE, Gallex, GNO, Kamiokande, Super-Kamiokande, SNO, and Borexino (BELLINI 11A) data and the SSM flux prediction in SERENELLI 11 (Astrophysical Journal **743** 24 (2011)) with the exception that the ${}^8\text{B}$ flux was left free. *CPT* invariance is assumed.
 - 21 BELLINI 11A obtained this result by a two-neutrino oscillation analysis using Homestake, SAGE, Gallex, GNO, Kamiokande, Super-Kamiokande, SNO, and Borexino (BELLINI 11A) data and the SSM flux prediction in SERENELLI 11 (Astrophysical Journal **743** 24 (2011)) with the exception that the ${}^8\text{B}$ flux was left free.
 - 22 GANDO 11 obtain this result with three-neutrino fit using the KamLAND + solar data. Superseded by GANDO 13.
 - 23 GANDO 11 obtain this result with three-neutrino fit using the KamLAND data only. Superseded by GANDO 13.
 - 24 AHARMIM 10 global solar neutrino data include SNO's low-energy-threshold analysis survival probability day/night curves, SNO Phase III integral rates (AHARMIM 08), CI (CLEVELAND 98), SAGE (ABDURASHITOV 09), Gallex/GNO (HAMPEL 99, ALTMANN 05), Borexino (ARPESELLA 08A), SK-I zenith (HOSAKA 06), and SK-II day/night spectra (CRAVENS 08).
 - 25 AHARMIM 10 obtained this result by a two-neutrino oscillation analysis using global solar neutrino data and KamLAND data (ABE 08A). *CPT* invariance is assumed.
 - 26 AHARMIM 10 obtained this result by a two-neutrino oscillation analysis using global solar neutrino data.
 - 27 AHARMIM 10 obtained this result by a three-neutrino oscillation analysis with the value of Δm_{31}^2 fixed to $2.3 \times 10^{-3} \text{ eV}^2$, using global solar neutrino data and KamLAND data (ABE 08A). *CPT* invariance is assumed.

- ²⁸ AHARMIM 10 obtained this result by a three-neutrino oscillation analysis with the value of Δm_{31}^2 fixed to $2.3 \times 10^{-3} \text{ eV}^2$, using global solar neutrino data.
- ²⁹ ABE 08A obtained this result by a rate + shape + time combined geoneutrino and reactor two-neutrino fit for Δm_{21}^2 and $\tan^2 \theta_{12}$, using KamLAND data only. Superseded by GANDO 11.
- ³⁰ ABE 08A obtained this result by means of a two-neutrino fit using KamLAND, Homestake, SAGE, GALLEX, GNO, SK (zenith angle and E-spectrum), the SNO χ^2 -map, and solar flux data. *CPT* invariance is assumed. Superseded by GANDO 11.
- ³¹ The result given by AHARMIM 08 is $\theta = (34.4^{+1.3}_{-1.2})^\circ$. This result is obtained by a two-neutrino oscillation analysis using solar neutrino data including those of Borexino (ARPESELLA 08A) and Super-Kamiokande-I (HOSAKA 06), and KamLAND data (ABE 08A). *CPT* invariance is assumed.
- ³² HOSAKA 06 obtained this result by a two-neutrino oscillation analysis using SK ν_e data, CC data from other solar neutrino experiments, and KamLAND data (ARAKI 05). *CPT* invariance is assumed.
- ³³ HOSAKA 06 obtained this result by a two-neutrino oscillation analysis using the data from Super-Kamiokande, SNO (AHMAD 02 and AHMAD 02B), and KamLAND (ARAKI 05) experiments. *CPT* invariance is assumed.
- ³⁴ HOSAKA 06 obtained this result by a two-neutrino oscillation analysis using the Super-Kamiokande and SNO (AHMAD 02 and AHMAD 02B) solar neutrino data.
- ³⁵ The result given by AHARMIM 05A is $\theta = (33.9 \pm 1.6)^\circ$. This result is obtained by a two-neutrino oscillation analysis using SNO pure deuteron and salt phase data, SK ν_e data, Cl and Ga CC data, and KamLAND data (ARAKI 05). *CPT* invariance is assumed. AHARMIM 05A also quotes $\theta = (33.9^{+2.4}_{-2.2})^\circ$ as the error enveloping the 68% CL two-dimensional region. This translates into $\sin^2 2\theta = 0.86^{+0.05}_{-0.06}$.
- ³⁶ AHARMIM 05A obtained this result by a two-neutrino oscillation analysis using the data from all solar neutrino experiments. The listed range of the parameter envelops the 95% CL two-dimensional region shown in figure 35a of AHARMIM 05A. AHARMIM 05A also quotes $\tan^2 \theta = 0.45^{+0.09}_{-0.08}$ as the error enveloping the 68% CL two-dimensional region. This translates into $\sin^2 2\theta = 0.86^{+0.05}_{-0.07}$.
- ³⁷ ARAKI 05 obtained this result by a two-neutrino oscillation analysis using KamLAND and solar neutrino data. *CPT* invariance is assumed. The 1σ error shown here is translated from the number provided by the KamLAND collaboration, $\tan^2 \theta = 0.40^{+0.07}_{-0.05}$. The corresponding number quoted in ARAKI 05 is $\tan^2 \theta = 0.40^{+0.10}_{-0.07}$ ($\sin^2 2\theta = 0.82 \pm 0.07$), which envelops the 68% CL two-dimensional region.
- ³⁸ The result given by AHMED 04A is $\theta = (32.5^{+1.7}_{-1.6})^\circ$. This result is obtained by a two-neutrino oscillation analysis using solar neutrino and KamLAND data (EGUCHI 03). *CPT* invariance is assumed. AHMED 04A also quotes $\theta = (32.5^{+2.4}_{-2.3})^\circ$ as the error enveloping the 68% CL two-dimensional region. This translates into $\sin^2 2\theta = 0.82 \pm 0.06$.
- ³⁹ AHMED 04A obtained this result by a two-neutrino oscillation analysis using the data from all solar neutrino experiments. The listed range of the parameter envelops the 95% CL two-dimensional region shown in Fig. 5(a) of AHMED 04A. The best-fit point is $\Delta(m^2) = 6.5 \times 10^{-5} \text{ eV}^2$, $\tan^2 \theta = 0.40$ ($\sin^2 2\theta = 0.82$).
- ⁴⁰ The result given by SMY 04 is $\tan^2 \theta = 0.44 \pm 0.08$. This result is obtained by a two-neutrino oscillation analysis using solar neutrino and KamLAND data (IANNI 03). *CPT* invariance is assumed.
- ⁴¹ SMY 04 obtained this result by a two-neutrino oscillation analysis using the data from all solar neutrino experiments. The 1σ errors are read from Fig. 6(a) of SMY 04.
- ⁴² SMY 04 obtained this result by a two-neutrino oscillation analysis using the Super-Kamiokande and SNO (AHMAD 02 and AHMAD 02B) solar neutrino data. The 1σ errors are read from Fig. 6(a) of SMY 04.

⁴³ AHMAD 02B obtained this result by a two-neutrino oscillation analysis using the data from all solar neutrino experiments. The listed range of the parameter envelops the 95% CL two-dimensional region shown in Fig. 4(b) of AHMAD 02B. The best fit point is $\Delta(m^2) = 5.0 \times 10^{-5} \text{ eV}^2$ and $\tan\theta = 0.34$ ($\sin^2 2\theta = 0.76$).

⁴⁴ FUKUDA 02 obtained this result by a two-neutrino oscillation analysis using the data from all solar neutrino experiments. The listed range of the parameter envelops the 95% CL two-dimensional region shown in Fig. 4 of FUKUDA 02. The best fit point is $\Delta(m^2) = 6.9 \times 10^{-5} \text{ eV}^2$ and $\tan^2\theta = 0.38$ ($\sin^2 2\theta = 0.80$).

Δm_{21}^2

VALUE (10^{-5} eV^2)	DOCUMENT ID	TECN	COMMENT
7.53±0.18	¹ GANDO	13	FIT KamLAND + global solar + SBL + accelerator: 3ν
● ● ● We do not use the following data for averages, fits, limits, etc. ● ● ●			
7.50 ^{+0.22} _{-0.20}	² SALAS	21	FIT global fit
7.42 ^{+0.21} _{-0.20}	³ ESTEBAN	20A	FIT Global fit
7.55 ^{+0.20} _{-0.16}	DE-SALAS	18	FIT Global fit
7.49 ^{+0.19} _{-0.18}	⁴ ABE	16C	FIT KamLAND+global solar; 3ν
4.8 ^{+1.3} _{-0.6}	⁵ ABE	16C	FIT SKAM+SNO; 3ν
4.8 ^{+1.5} _{-0.8}	⁶ ABE	16C	FIT SK-I+II+III+IV; 3ν
3.2 ^{+2.8} _{-0.2}	⁷ ABE	16C	FIT SK-IV; 3ν
7.6 ^{+0.19} _{-0.18}	⁸ FORERO	14	FIT 3ν
7.50 ^{+0.19} _{-0.17}	⁹ GONZALEZ...	14	FIT Either mass ordering; global fit
5.13 ^{+1.29} _{-0.96}	^{10,11} AHARMIM	13	FIT global solar: 2ν
5.13 ^{+1.49} _{-0.98}	^{11,12} AHARMIM	13	FIT global solar: 3ν
7.46 ^{+0.20} _{-0.19}	^{11,13} AHARMIM	13	FIT KamLAND + global solar: 3ν
7.53 ^{+0.19} _{-0.18}	¹⁴ GANDO	13	FIT KamLAND + global solar: 3ν
7.54 ^{+0.19} _{-0.18}	¹⁵ GANDO	13	FIT KamLAND: 3ν
7.6 ± 0.2	¹⁶ ABE	11	FIT KamLAND + global solar: 2ν
6.2 ^{+1.1} _{-1.9}	¹⁷ ABE	11	FIT global solar: 2ν
7.7 ± 0.3	¹⁸ ABE	11	FIT KamLAND + global solar: 3ν
6.0 ^{+2.2} _{-2.5}	¹⁹ ABE	11	FIT global solar: 3ν
7.50 ^{+0.16} _{-0.24}	²⁰ BELLINI	11A	FIT KamLAND + global solar: 2ν
5.2 ^{+1.5} _{-0.9}	²¹ BELLINI	11A	FIT global solar: 2ν
7.50 ^{+0.19} _{-0.20}	²² GANDO	11	FIT KamLAND + solar: 3ν
7.49±0.20	²³ GANDO	11	FIT KamLAND: 3ν
7.59 ^{+0.20} _{-0.21}	^{24,25} AHARMIM	10	FIT KamLAND + global solar: 2ν

$5.89^{+2.13}_{-2.16}$	24,26	AHARMIM	10	FIT	global solar: 2ν
7.59 ± 0.21	24,27	AHARMIM	10	FIT	KamLAND + global solar: 3ν
$6.31^{+2.49}_{-2.58}$	24,28	AHARMIM	10	FIT	global solar: 3ν
$7.58^{+0.14}_{-0.13} \pm 0.15$	29	ABE	08A	FIT	KamLAND
7.59 ± 0.21	30	ABE	08A	FIT	KamLAND + global solar
$7.59^{+0.19}_{-0.21}$	31	AHARMIM	08	FIT	KamLAND + global solar
8.0 ± 0.3	32	HOSAKA	06	FIT	KamLAND + global solar
8.0 ± 0.3	33	HOSAKA	06	FIT	SKAM+SNO+KamLAND
$6.3^{+3.7}_{-1.5}$	34	HOSAKA	06	FIT	SKAM+SNO
5–12	35	HOSAKA	06	FIT	SKAM day/night in the LMA region
$8.0^{+0.4}_{-0.3}$	36	AHARMIM	05A	FIT	KamLAND + global solar LMA
3.3–14.4	37	AHARMIM	05A	FIT	global solar
$7.9^{+0.4}_{-0.3}$	38	ARAKI	05	FIT	KamLAND + global solar
$7.1^{+1.0}_{-0.3}$	39	AHMED	04A	FIT	KamLAND + global solar
3.2–13.7	40	AHMED	04A	FIT	global solar
$7.1^{+0.6}_{-0.5}$	41	SMY	04	FIT	KamLAND + global solar
$6.0^{+1.7}_{-1.6}$	42	SMY	04	FIT	global solar
$6.0^{+2.5}_{-1.6}$	43	SMY	04	FIT	SKAM + SNO
2.8–12.0	44	AHMAD	02B	FIT	global solar
3.2–19.1	45	FUKUDA	02	FIT	global solar

¹ GANDO 13 obtained this result by a three-neutrino oscillation analysis using KamLAND, global solar neutrino, short-baseline (SBL) reactor, and accelerator data, assuming CPT invariance. Supersedes GANDO 11.

² SALAS 21 reports results of a global fit to neutrino oscillation data available at the time of the Neutrino 2020 conference.

³ ESTEBAN 20A reports results of a global fit to neutrino oscillation data available at the time of the Neutrino2020 conference.

⁴ ABE 16C obtained this result by a three-neutrino oscillation analysis, with a constraint of $\sin^2(\theta_{13}) = 0.0219 \pm 0.0014$ coming from reactor neutrino experiments, using all solar data and KamLAND data. CPT invariance is assumed.

⁵ ABE 16C obtained this result by a three-neutrino oscillation analysis, with a constraint of $\sin^2(\theta_{13}) = 0.0219 \pm 0.0014$ coming from reactor neutrino experiments, using Super-Kamiokande (I+II+III+IV) and SNO data.

⁶ ABE 16C obtained this result by a three-neutrino oscillation analysis, with a constraint of $\sin^2(\theta_{13}) = 0.0219 \pm 0.0014$ coming from reactor neutrino experiments, by combining the four phases of the Super-Kamiokande solar data.

⁷ ABE 16C obtained this result by a three-neutrino oscillation analysis, with a constraint of $\sin^2(\theta_{13}) = 0.0219 \pm 0.0014$ coming from reactor neutrino experiments, using the Super-Kamiokande-IV data.

⁸ FORERO 14 performs a global fit to Δm_{21}^2 using solar, reactor, long-baseline accelerator, and atmospheric neutrino data.

⁹ GONZALEZ-GARCIA 14 result comes from a frequentist global fit. The corresponding Bayesian global fit to the same data results are reported in BERGSTROM 15 as

- $(7.50^{+0.19}_{-0.17}) \times 10^{-5} \text{ eV}^2$ for normal and $(7.50^{+0.18}_{-0.17}) \times 10^{-5} \text{ eV}^2$ for inverted mass ordering.
- 10 AHARMIM 13 obtained this result by a two-neutrino oscillation analysis using global solar neutrino data.
 - 11 AHARMIM 13 global solar neutrino data include SNO's all-phases-combined analysis results on the total active ^8B neutrino flux and energy-dependent ν_e survival probability parameters, measurements of Cl (CLEVELAND 98), Ga (ABDURASHITOV 09 which contains combined analysis with GNO (ALTMANN 05 and Ph.D. thesis of F. Kaether)), and ^7Be (BELLINI 11A) rates, and ^8B solar-neutrino recoil electron measurements of SK-I (HOSAKA 06) zenith, SK-II (CRAVENS 08), and SK-III (ABE 11) day/night spectra, and Borexino (BELLINI 10A) spectra.
 - 12 AHARMIM 13 obtained this result by a three-neutrino oscillation analysis with the value of Δm_{31}^2 fixed to $2.45 \times 10^{-3} \text{ eV}^2$, using global solar neutrino data.
 - 13 AHARMIM 13 obtained this result by a three-neutrino oscillation analysis with the value of Δm_{31}^2 fixed to $2.45 \times 10^{-3} \text{ eV}^2$, using global solar neutrino and KamLAND data (GANDO 11). CPT invariance is assumed.
 - 14 GANDO 13 obtained this result by a three-neutrino oscillation analysis using KamLAND and global solar neutrino data, assuming CPT invariance. Supersedes GANDO 11.
 - 15 GANDO 13 obtained this result by a three-neutrino oscillation analysis using KamLAND data. Supersedes GANDO 11.
 - 16 ABE 11 obtained this result by a two-neutrino oscillation analysis using solar neutrino data including Super-Kamiokande, SNO, Borexino (ARPESELLA 08A), Homestake, GALLEX/GNO, SAGE, and KamLAND data. CPT invariance is assumed.
 - 17 ABE 11 obtained this result by a two-neutrino oscillation analysis using solar neutrino data including Super-Kamiokande, SNO, Borexino (ARPESELLA 08A), Homestake, GALLEX/GNO, and SAGE data.
 - 18 ABE 11 obtained this result by a three-neutrino oscillation analysis with the value of Δm_{32}^2 fixed to $2.4 \times 10^{-3} \text{ eV}^2$, using solar neutrino data including Super-Kamiokande, SNO, Borexino (ARPESELLA 08A), Homestake, GALLEX/GNO, SAGE, and KamLAND data. The normal neutrino mass ordering and CPT invariance are assumed.
 - 19 ABE 11 obtained this result by a three-neutrino oscillation analysis with the value of Δm_{32}^2 fixed to $2.4 \times 10^{-3} \text{ eV}^2$, using solar neutrino data including Super-Kamiokande, SNO, Borexino (ARPESELLA 08A), Homestake, and GALLEX/GNO data. The normal neutrino mass ordering is assumed.
 - 20 BELLINI 11A obtained this result by a two-neutrino oscillation analysis using KamLAND, Homestake, SAGE, Gallex, GNO, Kamiokande, Super-Kamiokande, SNO, and Borexino (BELLINI 11A) data and the SSM flux prediction in SERENELLI 11 (Astrophysical Journal **743** 24 (2011)) with the exception that the ^8B flux was left free. CPT invariance is assumed.
 - 21 BELLINI 11A obtained this result by a two-neutrino oscillation analysis using Homestake, SAGE, Gallex, GNO, Kamiokande, Super-Kamiokande, SNO, and Borexino (BELLINI 11A) data and the SSM flux prediction in SERENELLI 11 (Astrophysical Journal **743** 24 (2011)) with the exception that the ^8B flux was left free.
 - 22 GANDO 11 obtain this result with three-neutrino fit using the KamLAND + solar data. Superseded by GANDO 13.
 - 23 GANDO 11 obtain this result with three-neutrino fit using the KamLAND data only. Supersedes ABE 08A.
 - 24 AHARMIM 10 global solar neutrino data include SNO's low-energy-threshold analysis survival probability day/night curves, SNO Phase III integral rates (AHARMIM 08), Cl (CLEVELAND 98), SAGE (ABDURASHITOV 09), Gallex/GNO (HAMPEL 99, ALTMANN 05), Borexino (ARPESELLA 08A), SK-I zenith (HOSAKA 06), and SK-II day/night spectra (CRAVENS 08).
 - 25 AHARMIM 10 obtained this result by a two-neutrino oscillation analysis using global solar neutrino data and KamLAND data (ABE 08A). CPT invariance is assumed.

- ²⁶ AHARMIM 10 obtained this result by a two-neutrino oscillation analysis using global solar neutrino data.
- ²⁷ AHARMIM 10 obtained this result by a three-neutrino oscillation analysis with the value of Δm_{31}^2 fixed to $2.3 \times 10^{-3} \text{ eV}^2$, using global solar neutrino data and KamLAND data (ABE 08A). *CPT* invariance is assumed.
- ²⁸ AHARMIM 10 obtained this result by a three-neutrino oscillation analysis with the value of Δm_{31}^2 fixed to $2.3 \times 10^{-3} \text{ eV}^2$, using global solar neutrino data.
- ²⁹ ABE 08A obtained this result by a rate + shape + time combined geoneutrino and reactor two-neutrino fit for Δm_{21}^2 and $\tan^2 \theta_{12}$, using KamLAND data only. Superseded by GANDO 11.
- ³⁰ ABE 08A obtained this result by means of a two-neutrino fit using KamLAND, Homestake, SAGE, GALLEX, GNO, SK (zenith angle and E-spectrum), the SNO χ^2 -map, and solar flux data. *CPT* invariance is assumed. Superseded by GANDO 11.
- ³¹ AHARMIM 08 obtained this result by a two-neutrino oscillation analysis using all solar neutrino data including those of Borexino (ARPESELLA 08A) and Super-Kamiokande-I (HOSAKA 06), and KamLAND data (ABE 08A). *CPT* invariance is assumed.
- ³² HOSAKA 06 obtained this result by a two-neutrino oscillation analysis using solar neutrino and KamLAND data (ARAKI 05). *CPT* invariance is assumed.
- ³³ HOSAKA 06 obtained this result by a two-neutrino oscillation analysis using the data from Super-Kamiokande, SNO (AHMAD 02 and AHMAD 02B), and KamLAND (ARAKI 05) experiments. *CPT* invariance is assumed.
- ³⁴ HOSAKA 06 obtained this result by a two-neutrino oscillation analysis using the Super-Kamiokande and SNO (AHMAD 02 and AHMAD 02B) solar neutrino data.
- ³⁵ HOSAKA 06 obtained this result from the consistency between the observed and expected day-night flux asymmetry amplitude. The listed 68% CL range is derived from the 1σ boundary of the amplitude fit to the data. Oscillation parameters are constrained to be in the LMA region. The mixing angle is fixed at $\tan^2 \theta = 0.44$ because the fit depends only very weakly on it.
- ³⁶ AHARMIM 05A obtained this result by a two-neutrino oscillation analysis using solar neutrino and KamLAND data (ARAKI 05). *CPT* invariance is assumed. AHARMIM 05A also quotes $\Delta(m^2) = (8.0^{+0.6}_{-0.4}) \times 10^{-5} \text{ eV}^2$ as the error enveloping the 68% CL two-dimensional region.
- ³⁷ AHARMIM 05A obtained this result by a two-neutrino oscillation analysis using the data from all solar neutrino experiments. The listed range of the parameter envelops the 95% CL two-dimensional region shown in figure 35a of AHARMIM 05A. AHARMIM 05A also quotes $\Delta(m^2) = (6.5^{+4.4}_{-2.3}) \times 10^{-5} \text{ eV}^2$ as the error enveloping the 68% CL two-dimensional region.
- ³⁸ ARAKI 05 obtained this result by a two-neutrino oscillation analysis using KamLAND and solar neutrino data. *CPT* invariance is assumed. The 1σ error shown here is provided by the KamLAND collaboration. The error quoted in ARAKI 05, $\Delta(m^2) = (7.9^{+0.6}_{-0.5}) \times 10^{-5}$, envelops the 68% CL two-dimensional region.
- ³⁹ AHMED 04A obtained this result by a two-neutrino oscillation analysis using solar neutrino and KamLAND data (EGUCHI 03). *CPT* invariance is assumed. AHMED 04A also quotes $\Delta(m^2) = (7.1^{+1.2}_{-0.6}) \times 10^{-5} \text{ eV}^2$ as the error enveloping the 68% CL two-dimensional region.
- ⁴⁰ AHMED 04A obtained this result by a two-neutrino oscillation analysis using the data from all solar neutrino experiments. The listed range of the parameter envelops the 95% CL two-dimensional region shown in Fig. 5(a) of AHMED 04A. The best-fit point is $\Delta(m^2) = 6.5 \times 10^{-5} \text{ eV}^2$, $\tan^2 \theta = 0.40$ ($\sin^2 2\theta = 0.82$).
- ⁴¹ SMY 04 obtained this result by a two-neutrino oscillation analysis using solar neutrino and KamLAND data (IANNI 03). *CPT* invariance is assumed.
- ⁴² SMY 04 obtained this result by a two-neutrino oscillation analysis using the data from all solar neutrino experiments. The 1σ errors are read from Fig. 6(a) of SMY 04.

- ⁴³SMY 04 obtained this result by a two-neutrino oscillation analysis using the Super-Kamiokande and SNO (AHMAD 02 and AHMAD 02B) solar neutrino data. The 1σ errors are read from Fig. 6(a) of SMY 04.
- ⁴⁴AHMAD 02B obtained this result by a two-neutrino oscillation analysis using the data from all solar neutrino experiments. The listed range of the parameter envelops the 95% CL two-dimensional region shown in Fig. 4(b) of AHMAD 02B. The best fit point is $\Delta(m^2) = 5.0 \times 10^{-5} \text{ eV}^2$ and $\tan\theta = 0.34$ ($\sin^2 2\theta = 0.76$).
- ⁴⁵FUKUDA 02 obtained this result by a two-neutrino oscillation analysis using the data from all solar neutrino experiments. The listed range of the parameter envelops the 95% CL two-dimensional region shown in Fig. 4 of FUKUDA 02. The best fit point is $\Delta(m^2) = 6.9 \times 10^{-5} \text{ eV}^2$ and $\tan^2\theta = 0.38$ ($\sin^2 2\theta = 0.80$).

$\sin^2(\theta_{23})$

The reported limits below correspond to the projection onto the $\sin^2(\theta_{23})$ axis of the 90% CL contours in the $\sin^2(\theta_{23}) - \Delta m_{32}^2$ plane presented by the authors. Unless otherwise specified, the limits are 90% CL and the reported uncertainties are 68% CL.

If an experiment reports $\sin^2(2\theta_{23})$ we convert the value to $\sin^2(\theta_{23})$.

VALUE	DOCUMENT ID	TECN	COMMENT
$0.534^{+0.021}_{-0.024}$	OUR FIT		Assuming inverted mass ordering
$0.547^{+0.018}_{-0.024}$	OUR FIT		Assuming normal mass ordering
0.57 $^{+0.03}_{-0.04}$	1 ACERO	22 NOVA	Normal mass ordering; octant II for θ_{23}
0.56 ± 0.04	1 ACERO	22 NOVA	Inverted mass ordering; octant II for θ_{23}
0.53 $^{+0.03}_{-0.04}$	2 ABE	20F T2K	Both mass orderings
0.43 $^{+0.20}_{-0.04}$	3 ADAMSON	20A MINS	Normal mass ordering
0.42 $^{+0.07}_{-0.03}$	3 ADAMSON	20A MINS	Inverted mass ordering
0.51 $^{+0.07}_{-0.09}$	4 AARTSEN	18A ICCB	Normal mass ordering
0.588 $^{+0.031}_{-0.064}$	5 ABE	18B SKAM	Normal mass ordering, θ_{13} constrained
0.575 $^{+0.036}_{-0.073}$	5 ABE	18B SKAM	Inverted mass ordering, θ_{13} constrained
● ● ● We do not use the following data for averages, fits, limits, etc. ● ● ●			
0.51 $^{+0.06}_{-0.07}$	6 ABE	21A T2K	ν_μ disappearance
0.43 $^{+0.21}_{-0.05}$	6 ABE	21A T2K	$\bar{\nu}_\mu$ disappearance
0.574 ± 0.014	7 SALAS	21 FIT	Normal mass ordering, global fit
0.578 $^{+0.010}_{-0.017}$	7 SALAS	21 FIT	Inverted mass ordering, global fit
0.455	8 AARTSEN	20 ICCB	For both mass orderings
0.573 $^{+0.016}_{-0.020}$	9 ESTEBAN	20A FIT	Normal mass ordering, global fit
0.575 $^{+0.016}_{-0.019}$	9 ESTEBAN	20A FIT	Inverted mass ordering, global fit
0.58 $^{+0.04}_{-0.13}$	10 AARTSEN	19C ICCB	
0.56 $^{+0.04}_{-0.03}$	11 ACERO	19 NOVA	Normal mass order; octant II for θ_{23}

0.48	$+0.04$ -0.03	11,12 ACERO	19	NOVA	Normal mass order; octant I for θ_{23}
0.56	$+0.04$ -0.03	11,12 ACERO	19	NOVA	Inverted mass order; octant II for θ_{23}
0.47	$+0.04$ -0.03	11,12 ACERO	19	NOVA	Inverted mass order; octant I for θ_{23}
0.49	$+0.30$ -0.28	AGAFONOVA	19	OPER	
0.50	$+0.20$ -0.19	13 ALBERT	19	ANTR	Atmospheric ν , deep sea telescope
0.587	$+0.036$ -0.069	14 ABE	18B	SKAM	3ν osc: normal mass ordering, θ_{13} free
0.551	$+0.044$ -0.075	14 ABE	18B	SKAM	3ν osc: inverted mass ordering, θ_{13} free
0.526	$+0.032$ -0.036	15 ABE	18G	T2K	Normal mass ordering, θ_{13} constrained
0.530	$+0.030$ -0.034	15 ABE	18G	T2K	Inverted mass ordering, θ_{13} constrained
0.56	± 0.04	16 ACERO	18	NOVA	Normal mass order; octant II for θ_{23}
0.47	± 0.04	16 ACERO	18	NOVA	Normal mass order; octant I for θ_{23}
0.547	$+0.020$ -0.030	DE-SALAS	18	FIT	Normal mass ordering, global fit
0.551	$+0.018$ -0.030	DE-SALAS	18	FIT	Inverted mass order, global fit
0.532	$+0.061$ -0.087	17 ABE	17A	T2K	Normal mass ordering
0.534	$+0.061$ -0.087	17 ABE	17A	T2K	Inverted mass ordering
0.51	$+0.08$ -0.07	ABE	17C	T2K	Normal mass ordering with neutrinos
0.42	$+0.25$ -0.07	ABE	17C	T2K	Normal mass ordering with antineutrinos
0.52	$+0.075$ -0.09	ABE	17C	T2K	normal mass ordering with neutrinos and antineutrinos
0.55	$+0.05$ -0.09	17 ABE	17F	T2K	Normal mass ordering
0.55	$+0.05$ -0.08	17 ABE	17F	T2K	Inverted mass ordering
0.404	$+0.022$ -0.030	18 ADAMSON	17A	NOVA	Normal mass ordering; octant I for θ_{23}
0.624	$+0.022$ -0.030	18 ADAMSON	17A	NOVA	Normal mass ordering; octant II for θ_{23}
0.398	$+0.030$ -0.022	18 ADAMSON	17A	NOVA	Inverted mass ordering; octant I for θ_{23}
0.618	$+0.022$ -0.030	18 ADAMSON	17A	NOVA	Inverted mass ordering; octant II for θ_{23}
0.45	$+0.19$ -0.07	19 ABE	16D	T2K	3ν osc; normal mass ordering; $\bar{\nu}$ beam
0.38	to 0.65	20 ADAMSON	16A	NOVA	normal mass ordering
0.37	to 0.64	20 ADAMSON	16A	NOVA	Inverted mass ordering
0.53	$+0.09$ -0.12	21 AARTSEN	15A	ICCB	Normal mass ordering
0.51	$+0.09$ -0.11	21 AARTSEN	15A	ICCB	Inverted mass ordering
0.514	$+0.055$ -0.056	22 ABE	14	T2K	3ν osc.; normal mass ordering
0.511	± 0.055	22 ABE	14	T2K	3ν osc.; inverted mass ordering
0.41	$+0.23$ -0.06	23 ADAMSON	14	MINS	Normal mass ordering

0.41 ^{+0.26} _{-0.07}	23	ADAMSON	14	MINS	Inverted mass ordering
0.567 ^{+0.032} _{-0.128}	24	FORERO	14	FIT	Normal mass ordering
0.573 ^{+0.025} _{-0.043}	24	FORERO	14	FIT	Inverted mass ordering
0.452 ^{+0.052} _{-0.028}	25	GONZALEZ...	14	FIT	Normal mass ordering; global fit
0.579 ^{+0.025} _{-0.037}	25	GONZALEZ...	14	FIT	Inverted mass ordering; global fit
0.24 to 0.76	26	AARTSEN	13B	ICCB	DeepCore, 2ν oscillation
0.514±0.082	27	ABE	13G	T2K	3ν osc.; normal mass ordering
0.388 ^{+0.051} _{-0.053}	28	ADAMSON	13B	MINS	Beam + Atmospheric; identical ν & ν̄
0.3 to 0.7	29	ABE	12A	T2K	Off-axis beam
0.28 to 0.72	30	ADAMSON	12	MINS	ν̄ beam
0.25 to 0.75	31,32	ADAMSON	12B	MINS	MINOS atmospheric
0.27 to 0.73	31,33	ADAMSON	12B	MINS	MINOS pure atmospheric ν
0.21 to 0.79	31,33	ADAMSON	12B	MINS	MINOS pure atmospheric ν̄
0.15 to 0.85	34	ADRIAN-MAR.	12	ANTR	Atmospheric ν with deep see telescope
0.39 to 0.61	35	ABE	11C	SKAM	Super-Kamiokande
0.34 to 0.66		ADAMSON	11	MINS	2ν osc.; maximal mixing
0.31 ^{+0.10} _{-0.07}	36	ADAMSON	11B	MINS	ν̄ beam
0.41 to 0.59	37	WENDELL	10	SKAM	3ν osc. with solar terms; θ ₁₃ =0
0.39 to 0.61	38	WENDELL	10	SKAM	3ν osc.; normal mass ordering
0.37 to 0.63	39	WENDELL	10	SKAM	3ν osc.; inverted mass ordering
0.31 to 0.69		ADAMSON	08A	MINS	MINOS
0.05 to 0.95	40	ADAMSON	06	MINS	Atmospheric ν with far detector
0.18 to 0.82	41	AHN	06A	K2K	KEK to Super-K
0.23 to 0.77	42	MICHAEL	06	MINS	MINOS
0.18 to 0.82	43	ALIU	05	K2K	KEK to Super-K
0.18 to 0.82	44	ALLISON	05	SOU2	
0.36 to 0.64	45	ASHIE	05	SKAM	Super-Kamiokande
0.28 to 0.72	46	AMBROSIO	04	MCRO	MACRO
0.34 to 0.66	47	ASHIE	04	SKAM	L/E distribution
0.08 to 0.92	48	AHN	03	K2K	KEK to Super-K
0.13 to 0.87	49	AMBROSIO	03	MCRO	MACRO
0.26 to 0.74	50	AMBROSIO	03	MCRO	MACRO
0.15 to 0.85	51	SANCHEZ	03	SOU2	Soudan-2 Atmospheric
0.28 to 0.72	52	AMBROSIO	01	MCRO	Upward μ
0.29 to 0.71	53	AMBROSIO	01	MCRO	Upward μ
0.13 to 0.87	54	FUKUDA	99C	SKAM	Upward μ
0.23 to 0.77	55	FUKUDA	99D	SKAM	Upward μ
0.08 to 0.92	56	FUKUDA	99D	SKAM	Stop μ / through
0.29 to 0.71	57	FUKUDA	98C	SKAM	Super-Kamiokande
0.08 to 0.92	58	HATAKEYAMA	98	KAMI	Kamiokande
0.24 to 0.76	59	HATAKEYAMA	98	KAMI	Kamiokande
0.20 to 0.80	60	FUKUDA	94	KAMI	Kamiokande

¹ ACERO 22 uses data from Jun 29, 2016 to Feb 26, 2019 (12.5×10^{20} POT) and Feb 6, 2014 to Mar 20, 2020 (13.6×10^{20} POT). Best fit for octant I (lower octant) is 0.46 for both normal and inverted mass orderings. Supersedes ACERO 19.

- ² ABE 20F results are based on data collected between 2009 and 2018 in (anti)neutrino mode and include a neutrino beam exposure of 1.49×10^{21} (1.64×10^{21}) protons on target. Supersedes ABE 18G.
- ³ ADAMSON 20A uses the complete dataset from MINOS and MINOS+ experiments. The data were collected using a total exposure of 23.76×10^{20} protons on target and 60.75 kton·yr exposure to atmospheric neutrinos. Supersedes ADAMSON 14.
- ⁴ AARTSEN 18A uses three years (April 2012 – May 2015) of neutrino data from full sky with reconstructed energies between 5.6 and 56 GeV, measured with the low-energy subdetector DeepCore of the IceCube neutrino telescope. AARTSEN 18A also reports the best fit result for the inverted mass ordering as $\Delta m_{32}^2 = -2.32 \times 10^{-3} \text{ eV}^2$ and $\sin^2(\theta_{23}) = 0.51$. Uncertainties for the inverted mass ordering fits were not provided. Supersedes AARTSEN 15A.
- ⁵ ABE 18B uses 328 kton·years of Super-Kamiokande I-IV atmospheric neutrino data to obtain this result. The fit is performed over the three parameters, Δm_{32}^2 , $\sin^2(\theta_{23})$, and δ , while the solar parameters and $\sin^2(\theta_{13})$ are fixed to $\Delta m_{21}^2 = (7.53 \pm 0.18) \times 10^{-5} \text{ eV}^2$, $\sin^2(\theta_{12}) = 0.304 \pm 0.014$, and $\sin^2(\theta_{13}) = 0.0219 \pm 0.0012$.
- ⁶ ABE 21A results are based on 1.49×10^{21} POT in neutrino mode and 1.64×10^{21} POT in antineutrino mode.
- ⁷ SALAS 21 reports results of a global fit to neutrino oscillation data available at the time of the Neutrino 2020 conference.
- ⁸ AARTSEN 20 uses the data taken between May 2012 and April 2014 with the low-energy subdetector DeepCore of the IceCube neutrino telescope. The reconstructed energy range is between 4 (5) and 90 (80) GeV for the main (confirmatory) analysis. Though the observed best-fit is in the lower octant for both mass orderings, a substantial range of $\sin^2(\theta_{23}) > 0.5$ is still compatible with the observed data for both mass orderings.
- ⁹ ESTEBAN 20A reports results of a global fit to neutrino oscillation data available at the time of the Neutrino2020 conference.
- ¹⁰ AARTSEN 19C uses three years (April 2012 – May 2015) of neutrino data from full sky with reconstructed energies between 5.6 and 56 GeV, measured with the low-energy sub-detector DeepCore of the IceCube neutrino telescope. AARTSEN 19C adopts looser event selection criteria to prioritize the efficiency of selecting neutrino events, different from tighter event selection criteria which closely follow the criteria used by AARTSEN 18A to measure the ν_{μ} disappearance.
- ¹¹ ACERO 19 is based on a sample size of 12.33×10^{20} protons on target. The fit combines both antineutrino and neutrino data to extract the oscillation parameters. The results favor the normal mass ordering by 1.9σ and θ_{23} values in octant II by 1.6σ . Supersedes ACERO 18.
- ¹² Errors are from normal mass ordering and θ_{13} octant II fits.
- ¹³ ALBERT 19 measured the oscillation parameters of atmospheric neutrinos with the ANTARES deep sea neutrino telescope using the data taken from 2007 to 2016 (2830 days of total live time). Supersedes ADRIAN-MARTINEZ 12.
- ¹⁴ ABE 18B uses 328 kton·years of Super-Kamiokande I-IV atmospheric neutrino data to obtain this result. The fit is performed over the four parameters, Δm_{32}^2 , $\sin^2\theta_{23}$, $\sin^2\theta_{13}$, and δ , while the solar parameters are fixed to $\Delta m_{21}^2 = (7.53 \pm 0.18) \times 10^{-5} \text{ eV}^2$ and $\sin^2\theta_{12} = 0.304 \pm 0.014$.
- ¹⁵ ABE 18G data prefers normal mass ordering is with a posterior probability of 87%. Supersedes ABE 17F.
- ¹⁶ ACERO 18 performs a joint fit to the data for ν_{μ} disappearance and ν_e appearance. The overall best fit favors normal mass ordering and θ_{23} in octant II. No 1σ confidence intervals are presented for the inverted mass ordering scenarios. Superseded by ACERO 19.
- ¹⁷ Errors are from the projections of the 68% contour on 2D plot of Δm^2 versus $\sin^2(\theta_{23})$. ABE 17F supersedes ABE 17A. Superseded by ABE 18G.

- ¹⁸ Superseded by ACERO 18.
- ¹⁹ ABE 16D reports oscillation results using $\bar{\nu}_\mu$ disappearance in an off-axis beam.
- ²⁰ ADAMSON 16A obtains $\sin^2(\theta_{23})$ in the 68% C.L. range [0.38, 0.65] ([0.37, 0.64]), with two statistically degenerate best-fit values of 0.44 and 0.59 (0.44 and 0.59) for normal (inverted) mass ordering. Superseded by ADAMSON 17A.
- ²¹ AARTSEN 15A obtains this result by a three-neutrino oscillation analysis using 10–100 GeV muon neutrino sample from a total of 953 days of measurement with the low-energy subdetector DeepCore of the IceCube neutrino telescope. Superseded by AARTSEN 18A.
- ²² ABE 14 results are based on ν_μ disappearance using three-neutrino oscillation fit. The confidence intervals are derived from one dimensional profiled likelihoods. Superseded by ABE 17A.
- ²³ ADAMSON 14 uses a complete set of accelerator and atmospheric data. The analysis combines the ν_μ disappearance and ν_e appearance data using three-neutrino oscillation fit. The fit results are obtained for normal and inverted mass ordering assumptions. The best fit is for first θ_{23} octant and inverted mass ordering.
- ²⁴ FORERO 14 performs a global fit to neutrino oscillations using solar, reactor, long-baseline accelerator, and atmospheric neutrino data.
- ²⁵ GONZALEZ-GARCIA 14 result comes from a frequentist global fit. The corresponding Bayesian global fit to the same data results are reported in BERGSTROM 15 as 68% CL intervals of 0.433–0.496 or 0.530–0.594 for normal and 0.514–0.612 for inverted mass ordering.
- ²⁶ AARTSEN 13B obtained this result by a two-neutrino oscillation analysis using 20–100 GeV muon neutrino sample from a total of 318.9 days of live-time measurement with the low-energy subdetector DeepCore of the IceCube neutrino telescope.
- ²⁷ The best fit value is $\sin^2(\theta_{23}) = 0.514 \pm 0.082$. Superseded by ABE 14.
- ²⁸ ADAMSON 13B obtained this result from ν_μ and $\bar{\nu}_\mu$ disappearance using ν_μ (10.71×10^{20} POT) and $\bar{\nu}_\mu$ (3.36×10^{20} POT) beams, and atmospheric (37.88kton-years) data from MINOS. The fit assumed two-flavor neutrino hypothesis and identical ν_μ and $\bar{\nu}_\mu$ oscillation parameters. Superseded by ADAMSON 14.
- ²⁹ ABE 12A obtained this result by a two-neutrino oscillation analysis. The best-fit point is $\sin^2(2\theta_{23}) = 0.98$.
- ³⁰ ADAMSON 12 is a two-neutrino oscillation analysis using antineutrinos. The best fit value is $\sin^2(2\theta_{23}) = 0.95^{+0.10}_{-0.11} \pm 0.01$.
- ³¹ ADAMSON 12B obtained this result by a two-neutrino oscillation analysis of the L/E distribution using 37.9 kton-yr atmospheric neutrino data with the MINOS far detector.
- ³² The best fit point is $\Delta m^2 = 0.0019 \text{ eV}^2$ and $\sin^2 2\theta = 0.99$. The 90% single-parameter confidence interval at the best fit point is $\sin^2 2\theta > 0.86$.
- ³³ The data are separated into pure samples of ν_s and $\bar{\nu}_s$, and separate oscillation parameters for ν_s and $\bar{\nu}_s$ are fit to the data. The best fit point is $(\Delta m^2, \sin^2 2\theta) = (0.0022 \text{ eV}^2, 0.99)$ and $(\Delta \bar{m}^2, \sin^2 2\bar{\theta}) = (0.0016 \text{ eV}^2, 1.00)$. The quoted result is taken from the 90% C.L. contour in the $(\Delta m^2, \sin^2 2\theta)$ plane obtained by minimizing the four parameter log-likelihood function with respect to the other oscillation parameters.
- ³⁴ ADRIAN-MARTINEZ 12 measured the oscillation parameters of atmospheric neutrinos with the ANTARES deep sea neutrino telescope using the data taken from 2007 to 2010 (863 days of total live time). Superseded by ALBERT 19.
- ³⁵ ABE 11C obtained this result by a two-neutrino oscillation analysis using the Super-Kamiokande-I+II+III atmospheric neutrino data. ABE 11C also reported results under a two-neutrino disappearance model with separate mixing parameters between ν and $\bar{\nu}$, and obtained $\sin^2 2\theta > 0.93$ for ν and $\sin^2 2\theta > 0.83$ for $\bar{\nu}$ at 90% C.L.
- ³⁶ ADAMSON 11B obtained this result by a two-neutrino oscillation analysis of antineutrinos in an antineutrino enhanced beam with 1.71×10^{20} protons on target. This result is consistent with the neutrino measurements of ADAMSON 11 at 2% C.L.

- 37 WENDELL 10 obtained this result ($\sin^2\theta_{23} = 0.407\text{--}0.583$) by a three-neutrino oscillation analysis using the Super-Kamiokande-I+II+III atmospheric neutrino data, assuming $\theta_{13} = 0$ but including the solar oscillation parameters Δm_{21}^2 and $\sin^2\theta_{12}$ in the fit.
- 38 WENDELL 10 obtained this result ($\sin^2\theta_{23} = 0.43\text{--}0.61$) by a three-neutrino oscillation analysis with one mass scale dominance ($\Delta m_{21}^2 = 0$) using the Super-Kamiokande-I+II+III atmospheric neutrino data, and updates the HOSAKA 06A result.
- 39 WENDELL 10 obtained this result ($\sin^2\theta_{23} = 0.44\text{--}0.63$) by a three-neutrino oscillation analysis with one mass scale dominance ($\Delta m_{21}^2 = 0$) using the Super-Kamiokande-I+II+III atmospheric neutrino data, and updates the HOSAKA 06A result.
- 40 ADAMSON 06 obtained this result by a two-neutrino oscillation analysis of the L/E distribution using 4.54 kton yr atmospheric neutrino data with the MINOS far detector.
- 41 Supercedes ALIU 05.
- 42 MICHAEL 06 best fit is for maximal mixing. See also ADAMSON 08.
- 43 The best fit is for maximal mixing.
- 44 ALLISON 05 result is based upon atmospheric neutrino interactions including upward-stopping muons, with an exposure of 5.9 kton yr. From a two-flavor oscillation analysis the best-fit point is $\Delta m^2 = 0.0017 \text{ eV}^2$ and $\sin^2(2\theta) = 0.97$.
- 45 ASHIE 05 obtained this result by a two-neutrino oscillation analysis using 92 kton yr atmospheric neutrino data from the complete Super-Kamiokande I running period.
- 46 AMBROSIO 04 obtained this result, without using the absolute normalization of the neutrino flux, by combining the angular distribution of upward through-going muon tracks with $E_\mu > 1 \text{ GeV}$, N_{low} and N_{high} , and the numbers of InDown + UpStop and InUp events. Here, N_{low} and N_{high} are the number of events with reconstructed neutrino energies $< 30 \text{ GeV}$ and $> 130 \text{ GeV}$, respectively. InDown and InUp represent events with downward and upward-going tracks starting inside the detector due to neutrino interactions, while UpStop represents entering upward-going tracks which stop in the detector. The best fit is for maximal mixing.
- 47 ASHIE 04 obtained this result from the $L(\text{flight length})/E(\text{estimated neutrino energy})$ distribution of ν_μ disappearance probability, using the Super-Kamiokande-I 1489 live-day atmospheric neutrino data.
- 48 There are several islands of allowed region from this K2K analysis, extending to high values of Δm^2 . We only include the one that overlaps atmospheric neutrino analyses. The best fit is for maximal mixing.
- 49 AMBROSIO 03 obtained this result on the basis of the ratio $R = N_{low}/N_{high}$, where N_{low} and N_{high} are the number of upward through-going muon events with reconstructed neutrino energy $< 30 \text{ GeV}$ and $> 130 \text{ GeV}$, respectively. The data came from the full detector run started in 1994. The method of FELDMAN 98 is used to obtain the limits.
- 50 AMBROSIO 03 obtained this result by using the ratio R and the angular distribution of the upward through-going muons. R is given in the previous note and the angular distribution is reported in AMBROSIO 01. The method of FELDMAN 98 is used to obtain the limits. The best fit is to maximal mixing.
- 51 SANCHEZ 03 is based on an exposure of 5.9 kton yr. The result is obtained using a likelihood analysis of the neutrino L/E distribution for a selection μ flavor sample while the e -flavor sample provides flux normalization. The method of FELDMAN 98 is used to obtain the allowed region. The best fit is $\sin^2(2\theta) = 0.97$.
- 52 AMBROSIO 01 result is based on the angular distribution of upward through-going muon tracks with $E_\mu > 1 \text{ GeV}$. The data came from three different detector configurations, but the statistics is largely dominated by the full detector run, from May 1994 to December 2000. The total live time, normalized to the full detector configuration is 6.17 years. The best fit is obtained outside the physical region. The method of FELDMAN 98 is used to obtain the limits. The best fit is for maximal mixing.
- 53 AMBROSIO 01 result is based on the angular distribution and normalization of upward through-going muon tracks with $E_\mu > 1 \text{ GeV}$. See the previous footnote.

- ⁵⁴ FUKUDA 99C obtained this result from a total of 537 live days of upward through-going muon data in Super-Kamiokande between April 1996 to January 1998. With a threshold of $E_\mu > 1.6$ GeV, the observed flux is $(1.74 \pm 0.07 \pm 0.02) \times 10^{-13} \text{ cm}^{-2}\text{s}^{-1}\text{sr}^{-1}$. The best fit is $\sin^2(2\theta) = 0.95$.
- ⁵⁵ FUKUDA 99D obtained this result from a simultaneous fitting to zenith angle distributions of upward-stopping and through-going muons. The flux of upward-stopping muons of minimum energy of 1.6 GeV measured between April 1996 and January 1998 is $(0.39 \pm 0.04 \pm 0.02) \times 10^{-13} \text{ cm}^{-2}\text{s}^{-1}\text{sr}^{-1}$. This is compared to the expected flux of $(0.73 \pm 0.16 \text{ (theoretical error)}) \times 10^{-13} \text{ cm}^{-2}\text{s}^{-1}\text{sr}^{-1}$. The best fit is to maximal mixing.
- ⁵⁶ FUKUDA 99D obtained this result from the zenith dependence of the upward-stopping/through-going flux ratio. The best fit is to maximal mixing.
- ⁵⁷ FUKUDA 98C obtained this result by an analysis of 33.0 kton yr atmospheric neutrino data. The best fit is for maximal mixing.
- ⁵⁸ HATAKEYAMA 98 obtained this result from a total of 2456 live days of upward-going muon data in Kamiokande between December 1985 and May 1995. With a threshold of $E_\mu > 1.6$ GeV, the observed flux of upward through-going muons is $(1.94 \pm 0.10^{+0.07}_{-0.06}) \times 10^{-13} \text{ cm}^{-2}\text{s}^{-1}\text{sr}^{-1}$. This is compared to the expected flux of $(2.46 \pm 0.54 \text{ (theoretical error)}) \times 10^{-13} \text{ cm}^{-2}\text{s}^{-1}\text{sr}^{-1}$. The best fit is for maximal mixing.
- ⁵⁹ HATAKEYAMA 98 obtained this result from a combined analysis of Kamiokande contained events (FUKUDA 94) and upward going muon events. The best fit is $\sin^2(2\theta) = 0.95$.
- ⁶⁰ FUKUDA 94 obtained the result by a combined analysis of sub- and multi-GeV atmospheric neutrino events in Kamiokande. The best fit is for maximal mixing.

Δm_{32}^2

The sign of Δm_{32}^2 is not known at this time. If given, values are shown separately for the normal and inverted mass ordering. Unless otherwise specified, the ranges below correspond to the projection onto the Δm_{32}^2 axis of the 90% CL contours in the $\sin^2(2\theta_{23}) - \Delta m_{32}^2$ plane presented by the authors. If uncertainties are reported with the value, they correspond to one standard deviation uncertainty.

<u>VALUE (10^{-3} eV^2)</u>	<u>DOCUMENT ID</u>	<u>TECN</u>	<u>COMMENT</u>
-2.519±0.033 OUR FIT	Assuming inverted ordering		
2.437±0.033 OUR FIT	Assuming normal ordering		
2.41 ± 0.07	¹ ACERO	22 NOVA	Normal mass ordering, octant II for θ_{23} , θ_{13} constrained
-2.45 ± 0.07	¹ ACERO	22 NOVA	Inverted mass ordering, octant II for θ_{23} , θ_{13} constrained
2.45 ± 0.07	² ABE	20F T2K	Normal mass ordering, θ_{13} constrained
-2.51 ± 0.07	^{2,3} ABE	20F T2K	Inverted mass ordering, θ_{13} constrained
2.40 $^{+0.08}_{-0.09}$	⁴ ADAMSON	20A MINS	Accel., atmospheric, normal mass ordering
-2.45 $^{+0.08}_{-0.07}$	⁴ ADAMSON	20A MINS	Accel., atmospheric, inverted mass ordering
2.31 $^{+0.11}_{-0.13}$	⁵ AARTSEN	18A ICCB	Normal mass ordering
2.50 $^{+0.13}_{-0.20}$	⁶ ABE	18B SKAM	Normal mass ordering, θ_{13} constrained

-2.58	$\begin{matrix} +0.08 \\ -0.37 \end{matrix}$	6 ABE	18B SKAM	Inverted mass ordering, θ_{13} constrained
2.471	$\begin{matrix} +0.068 \\ -0.070 \end{matrix}$	7 ADEY	18A DAYA	Normal mass ordering
-2.575	$\begin{matrix} +0.068 \\ -0.070 \end{matrix}$	7 ADEY	18A DAYA	Inverted mass ordering
2.63	± 0.14	8 BAK	18 RENO	Normal mass ordering
-2.73	± 0.14	8 BAK	18 RENO	Inverted mass ordering
● ● ● We do not use the following data for averages, fits, limits, etc. ● ● ●				
2.47	$\begin{matrix} +0.08 \\ -0.09 \end{matrix}$	9 ABE	21A T2K	ν_{μ} disappearance
2.50	$\begin{matrix} +0.18 \\ -0.13 \end{matrix}$	9 ABE	21A T2K	$\bar{\nu}_{\mu}$ disappearance
2.517	$\begin{matrix} +0.026 \\ -0.028 \end{matrix}$	10 ESTEBAN	20A FIT	Normal mass ordering, global fit
-2.498	$\begin{matrix} +0.028 \\ -0.028 \end{matrix}$	10 ESTEBAN	20A FIT	Inverted mass ordering, global fit
2.55	$\begin{matrix} +0.12 \\ -0.11 \end{matrix}$	11 AARTSEN	19C ICCB	
2.48	$\begin{matrix} +0.11 \\ -0.06 \end{matrix}$	12 ACERO	19 NOVA	Normal mass ordering, octant II for θ_{23}
-2.54	$\begin{matrix} +0.06 \\ -0.11 \end{matrix}$	12 ACERO	19 NOVA	Inverted mass ordering, octant II for θ_{23}
< 4.1 at 90% CL		AGAFONOVA	19 OPER	
2.0	$\begin{matrix} +0.4 \\ -0.3 \end{matrix}$	13 ALBERT	19 ANTR	Atmospheric ν , deep sea telescope
2.50	$\begin{matrix} +0.13 \\ -0.31 \end{matrix}$	14 ABE	18B SKAM	3ν osc: normal mass ordering, θ_{13} free
-2.28	$\begin{matrix} +0.33 \\ -0.13 \end{matrix}$	14 ABE	18B SKAM	3ν osc: inverted mass ordering, θ_{13} free
2.463	$\begin{matrix} +0.071 \\ -0.070 \end{matrix}$	15 ABE	18G T2K	Normal mass ordering, θ_{13} constrained
-2.507	± 0.070	15,16 ABE	18G T2K	Inverted mass ordering, θ_{13} constrained
2.44	$\begin{matrix} +0.08 \\ -0.07 \end{matrix}$	17 ACERO	18 NOVA	Normal mass order, octant II for θ_{23}
2.45	$\begin{matrix} +0.07 \\ -0.08 \end{matrix}$	17,18 ACERO	18 NOVA	Normal mass order; octant I for θ_{23}
2.7	$\begin{matrix} +0.7 \\ -0.6 \end{matrix}$	19 AGAFONOVA	18 OPER	OPERA ν_{τ} appearance
2.42	± 0.03	DE-SALAS	18 FIT	Normal mass ordering, global fit
-2.50	$\begin{matrix} +0.03 \\ -0.04 \end{matrix}$	DE-SALAS	18 FIT	Inverted mass order, global fit
2.57	$\begin{matrix} +0.21 & +0.12 \\ -0.23 & -0.13 \end{matrix}$	20 SEO	18 RENO	Normal mass ordering
-2.67	$\begin{matrix} +0.23 & +0.13 \\ -0.21 & -0.12 \end{matrix}$	20 SEO	18 RENO	Inverted mass ordering
2.53	$\begin{matrix} +0.15 \\ -0.13 \end{matrix}$	ABE	17C T2K	Normal mass ordering with neutrinos
2.55	$\begin{matrix} +0.33 \\ -0.27 \end{matrix}$	ABE	17C T2K	Normal mass ordering with antineutrinos
2.55	$\begin{matrix} +0.08 \\ -0.08 \end{matrix}$	ABE	17C T2K	Normal mass ordering with neutrinos and antineutrinos

-2.63	$\begin{matrix} +0.08 \\ -0.08 \end{matrix}$	ABE	17C	T2K	Inverted mass ordering with neutrinos and antineutrinos
2.54	± 0.08	21 ABE	17F	T2K	Normal mass ordering; $\nu + \bar{\nu}$
-2.51	± 0.08	21 ABE	17F	T2K	Inverted mass ordering; $\nu + \bar{\nu}$
2.67	± 0.11	22 ADAMSON	17A	NOVA	3ν osc; normal mass ordering
-2.72	± 0.11	22 ADAMSON	17A	NOVA	3ν osc; inverted mass ordering
2.45	± 0.06	± 0.06 23 AN	17A	DAYA	Normal mass ordering
-2.56	± 0.06	± 0.06 23 AN	17A	DAYA	Inverted mass ordering
2.51	$\begin{matrix} +0.29 \\ -0.25 \end{matrix}$	24 ABE	16D	T2K	3ν osc.; normal mass ordering; $\bar{\nu}$ beam
2.52	$\begin{matrix} +0.20 \\ -0.18 \end{matrix}$	25 ADAMSON	16A	NOVA	3ν osc; normal mass ordering
-2.56	± 0.19	25 ADAMSON	16A	NOVA	3ν osc; inverted mass ordering
2.56	$\begin{matrix} +0.21 & +0.12 \\ -0.23 & -0.13 \end{matrix}$	26 CHOI	16	RENO	3ν osc; normal mass ordering
-2.69	$\begin{matrix} +0.23 & +0.13 \\ -0.21 & -0.12 \end{matrix}$	26 CHOI	16	RENO	3ν osc; inverted mass ordering
2.72	$\begin{matrix} +0.19 \\ -0.20 \end{matrix}$	27 AARTSEN	15A	ICCB	Normal mass ordering
-2.73	$\begin{matrix} +0.21 \\ -0.18 \end{matrix}$	27 AARTSEN	15A	ICCB	Inverted mass ordering
2.0-5.0		28 AGAFONOVA	15A	OPER	90% CL, 5 events
2.37	± 0.11	29 AN	15	DAYA	3ν osc.; normal mass ordering
-2.47	± 0.11	29 AN	15	DAYA	3ν osc.; inverted mass ordering
2.51	± 0.10	30 ABE	14	T2K	3ν osc.; normal mass ordering
-2.56	± 0.10	30 ABE	14	T2K	3ν osc.; inverted mass ordering
2.37	± 0.09	31 ADAMSON	14	MINS	Accel., atmospheric, normal mass ordering
-2.41	$\begin{matrix} +0.09 \\ -0.12 \end{matrix}$	31 ADAMSON	14	MINS	Accel., atmospheric, inverted mass ordering
2.54	$\begin{matrix} +0.19 \\ -0.20 \end{matrix}$	32 AN	14	DAYA	3ν osc.; normal mass ordering
-2.64	$\begin{matrix} +0.20 \\ -0.19 \end{matrix}$	32 AN	14	DAYA	3ν osc.; inverted mass ordering
2.48	$\begin{matrix} +0.05 \\ -0.07 \end{matrix}$	33 FORERO	14	FIT	3ν ; normal mass ordering
-2.38	$\begin{matrix} +0.06 \\ -0.05 \end{matrix}$	33 FORERO	14	FIT	3ν ; inverted mass ordering
2.457	± 0.047	34,35 GONZALEZ...	14	FIT	Normal mass ordering; global fit
-2.449	$\begin{matrix} +0.047 \\ -0.048 \end{matrix}$	34 GONZALEZ...	14	FIT	Inverted mass ordering; global fit
2.3	$\begin{matrix} +0.6 \\ -0.5 \end{matrix}$	36 AARTSEN	13B	ICCB	DeepCore, 2ν oscillation
2.44	$\begin{matrix} +0.17 \\ -0.15 \end{matrix}$	37 ABE	13G	T2K	3ν osc.; normal mass ordering
2.41	$\begin{matrix} +0.09 \\ -0.10 \end{matrix}$	38 ADAMSON	13B	MINS	2ν osc.; beam + atmospheric; identical ν & $\bar{\nu}$
2.2-3.1		39 ABE	12A	T2K	off-axis beam
2.62	$\begin{matrix} +0.31 \\ -0.28 \end{matrix}$	± 0.09 40 ADAMSON	12	MINS	$\bar{\nu}$ beam
1.35-2.55		41,42 ADAMSON	12B	MINS	MINOS atmospheric
1.4-5.6		41,43 ADAMSON	12B	MINS	MINOS pure atmospheric ν
0.9-2.5		41,43 ADAMSON	12B	MINS	MINOS pure atmospheric $\bar{\nu}$
1.8-5.0		44 ADRIAN-MAR..	12	ANTR	Atmospheric ν with deep sea telescope

1.3–4.0	45 ABE	11C SKAM	atmospheric $\bar{\nu}$
2.32 $^{+0.12}_{-0.08}$	ADAMSON	11 MINS	2ν oscillation; maximal mixing
3.36 $^{+0.46}_{-0.40}$	46 ADAMSON	11B MINS	$\bar{\nu}$ beam
< 3.37	47 ADAMSON	11C MINS	MINOS
1.9–2.6	48 WENDELL	10 SKAM	3ν osc.; normal mass ordering
–1.7– – 2.7	48 WENDELL	10 SKAM	3ν osc.; inverted mass ordering
2.43 ± 0.13	ADAMSON	08A MINS	MINOS
0.07–50	49 ADAMSON	06 MINS	atmospheric ν with far detector
1.9–4.0	50,51 AHN	06A K2K	KEK to Super-K
2.2–3.8	52 MICHAEL	06 MINS	MINOS
1.9–3.6	50 ALIU	05 K2K	KEK to Super-K
0.3–12	53 ALLISON	05 SOU2	
1.5–3.4	54 ASHIE	05 SKAM	atmospheric neutrino
0.6–8.0	55 AMBROSIO	04 MCRO	MACRO
1.9 to 3.0	56 ASHIE	04 SKAM	L/E distribution
1.5–3.9	57 AHN	03 K2K	KEK to Super-K
0.25–9.0	58 AMBROSIO	03 MCRO	MACRO
0.6–7.0	59 AMBROSIO	03 MCRO	MACRO
0.15–15	60 SANCHEZ	03 SOU2	Soudan-2 Atmospheric
0.6–15	61 AMBROSIO	01 MCRO	upward μ
1.0–6.0	62 AMBROSIO	01 MCRO	upward μ
1.0–50	63 FUKUDA	99C SKAM	upward μ
1.5–15.0	64 FUKUDA	99D SKAM	upward μ
0.7–18	65 FUKUDA	99D SKAM	stop μ / through
0.5–6.0	66 FUKUDA	98C SKAM	Super-Kamiokande
0.55–50	67 HATAKEYAMA98	KAMI	Kamiokande
4–23	68 HATAKEYAMA98	KAMI	Kamiokande
5–25	69 FUKUDA	94 KAMI	Kamiokande

¹ ACERO 22 uses data from Jun 29, 2016 to Feb 26, 2019 (12.5×10^{20} POT) and Feb 6, 2014 to Mar 20, 2020 (13.6×10^{20} POT). For normal mass ordering and θ_{23} octant I (lower octant), best fit is 0.00239 eV^2 ; for inverted mass ordering and octant I, best fit is -0.00244 eV^2 . Supersedes ACERO 19.

² ABE 20F results are based on data collected between 2009 and 2018 in (anti)neutrino mode and include a neutrino beam exposure of 1.49×10^{21} (1.64×10^{21}) protons on target. Supersedes ABE 18G.

³ ABE 20F reports $\Delta m_{13}^2 = (2.43 \pm 0.07) \times 10^{-3} \text{ eV}^2$ for inverted mass ordering. We convert to Δm_{32}^2 using PDG 20 value of $\Delta m_{21}^2 = (7.53 \pm 0.18) \times 10^{-5} \text{ eV}^2$.

⁴ ADAMSON 20A uses the complete dataset from MINOS and MINOS+ experiments. The data were collected using a total exposure of 23.76×10^{20} protons on target and 60.75 kton·yr exposure to atmospheric neutrinos. Supersedes ADAMSON 14.

⁵ AARTSEN 18A uses three years (April 2012 – May 2015) of neutrino data from full sky with reconstructed energies between 5.6 and 56 GeV, measured with the low-energy subdetector DeepCore of the IceCube neutrino telescope. AARTSEN 18A also reports the best fit values for the inverted mass ordering as $\Delta m_{32}^2 = -2.32 \times 10^{-3} \text{ eV}^2$ and $\sin^2(\theta_{23}) = 0.51$. Uncertainties for the inverted mass ordering fits were not provided. Supersedes AARTSEN 15A.

⁶ ABE 18B uses 328 kton·years of Super-Kamiokande I-IV atmospheric neutrino data to obtain this result. The fit is performed over the three parameters, Δm_{32}^2 , $\sin^2(\theta_{23})$, and

- δ , while the solar parameters and $\sin^2(\theta_{13})$ are fixed to $\Delta m_{21}^2 = (7.53 \pm 0.18) \times 10^{-5} \text{ eV}^2$, $\sin^2(\theta_{12}) = 0.304 \pm 0.014$, and $\sin^2(\theta_{13}) = 0.0219 \pm 0.0012$.
- 7 ADEY 18A reports results from analysis of 1958 days of data taking with the Daya-Bay experiment, with $3.9 \times 10^6 \bar{\nu}_e$ candidates. The fit to the data gives $\Delta m_{ee}^2 = (2.522_{-0.070}^{+0.068}) \times 10^{-3} \text{ eV}^2$. Solar oscillation parameters are fixed in the analysis using the global averages, $\sin^2(\theta_{12}) = 0.307_{-0.012}^{+0.013}$, $\Delta m_{21}^2 = (7.53 \pm 0.18) \times 10^{-5} \text{ eV}^2$, from PDG 18. Supersedes AN 17A.
 - 8 BAK 18 reports results of the RENO experiment using about 2200 live-days of data taken with detectors placed at 410.6 and 1445.7 m from reactors of the Hanbit Nuclear Power Plant. We convert the results to Δm_{32}^2 using the PDG 18 values of $\sin^2\theta_{12} = 0.307_{-0.012}^{+0.013}$ and $\Delta m_{21}^2 = (7.53 \pm 0.18) \times 10^{-5} \text{ eV}^2$. Supersedes SEO 18.
 - 9 ABE 21A results are based on 1.49×10^{21} POT in neutrino mode and 1.64×10^{21} POT in antineutrino mode.
 - 10 ESTEBAN 20A reports results of a global fit to neutrino oscillation data available at the time of the Neutrino2020 conference.
 - 11 AARTSEN 19C uses three years (April 2012 – May 2015) of neutrino data from full sky with reconstructed energies between 5.6 and 56 GeV, measured with the low-energy sub-detector DeepCore of the IceCube neutrino telescope. AARTSEN 19C adopts looser event selection criteria to prioritize the efficiency of selecting neutrino events, different from tighter event selection criteria which closely follow the criteria used by AARTSEN 18A to measure the ν_μ disappearance.
 - 12 ACERO 19 is based on a sample size of 12.33×10^{20} protons on target. The fit combines both antineutrino and neutrino data to extract the oscillation parameters. The results favor the normal mass ordering by 1.9σ and θ_{23} values in octant II by 1.6σ . Superseded by ACERO 22.
 - 13 ALBERT 19 measured the oscillation parameters of atmospheric neutrinos with the ANTARES deep sea neutrino telescope using the data taken from 2007 to 2016 (2830 days of total live time). Supersedes ADRIAN-MARTINEZ 12.
 - 14 ABE 18B uses 328 kton-years of Super-Kamiokande I-IV atmospheric neutrino data to obtain this result. The fit is performed over the four parameters, Δm_{32}^2 , $\sin^2\theta_{23}$, $\sin^2\theta_{13}$, and δ , while the solar parameters are fixed to $\Delta m_{21}^2 = (7.53 \pm 0.18) \times 10^{-5} \text{ eV}^2$ and $\sin^2\theta_{12} = 0.304 \pm 0.014$.
 - 15 ABE 18G data prefers normal ordering with a posterior probability of 87%. Supersedes ABE 17F.
 - 16 ABE 18G reports $\Delta m_{13}^2 = (2.432 \pm 0.070) \times 10^{-3} \text{ eV}^2$ for inverted mass ordering. We convert to Δm_{32}^2 using PDG 18 value of $\Delta m_{21}^2 = (7.53 \pm 0.18) \times 10^{-5} \text{ eV}^2$.
 - 17 ACERO 18 performs a joint fit to the data for ν_μ disappearance and ν_e appearance. The overall best fit favors normal mass ordering and θ_{23} in octant II. No 1σ confidence intervals are presented for the inverted mass ordering scenarios. Superseded by ACERO 19.
 - 18 The error for octant I is taken from the result for octant II.
 - 19 AGAFONOVA 18 assumes maximal θ_{23} mixing.
 - 20 SEO 18 reports result of the RENO experiment from a rate and shape analysis of 500 days of data. A simultaneous fit to θ_{13} and Δm_{ee}^2 yields $\Delta m_{ee}^2 = (2.62_{-0.23}^{+0.21+0.12}) \times 10^{-3} \text{ eV}^2$. We convert the results to Δm_{32}^2 using the PDG 18 values of $\sin^2\theta_{12}$ and Δm_{21}^2 . SEO 18 is a detailed description of the results published in CHOI 16, which it supersedes. Superseded by BAK 18
 - 21 ABE 17F confidence intervals are obtained using a frequentist analysis including θ_{13} constraint from reactor experiments. Bayesian intervals based on Markov Chain Monte Carlo method are also provided by the authors. Superseded by ABE 18G.
 - 22 Superseded by ACERO 18.

- ²³ AN 17A report results from combined rate and spectral shape analysis of 1230 days of data taken with the Daya Bay reactor experiment. The data set contains more than 2.5×10^6 inverse beta-decay events with neutron capture on Gd. The fit to the data gives $\Delta m_{ee}^2 = (2.50 \pm 0.06 \pm 0.06) \times 10^{-3}$ eV. Superseded by ADEY 18A.
- ²⁴ ABE 16D reports oscillation results using $\bar{\nu}_\mu$ disappearance in an off-axis beam.
- ²⁵ Superseded by ADAMSON 17A.
- ²⁶ CHOI 16 reports result of the RENO experiment from a rate and shape analysis of 500 days of data. A simultaneous fit to θ_{13} and Δm_{ee}^2 yields $\Delta m_{ee}^2 = (2.62^{+0.21+0.12}_{-0.23-0.13}) \times 10^{-3}$ eV. We convert the results to Δm_{32}^2 using PDG 18 values of $\sin^2(\theta_{12})$ and Δm_{21}^2 .
- ²⁷ AARTSEN 15A obtains this result by a three-neutrino oscillation analysis using 10–100 GeV muon neutrino sample from a total of 953 days of measurements with the low-energy subdetector DeepCore of the IceCube neutrino telescope. Superseded by AARTSEN 18A.
- ²⁸ AGAFONOVA 15A result is based on $5 \nu_\mu \rightarrow \nu_\tau$ appearance candidates with an expected background of 0.25 ± 0.05 events. The best fit is for $\Delta m_{32}^2 = 3.3 \times 10^{-3}$ eV².
- ²⁹ AN 15 uses all eight identical detectors, with four placed near the reactor cores and the remaining four at the far hall to determine prompt energy spectra. The results correspond to the exposure of 6.9×10^5 GW_{th}-ton-days. They derive $\Delta m_{ee}^2 = (2.42 \pm 0.11) \times 10^{-3}$ eV². Assuming the normal (inverted) ordering, the fitted $\Delta m_{32}^2 = (2.37 \pm 0.11) \times 10^{-3}$ ($(2.47 \pm 0.11) \times 10^{-3}$) eV². Superseded by AN 17A.
- ³⁰ ABE 14 results are based on ν_μ disappearance using three-neutrino oscillation fit. The confidence intervals are derived from one dimensional profiled likelihoods. In ABE 14 the inverted mass ordering result is reported as $\Delta m_{13}^2 = (2.48 \pm 0.10) \times 10^{-3}$ eV² which we converted to Δm_{32}^2 by adding PDG 14 value of $\Delta m_{21}^2 = (7.53 \pm 0.18) \times 10^{-5}$ eV². Superseded by ABE 17C.
- ³¹ ADAMSON 14 uses a complete set of accelerator and atmospheric data. The analysis combines The analysis combines the ν_μ disappearance and ν_e appearance data using three-neutrino oscillation fit. The fit results are obtained for normal and inverted mass ordering assumptions.
- ³² AN 14 uses six identical detectors, with three placed near the reactor cores (flux-weighted baselines of 512 and 561 m) and the remaining three at the far hall (at the flux averaged distance of 1579 m from all six reactor cores) to determine prompt energy spectra and derive $\Delta m_{ee}^2 = (2.59^{+0.19}_{-0.20}) \times 10^{-3}$ eV². Assuming the normal (inverted) ordering, the fitted $\Delta m_{32}^2 = (2.54^{+0.19}_{-0.20}) \times 10^{-3}$ ($(2.64^{+0.19}_{-0.20}) \times 10^{-3}$) eV². Superseded by AN 15.
- ³³ FORERO 14 performs a global fit to Δm_{31}^2 using solar, reactor, long-baseline accelerator, and atmospheric neutrino data.
- ³⁴ GONZALEZ-GARCIA 14 result comes from a frequentist global fit. The corresponding Bayesian global fit to the same data results are reported in BERGSTROM 15 as $(2.460 \pm 0.046) \times 10^{-3}$ eV² for normal and $(2.445^{+0.047}_{-0.045}) \times 10^{-3}$ eV² for inverted mass ordering.
- ³⁵ The value for normal mass ordering is actually a measurement of Δm_{31}^2 which differs from Δm_{32}^2 by a much smaller value of Δm_{12}^2 .
- ³⁶ AARTSEN 13B obtained this result by a two-neutrino oscillation analysis using 20–100 GeV muon neutrino sample from a total of 318.9 days of live-time measurement with the low-energy subdetector DeepCore of the IceCube neutrino telescope.
- ³⁷ Based on the observation of 58 ν_μ events with 205 ± 17 (syst) expected in the absence of neutrino oscillations. Superseded by ABE 14.
- ³⁸ ADAMSON 13B obtained this result from ν_μ and $\bar{\nu}_\mu$ disappearance using ν_μ (10.71×10^{20} POT) and $\bar{\nu}_\mu$ (3.36×10^{20} POT) beams, and atmospheric (37.88 kton-years) data

- from MINOS. The fit assumed two-flavor neutrino hypothesis and identical ν_μ and $\bar{\nu}_\mu$ oscillation parameters.
- 39 ABE 12A obtained this result by a two-neutrino oscillation analysis. The best-fit point is $\Delta m_{32}^2 = 2.65 \times 10^{-3} \text{ eV}^2$.
- 40 ADAMSON 12 is a two-neutrino oscillation analysis using antineutrinos.
- 41 ADAMSON 12B obtained this result by a two-neutrino oscillation analysis of the L/E distribution using 37.9 kton-yr atmospheric neutrino data with the MINOS far detector.
- 42 The 90% single-parameter confidence interval at the best fit point is $\Delta m^2 = 0.0019 \pm 0.0004 \text{ eV}^2$.
- 43 The data are separated into pure samples of ν_s and $\bar{\nu}_s$, and separate oscillation parameters for ν_s and $\bar{\nu}_s$ are fit to the data. The best fit point is $(\Delta m^2, \sin^2 2\theta) = (0.0022 \text{ eV}^2, 0.99)$ and $(\Delta \bar{m}^2, \sin^2 2\bar{\theta}) = (0.0016 \text{ eV}^2, 1.00)$. The quoted result is taken from the 90% C.L. contour in the $(\Delta m^2, \sin^2 2\theta)$ plane obtained by minimizing the four parameter log-likelihood function with respect to the other oscillation parameters.
- 44 ADRIAN-MARTINEZ 12 measured the oscillation parameters of atmospheric neutrinos with the ANTARES deep sea neutrino telescope using the data taken from 2007 to 2010 (863 days of total live time). Superseded by ALBERT 19
- 45 ABE 11C obtained this result by a two-neutrino oscillation analysis with separate mixing parameters between neutrinos and antineutrinos, using the Super-Kamiokande-I+II+III atmospheric neutrino data. The corresponding 90% CL neutrino oscillation parameter range obtained from this analysis is $\Delta m^2 = 1.7\text{--}3.0 \times 10^{-3} \text{ eV}^2$.
- 46 ADAMSON 11B obtained this result by a two-neutrino oscillation analysis of antineutrinos in an antineutrino enhanced beam with 1.71×10^{20} protons on target. This results is consistent with the neutrino measurements of ADAMSON 11 at 2% C.L.
- 47 ADAMSON 11C obtains this result based on a study of antineutrinos in a neutrino beam and assumes maximal mixing in the two-flavor approximation.
- 48 WENDELL 10 obtained this result by a three-neutrino oscillation analysis with one mass scale dominance ($\Delta m_{21}^2 = 0$) using the Super-Kamiokande-I+II+III atmospheric neutrino data, and updates the HOSAKA 06A result.
- 49 ADAMSON 06 obtained this result by a two-neutrino oscillation analysis of the L/E distribution using 4.54 kton yr atmospheric neutrino data with the MINOS far detector.
- 50 The best fit in the physical region is for $\Delta m^2 = 2.8 \times 10^{-3} \text{ eV}^2$.
- 51 Supercedes ALIU 05.
- 52 MICHAEL 06 best fit is $2.74 \times 10^{-3} \text{ eV}^2$. See also ADAMSON 08.
- 53 ALLISON 05 result is based on an atmospheric neutrino observation with an exposure of 5.9 kton yr. From a two-flavor oscillation analysis the best-fit point is $\Delta m^2 = 0.0017 \text{ eV}^2$ and $\sin^2 2\theta = 0.97$.
- 54 ASHIE 05 obtained this result by a two-neutrino oscillation analysis using 92 kton yr atmospheric neutrino data from the complete Super-Kamiokande I running period. The best fit is for $\Delta m^2 = 2.1 \times 10^{-3} \text{ eV}^2$.
- 55 AMBROSIO 04 obtained this result, without using the absolute normalization of the neutrino flux, by combining the angular distribution of upward through-going muon tracks with $E_\mu > 1 \text{ GeV}$, N_{low} and N_{high} , and the numbers of InDown + UpStop and InUp events. Here, N_{low} and N_{high} are the number of events with reconstructed neutrino energies $< 30 \text{ GeV}$ and $> 130 \text{ GeV}$, respectively. InDown and InUp represent events with downward and upward-going tracks starting inside the detector due to neutrino interactions, while UpStop represents entering upward-going tracks which stop in the detector. The best fit is for $\Delta m^2 = 2.3 \times 10^{-3} \text{ eV}^2$.
- 56 ASHIE 04 obtained this result from the $L(\text{flight length})/E(\text{estimated neutrino energy})$ distribution of ν_μ disappearance probability, using the Super-Kamiokande-I 1489 live-day atmospheric neutrino data. The best fit is for $\Delta m^2 = 2.4 \times 10^{-3} \text{ eV}^2$.

- 57 There are several islands of allowed region from this K2K analysis, extending to high values of Δm^2 . We only include the one that overlaps atmospheric neutrino analyses. The best fit is for $\Delta m^2 = 2.8 \times 10^{-3} \text{ eV}^2$.
- 58 AMBROSIO 03 obtained this result on the basis of the ratio $R = N_{low}/N_{high}$, where N_{low} and N_{high} are the number of upward through-going muon events with reconstructed neutrino energy $< 30 \text{ GeV}$ and $> 130 \text{ GeV}$, respectively. The data came from the full detector run started in 1994. The method of FELDMAN 98 is used to obtain the limits. The best fit is for $\Delta m^2 = 2.5 \times 10^{-3} \text{ eV}^2$.
- 59 AMBROSIO 03 obtained this result by using the ratio R and the angular distribution of the upward through-going muons. R is given in the previous note and the angular distribution is reported in AMBROSIO 01. The method of FELDMAN 98 is used to obtain the limits. The best fit is for $\Delta m^2 = 2.5 \times 10^{-3} \text{ eV}^2$.
- 60 SANCHEZ 03 is based on an exposure of 5.9 kton yr . The result is obtained using a likelihood analysis of the neutrino L/E distribution for a selection μ flavor sample while the e -flavor sample provides flux normalization. The method of FELDMAN 98 is used to obtain the allowed region. The best fit is for $\Delta m^2 = 5.2 \times 10^{-3} \text{ eV}^2$.
- 61 AMBROSIO 01 result is based on the angular distribution of upward through-going muon tracks with $E_\mu > 1 \text{ GeV}$. The data came from three different detector configurations, but the statistics is largely dominated by the full detector run, from May 1994 to December 2000. The total live time, normalized to the full detector configuration is 6.17 years . The best fit is obtained outside the physical region. The method of FELDMAN 98 is used to obtain the limits.
- 62 AMBROSIO 01 result is based on the angular distribution and normalization of upward through-going muon tracks with $E_\mu > 1 \text{ GeV}$. See the previous footnote.
- 63 FUKUDA 99C obtained this result from a total of 537 live days of upward through-going muon data in Super-Kamiokande between April 1996 to January 1998. With a threshold of $E_\mu > 1.6 \text{ GeV}$, the observed flux is $(1.74 \pm 0.07 \pm 0.02) \times 10^{-13} \text{ cm}^{-2}\text{s}^{-1}\text{sr}^{-1}$. The best fit is for $\Delta m^2 = 5.9 \times 10^{-3} \text{ eV}^2$.
- 64 FUKUDA 99D obtained this result from a simultaneous fitting to zenith angle distributions of upward-stopping and through-going muons. The flux of upward-stopping muons of minimum energy of 1.6 GeV measured between April 1996 and January 1998 is $(0.39 \pm 0.04 \pm 0.02) \times 10^{-13} \text{ cm}^{-2}\text{s}^{-1}\text{sr}^{-1}$. This is compared to the expected flux of $(0.73 \pm 0.16 \text{ (theoretical error)}) \times 10^{-13} \text{ cm}^{-2}\text{s}^{-1}\text{sr}^{-1}$. The best fit is for $\Delta m^2 = 3.9 \times 10^{-3} \text{ eV}^2$.
- 65 FUKUDA 99D obtained this result from the zenith dependence of the upward-stopping/through-going flux ratio. The best fit is for $\Delta m^2 = 3.1 \times 10^{-3} \text{ eV}^2$.
- 66 FUKUDA 98C obtained this result by an analysis of 33.0 kton yr atmospheric neutrino data. The best fit is for $\Delta m^2 = 2.2 \times 10^{-3} \text{ eV}^2$.
- 67 HATAKEYAMA 98 obtained this result from a total of 2456 live days of upward-going muon data in Kamiokande between December 1985 and May 1995. With a threshold of $E_\mu > 1.6 \text{ GeV}$, the observed flux of upward through-going muons is $(1.94 \pm 0.10^{+0.07}_{-0.06}) \times 10^{-13} \text{ cm}^{-2}\text{s}^{-1}\text{sr}^{-1}$. This is compared to the expected flux of $(2.46 \pm 0.54 \text{ (theoretical error)}) \times 10^{-13} \text{ cm}^{-2}\text{s}^{-1}\text{sr}^{-1}$. The best fit is for $\Delta m^2 = 2.2 \times 10^{-3} \text{ eV}^2$.
- 68 HATAKEYAMA 98 obtained this result from a combined analysis of Kamiokande contained events (FUKUDA 94) and upward going muon events. The best fit is for $\Delta m^2 = 13 \times 10^{-3} \text{ eV}^2$.
- 69 FUKUDA 94 obtained the result by a combined analysis of sub- and multi-GeV atmospheric neutrino events in Kamiokande. The best fit is for $\Delta m^2 = 16 \times 10^{-3} \text{ eV}^2$.

$\sin^2(\theta_{13})$

At present time direct measurements of $\sin^2(\theta_{13})$ are derived from the reactor $\bar{\nu}_e$ disappearance at distances corresponding to the Δm_{32}^2 value, i.e. $L \sim 1\text{km}$. Alternatively, limits can also be obtained from the analysis of the solar neutrino data and accelerator-based $\nu_\mu \rightarrow \nu_e$ experiments.

If an experiment reports $\sin^2(2\theta_{13})$ we convert the value to $\sin^2(\theta_{13})$.

VALUE (units 10^{-2})	CL%	DOCUMENT ID	TECN	COMMENT
2.20 ± 0.07				OUR AVERAGE
2.70 ± 0.37		¹ DE-KERRET	20 DCHZ	Chooz reactors
2.22 ± 0.21 ± 0.37		² SHIN	20 RENO	Yonggwang reactors
2.188 ± 0.076		³ ADEY	18A DAYA	DayaBay, LingAo/Ao II reactors
2.29 ± 0.18		⁴ BAK	18 RENO	Yonggwang reactors
1.81 ± 0.29		⁵ AN	16A DAYA	DayaBay, Ling Ao/Ao II reactors
● ● ● We do not use the following data for averages, fits, limits, etc. ● ● ●				
2.41 ± 0.45		⁶ ABRAHAO	21 DCHZ	Chooz reactors
2.200 ⁺ ₋ 0.069 0.062		⁷ SALAS	21 FIT	Normal mass ordering, global fit
2.225 ⁺ ₋ 0.064 0.070		⁷ SALAS	21 FIT	Inverted mass ordering, global fit
2.219 ⁺ ₋ 0.062 0.063		⁸ ESTEBAN	20A FIT	Normal mass ordering, global fit
2.238 ⁺ ₋ 0.063 0.062		⁸ ESTEBAN	20A FIT	Inverted mass ordering, global fit
< 3.9	68	AGAFONOVA	19 OPER	
1.8 ⁺ ₋ 2.9 1.3		⁹ ABE	18B SKAM	3ν osc: normal mass ordering, θ_{13} free
0.8 ⁺ ₋ 1.7 0.7		⁹ ABE	18B SKAM	3ν osc: inverted mass ordering, θ_{13} free
<12	90	¹⁰ AGAFONOVA	18A OPER	OPERA: ν_e appearance
2.160 ⁺ ₋ 0.083 0.069		DE-SALAS	18 FIT	Normal mass ordering, global fit
2.220 ⁺ ₋ 0.074 0.076		DE-SALAS	18 FIT	Inverted mass ordering, global fit
2.09 ± 0.23 ± 0.16		¹¹ SEO	18 RENO	Yonggwang reactors
2.7 ± 0.7		¹² ABE	17F T2K	Normal mass ordering, T2K only
2.149 ± 0.071 ± 0.050		¹³ AN	17A DAYA	DayaBay, LingAo/Ao II reactors
2.25 ⁺ ₋ 0.87 0.86		¹⁴ ABE	16B DCHZ	Chooz reactors
2.09 ± 0.23 ± 0.16		¹⁵ CHOI	16 RENO	Yonggwang reactors
2.15 ± 0.13		¹⁶ AN	15 DAYA	DayaBay, Ling Ao/Ao II reactors
2.6 ⁺ ₋ 1.2 1.1		¹⁷ ABE	14A DCHZ	Chooz reactors
3.0 ⁺ ₋ 1.3 1.0		¹⁸ ABE	14C T2K	Inverted mass ordering
3.6 ⁺ ₋ 1.0 0.9		¹⁸ ABE	14C T2K	Normal mass ordering

2.3	$\begin{matrix} + 0.9 \\ - 0.8 \end{matrix}$		19	ABE	14H	DCHZ	Chooz reactors
2.3	± 0.2		20	AN	14	DAYA	DayaBay, Ling Ao/Ao II reactors
2.12	± 0.47		21	AN	14B	DAYA	DayaBay, Ling Ao/Ao II reactors
2.34	± 0.20		22	FORERO	14	FIT	Normal mass ordering
2.40	± 0.19		22	FORERO	14	FIT	Inverted mass ordering
2.18	± 0.10		23	GONZALEZ...	14	FIT	Normal mass ordering; global fit
2.19	$\begin{matrix} + 0.11 \\ - 0.10 \end{matrix}$		23	GONZALEZ...	14	FIT	Inverted mass ordering; global fit
2.5	± 0.9	± 0.9	24	ABE	13C	DCHZ	Chooz reactors
2.3	$\begin{matrix} + 1.3 \\ - 1.0 \end{matrix}$		25	ABE	13E	T2K	Normal mass ordering
2.8	$\begin{matrix} + 1.6 \\ - 1.2 \end{matrix}$		25	ABE	13E	T2K	Inverted mass ordering
1.6	$\begin{matrix} + 1.3 \\ - 0.9 \end{matrix}$		26	ADAMSON	13A	MINS	Normal mass ordering
3.0	$\begin{matrix} + 1.8 \\ - 1.6 \end{matrix}$		26	ADAMSON	13A	MINS	Inverted mass ordering
< 13		90		AGAFONOVA	13	OPER	OPERA: 3ν
< 3.6		95	27	AHARMIM	13	FIT	global solar: 3ν
2.3	± 0.3	± 0.1	28	AN	13	DAYA	DayaBay, Ling Ao/Ao II reactors
2.2	± 1.1	± 0.8	29	ABE	12	DCHZ	Chooz reactors
2.8	± 0.8	± 0.7	30	ABE	12B	DCHZ	Chooz reactors
2.9	± 0.3	± 0.5	31	AHN	12	RENO	Yonggwang reactors
2.4	± 0.4	± 0.1	32	AN	12	DAYA	DayaBay, Ling Ao/Ao II reactors
2.5	$\begin{matrix} + 1.8 \\ - 1.6 \end{matrix}$		33	ABE	11	FIT	KamLAND + global solar
< 6.1		95	34	ABE	11	FIT	Global solar
1.3	to 5.6	68	35	ABE	11A	T2K	Normal mass ordering
1.5	to 5.6	68	36	ABE	11A	T2K	Inverted mass ordering
0.3	to 2.3	68	37	ADAMSON	11D	MINS	Normal mass ordering
0.8	to 3.9	68	38	ADAMSON	11D	MINS	Inverted mass ordering
8	± 3		39	FOGLI	11	FIT	Global neutrino data
7.8	± 6.2		40	GANDO	11	FIT	KamLAND + solar: 3ν
12.4	± 13.3		41	GANDO	11	FIT	KamLAND: 3ν
3	$\begin{matrix} + 9 \\ - 7 \end{matrix}$	90	42	ADAMSON	10A	MINS	Normal mass ordering
6	$\begin{matrix} + 14 \\ - 6 \end{matrix}$	90	43	ADAMSON	10A	MINS	Inverted mass ordering
8	$\begin{matrix} + 8 \\ - 7 \end{matrix}$		44,45	AHARMIM	10	FIT	KamLAND + global solar: 3ν
< 30		95	44,46	AHARMIM	10	FIT	global solar: 3ν
< 15		90	47	WENDELL	10	SKAM	3ν osc.; normal m ordering
< 33		90	47	WENDELL	10	SKAM	3ν osc.; inverted m ordering
11	$\begin{matrix} + 11 \\ - 8 \end{matrix}$		48	ADAMSON	09	MINS	Normal mass ordering
18	$\begin{matrix} + 15 \\ - 11 \end{matrix}$		49	ADAMSON	09	MINS	Inverted mass ordering
6	± 4		50	FOGLI	08	FIT	Global neutrino data

8	± 7	51	FOGLI	08	FIT	Solar + KamLAND data
5	± 5	52	FOGLI	08	FIT	Atmospheric + LBL + CHOOZ
< 36		90	53 YAMAMOTO	06	K2K	Accelerator experiment
< 48		90	54 AHN	04	K2K	Accelerator experiment
< 36		90	55 BOEHM	01		Palo Verde react.
< 45		90	56 BOEHM	00		Palo Verde react.
< 15		90	57 APOLLONIO	99	CHOZ	Reactor Experiment

¹ DE-KERRET 20 uses 481 days of data from single detector operation and also 384 days of data with both near and far detectors operating. A rate and shape analysis is performed on combined neutron captures on H and Gd. Supersedes ABE 16B.

² SHIN 20 uses the RENO detector and 1500 live days of data. The near (far) detector observed 567,690 (90,747) $\bar{\nu}_e$ candidate events with a delayed neutron capture on hydrogen. The extracted value of $\sin^2\theta_{13}$ is consistent with the previous analysis with neutron capture on Gd in BAK 18.

³ ADEY 18A reports results from analysis of 1958 days of data taking with the Daya-Bay experiment, with 3.9×10^6 $\bar{\nu}_e$ candidates. The fit to the data gives $\Delta m_{ee}^2 = (2.522_{-0.070}^{+0.068}) \times 10^{-3} \text{ eV}^2$. Solar oscillation parameters are fixed in the analysis using the global averages, $\sin^2(\theta_{12}) = 0.307_{-0.012}^{+0.013}$, $\Delta m_{21}^2 = (7.53 \pm 0.18) \times 10^{-5} \text{ eV}^2$, from PDG 18. Supersedes AN 17A.

⁴ BAK 18 reports results of the RENO experiment using about 2200 live-days of data taken with detectors placed at 410.6 and 1445.7 m from reactors of the Hanbit Nuclear Power Plant. Supersedes SEO 18.

⁵ AN 16A uses data from the eight antineutrino detectors (404 days) and six antineutrino detectors (217 days) runs to determine the mixing parameter $\sin^2(2\theta_{13})$ using the neutron capture on H only. Supersedes AN 14B.

⁶ ABRAHAO 21 uses 865 days of data collected in both near and far detectors with at least one reactor in operation. The analysis is based on a background model independent approach, so called Reactor Rate Modulation, to determine the mixing angle θ_{13} . Adding the background model reduces the uncertainty to 0.0041. Supersedes ABE 16B.

⁷ SALAS 21 reports results of a global fit to neutrino oscillation data available at the time of the Neutrino 2020 conference.

⁸ ESTEBAN 20A reports results of a global fit to neutrino oscillation data available at the time of the Neutrino2020 conference.

⁹ ABE 18B uses 328 kton-years of Super-Kamiokande I-IV atmospheric neutrino data to obtain this result. The fit is performed over the four parameters, Δm_{32}^2 , $\sin^2\theta_{23}$, $\sin^2\theta_{13}$, and δ , while the solar parameters are fixed to $\Delta m_{21}^2 = (7.53 \pm 0.18) \times 10^{-5} \text{ eV}^2$ and $\sin^2\theta_{12} = 0.304 \pm 0.014$.

¹⁰ AGAFONOVA 18A reports $\sin^2(2\theta_{13}) < 0.43$ at 90% C.L. The result on the sterile neutrino search in the context of 3+1 model is also reported. A 90% C.L. upper limit on $\sin^2(2\theta_{\mu e}) = 0.021$ for $\Delta m_{41}^2 \geq 0.1 \text{ eV}^2$ is set.

¹¹ SEO 18 reports results of the RENO experiment using about 500 days of data, performing a rate and shape analysis. Compared to AHN 12, a significant reduction of the systematic uncertainties is reported. A 3% excess of events near 5 MeV of the prompt energy is observed. SEO 18 is a detailed description of the results published in CHOI 16, which it supersedes. Superseded by BAK 18.

¹² Using T2K data only. For inverted mass ordering, all values of θ_{13} are ruled out at 68% CL.

¹³ AN 17A reports results from combined rate and spectral shape analysis of 1230 days of data taken with the Daya Bay reactor experiment. The data set contains more than 2.5×10^6 inverse beta-decay events with neutron capture on Gd. A simultaneous fit to θ_{13} and Δm_{ee}^2 is performed. Superseded by ADEY 18A.

- ¹⁴ ABE 16B uses 455.57 live days of data from a detector 1050 m away from two reactor cores of the Chooz nuclear power station, to determine the mixing parameter $\sin^2(2\theta_{13})$. This analysis uses 7.15 reactor-off days for constraining backgrounds. A rate and shape analysis is performed on combined neutron captures on H and Gd. Supersedes ABE 14H and ABE 13C.
- ¹⁵ CHOI 16 reports results of the RENO experiment using about 500 days of data, performing a rate and shape analysis. Compared to AHN 12, a significant reduction of the systematic uncertainties is reported. A 3% excess of events near 5 MeV of the prompt energy is observed. Supersedes AHN 12.
- ¹⁶ AN 15 uses all eight identical detectors, with four placed near the reactor cores and the remaining four at the far hall to determine the mixing angle θ_{13} using the $\bar{\nu}_e$ observed interaction rates with neutron capture on Gd and energy spectra. The result corresponds to the exposure of 6.9×10^5 GW_{th}-ton-days. Superseded by AN 17A.
- ¹⁷ ABE 14A uses 467.9 live days of one detector, 1050 m away from two reactor cores of the Chooz nuclear power station, to determine the mixing parameter $\sin^2(2\theta_{13})$. The Bugey4 data (DECLAIS 94) is used to constrain the neutrino flux. The data set includes 7.24 reactor-off days. A "rate-modulation" analysis is performed. Supersedes ABE 12B.
- ¹⁸ ABE 14C result is for ν_e appearance and assumes $\Delta m_{32}^2 = 2.4 \times 10^{-3}$ eV², $\sin^2(\theta_{23}) = 0.5$, and $\delta = 0$.
- ¹⁹ ABE 14H uses 467.9 live days of one detector, 1050 m away from two reactor cores of the Chooz nuclear power station, to determine the mixing parameter $\sin^2(2\theta_{13})$. The Bugey4 data (DECLAIS 94) is used to constrain the neutrino flux. The data set includes 7.24 reactor-off days. A rate and shape analysis is performed. Superseded by ABE 16B.
- ²⁰ AN 14 uses six identical detectors, with three placed near the reactor cores (flux-weighted baselines of 512 and 561 m) and the remaining three at the far hall (at the flux averaged distance of 1579 m from all six reactor cores) to determine the mixing angle θ_{13} using the $\bar{\nu}_e$ observed interaction rates with neutron capture on Gd and energy spectra. Supersedes AN 13 and superseded by AN 15.
- ²¹ AN 14B uses six identical anti-neutrino detectors with flux-weighted baselines of ~ 500 m and ~ 1.6 km to six power reactors. This rate analysis uses a 217-day data set and neutron capture on protons (not Gd) only. $\Delta m_{31}^2 = 2.32 \times 10^{-3}$ eV² is assumed. Superseded by AN 16A.
- ²² FORERO 14 performs a global fit to neutrino oscillations using solar, reactor, long-baseline accelerator, and atmospheric neutrino data.
- ²³ GONZALEZ-GARCIA 14 result comes from a frequentist global fit. The corresponding Bayesian global fit to the same data results are reported in BERGSTROM 15 as $(2.18^{+0.10}_{-0.11}) \times 10^{-2}$ eV² for normal and $(2.19^{+0.12}_{-0.10}) \times 10^{-2}$ eV² for inverted mass ordering.
- ²⁴ ABE 13C uses delayed neutron capture on hydrogen instead of on Gd used previously. The physical volume is thus three times larger. The fit is based on the rate and shape analysis as in ABE 12B. The Bugey4 data (DECLAIS 94) is used to constrain the neutrino flux. Superseded by ABE 16B.
- ²⁵ ABE 13E assumes maximal θ_{23} mixing and *CP* phase $\delta = 0$.
- ²⁶ ADAMSON 13A results obtained from ν_e appearance, assuming $\delta = 0$, and $\sin^2(2\theta_{23}) = 0.957$.
- ²⁷ AHARMIM 13 obtained this result by a three-neutrino oscillation analysis with the value of Δm_{32}^2 fixed to 2.45×10^{-3} eV², using global solar neutrino data. AHARMIM 13 global solar neutrino data include SNO's all-phases-combined analysis results on the total active ⁸B neutrino flux and energy-dependent ν_e survival probability parameters, measurements of Cl (CLEVELAND 98), Ga (ABDURASHITOV 09 which contains combined analysis with GNO (ALTMANN 05 and Ph.D. thesis of F. Kaether)), and ⁷Be (BELLINI 11A) rates, and ⁸B solar-neutrino recoil electron measurements of SK-I (HOSAKA 06) zenith, SK-II (CRAVENS 08) and SK-III (ABE 11) day/night spectra, and Borexino (BELLINI 10A) spectra. AHARMIM 13 also reported a result combining global solar and KamLAND data, which is $\sin^2(2\theta_{13}) = (9.1^{+2.9}_{-3.1}) \times 10^{-2}$.

- ²⁸ AN 13 uses six identical detectors, with three placed near the reactor cores (flux-weighted baselines of 498 and 555 m) and the remaining three at the far hall (at the flux averaged distance of 1628 m from all six reactor cores) to determine the $\bar{\nu}_e$ interaction rate ratios. Superseded by AN 14.
- ²⁹ ABE 12 determines the $\bar{\nu}_e$ interaction rate in a single detector, located 1050 m from the cores of two reactors. A rate and shape analysis is performed. The rate normalization is fixed by the results of the Bugey4 reactor experiment, thus avoiding any dependence on possible very short baseline oscillations. The value of $\Delta m_{31}^2 = 2.4 \times 10^{-3} \text{ eV}^2$ is used in the analysis. Superseded by ABE 12B.
- ³⁰ ABE 12B determines the neutrino mixing angle θ_{13} using a single detector, located 1050 m from the cores of two reactors. This result is based on a spectral shape and rate analysis. The Bugey4 data (DECLAIS 94) is used to constrain the neutrino flux. Superseded by ABE 14A.
- ³¹ AHN 12 uses two identical detectors, placed at flux weighted distances of 408.56 m and 1433.99 m from six reactor cores, to determine the mixing angle θ_{13} . This rate-only analysis excludes the no-oscillation hypothesis at 4.9 standard deviations. The value of $\Delta m_{31}^2 = (2.32_{-0.08}^{+0.12}) \times 10^{-3} \text{ eV}^2$ was assumed in the analysis. Superseded by CHOI 16.
- ³² AN 12 uses six identical detectors with three placed near the reactor cores (flux-weighted baselines of 470 m and 576 m) and the remaining three at the far hall (at the flux averaged distance of 1648 m from all six reactor cores) to determine the mixing angle θ_{13} using the $\bar{\nu}_e$ observed interaction rate ratios. This rate-only analysis excludes the no-oscillation hypothesis at 5.2 standard deviations. The value of $\Delta m_{31}^2 = (2.32_{-0.08}^{+0.12}) \times 10^{-3} \text{ eV}^2$ was assumed in the analysis. Superseded by AN 13.
- ³³ ABE 11 obtained this result by a three-neutrino oscillation analysis with the value of Δm_{32}^2 fixed to $2.4 \times 10^{-3} \text{ eV}^2$, using solar neutrino data including Super-Kamiokande, SNO, Borexino (ARPESELLA 08A), Homestake, GALLEX/GNO, SAGE, and KamLAND data. This result implies an upper bound of $\sin^2\theta_{13} < 0.059$ (95% CL) or $\sin^2 2\theta_{13} < 0.22$ (95% CL). The normal neutrino mass ordering and CPT invariance are assumed.
- ³⁴ ABE 11 obtained this result by a three-neutrino oscillation analysis with the value of Δm_{32}^2 fixed to $2.4 \times 10^{-3} \text{ eV}^2$, using solar neutrino data including Super-Kamiokande, SNO, Borexino (ARPESELLA 08A), Homestake, and GALLEX/GNO data. The normal neutrino mass ordering is assumed.
- ³⁵ The quoted limit is for $\Delta m_{32}^2 = 2.4 \times 10^{-3} \text{ eV}^2$, $\theta_{23} = \pi/2$, $\delta = 0$, and the normal mass ordering. For other values of δ , the 68% region spans from 0.03 to 0.25, and the 90% region from 0.02 to 0.32.
- ³⁶ The quoted limit is for $\Delta m_{32}^2 = 2.4 \times 10^{-3} \text{ eV}^2$, $\theta_{23} = \pi/2$, $\delta = 0$, and the inverted mass ordering. For other values of δ , the 68% region spans from 0.04 to 0.30, and the 90% region from 0.02 to 0.39.
- ³⁷ The quoted limit is for $\Delta m_{32}^2 = 2.32 \times 10^{-3} \text{ eV}^2$, $\theta_{23} = \pi/2$, $\delta = 0$, and the normal mass ordering. For other values of δ , the 68% region spans from 0.02 to 0.12, and the 90% region from 0 to 0.16.
- ³⁸ The quoted limit is for $\Delta m_{32}^2 = 2.32 \times 10^{-3} \text{ eV}^2$, $\theta_{23} = \pi/2$, $\delta = 0$, and the inverted mass ordering. For other values of δ , the 68% region spans from 0.02 to 0.16, and the 90% region from 0 to 0.21.
- ³⁹ FOGLI 11 obtained this result from an analysis using the atmospheric, accelerator long baseline, CHOOZ, solar, and KamLAND data. Recently, MUELLER 11 suggested an average increase of about 3.5% in normalization of the reactor $\bar{\nu}_e$ fluxes, and using these fluxes, the fitted result becomes 0.10 ± 0.03 .
- ⁴⁰ GANDO 11 report $\sin^2\theta_{13} = 0.020 \pm 0.016$. This result was obtained with three-neutrino fit using the KamLAND + solar data.
- ⁴¹ GANDO 11 report $\sin^2\theta_{13} = 0.032 \pm 0.037$. This result was obtained with three-neutrino fit using the KamLAND data only.

- 42 This result corresponds to the limit of <0.12 at 90% CL for $\Delta m_{32}^2 = 2.43 \times 10^{-3} \text{ eV}^2$, $\theta_{23} = \pi/2$, and $\delta = 0$. For other values of δ , the 90% CL region spans from 0 to 0.16.
- 43 This result corresponds to the limit of <0.20 at 90% CL for $\Delta m_{32}^2 = 2.43 \times 10^{-3} \text{ eV}^2$, $\theta_{23} = \pi/2$, and $\delta = 0$. For other values of δ , the 90% CL region spans from 0 to 0.21.
- 44 AHARMIM 10 global solar neutrino data include SNO's low-energy-threshold analysis survival probability day/night curves, SNO Phase III integral rates (AHARMIM 08), CI (CLEVELAND 98), SAGE (ABDURASHITOV 09), Gallex/GNO (HAMPEL 99, ALTMANN 05), Borexino (ARPESELLA 08A), SK-I zenith (HOSAKA 06), and SK-II day/night spectra (CRAVENS 08).
- 45 AHARMIM 10 obtained this result by a three-neutrino oscillation analysis with the value of Δm_{31}^2 fixed to $2.3 \times 10^{-3} \text{ eV}^2$, using global solar neutrino data and KamLAND data (ABE 08A). *CPT* invariance is assumed. This result implies an upper bound of $\sin^2 \theta_{13} < 0.057$ (95% CL) or $\sin^2 2\theta_{13} < 0.22$ (95% CL).
- 46 AHARMIM 10 obtained this result by a three-neutrino oscillation analysis with the value of Δm_{31}^2 fixed to $2.3 \times 10^{-3} \text{ eV}^2$, using global solar neutrino data.
- 47 WENDELL 10 obtained this result by a three-neutrino oscillation analysis with one mass scale dominance ($\Delta m_{21}^2 = 0$) using the Super-Kamiokande-I+II+III atmospheric neutrino data, and updates the HOSAKA 06A result.
- 48 The quoted limit is for $\Delta m_{32}^2 = 2.43 \times 10^{-3} \text{ eV}^2$, $\theta_{23} = \pi/2$, and $\delta = 0$. For other values of δ , the 68% CL region spans from 0.02 to 0.26.
- 49 The quoted limit is for $\Delta m_{32}^2 = 2.43 \times 10^{-3} \text{ eV}^2$, $\theta_{23} = \pi/2$, and $\delta = 0$. For other values of δ , the 68% CL region spans from 0.04 to 0.34.
- 50 FOGLI 08 obtained this result from a global analysis of all neutrino oscillation data, that is, solar + KamLAND + atmospheric + accelerator long baseline + CHOOZ.
- 51 FOGLI 08 obtained this result from an analysis using the solar and KamLAND neutrino oscillation data.
- 52 FOGLI 08 obtained this result from an analysis using the atmospheric, accelerator long baseline, and CHOOZ neutrino oscillation data.
- 53 YAMAMOTO 06 searched for $\nu_\mu \rightarrow \nu_e$ appearance. Assumes $2 \sin^2(2\theta_{\mu e}) = \sin^2(2\theta_{13})$. The quoted limit is for $\Delta m_{32}^2 = 1.9 \times 10^{-3} \text{ eV}^2$. That value of Δm_{32}^2 is the one- σ low value for AHN 06A. For the AHN 06A best fit value of $2.8 \times 10^{-3} \text{ eV}^2$, the $\sin^2(2\theta_{13})$ limit is < 0.26 . Supersedes AHN 04.
- 54 AHN 04 searched for $\nu_\mu \rightarrow \nu_e$ appearance. Assuming $2 \sin^2(2\theta_{\mu e}) = \sin^2(2\theta_{13})$, a limit on $\sin^2(2\theta_{\mu e})$ is converted to a limit on $\sin^2(2\theta_{13})$. The quoted limit is for $\Delta m_{32}^2 = 1.9 \times 10^{-3} \text{ eV}^2$. That value of Δm_{32}^2 is the one- σ low value for ALIU 05. For the ALIU 05 best fit value of $2.8 \times 10^{-3} \text{ eV}^2$, the $\sin^2(2\theta_{13})$ limit is < 0.30 .
- 55 The quoted limit is for $\Delta m_{32}^2 = 1.9 \times 10^{-3} \text{ eV}^2$. That value of Δm_{32}^2 is the 1- σ low value for ALIU 05. For the ALIU 05 best fit value of $2.8 \times 10^{-3} \text{ eV}^2$, the $\sin^2 2\theta_{13}$ limit is < 0.19 . In this range, the θ_{13} limit is larger for lower values of Δm_{32}^2 , and smaller for higher values of Δm_{32}^2 .
- 56 The quoted limit is for $\Delta m_{32}^2 = 1.9 \times 10^{-3} \text{ eV}^2$. That value of Δm_{32}^2 is the 1- σ low value for ALIU 05. For the ALIU 05 best fit value of $2.8 \times 10^{-3} \text{ eV}^2$, the $\sin^2 2\theta_{13}$ limit is < 0.23 .
- 57 The quoted limit is for $\Delta m_{32}^2 = 2.43 \times 10^{-3} \text{ eV}^2$. That value of Δm_{32}^2 is the central value for ADAMSON 08. For the ADAMSON 08 1- σ low value of $2.30 \times 10^{-3} \text{ eV}^2$, the $\sin^2 2\theta_{13}$ limit is < 0.16 . See also APOLLONIO 03 for a detailed description of the experiment.

————— **CP violating phase** —————

δ , CP violating phase

Measurements of δ come from atmospheric and accelerator experiments looking at ν_e appearance. We encode values between 0 and 2π , though it is equivalent to use $-\pi$ to π .

<u>VALUE (π rad)</u>	<u>CL%</u>	<u>DOCUMENT ID</u>	<u>TECN</u>	<u>COMMENT</u>	
1.23\pm0.21	OUR AVERAGE	Error includes scale factor of 1.3. See the ideogram below.			
0.82 ^{+0.27} _{-0.87}	1,2	ACERO	22 NOVA	Normal mass ordering, octant II for θ_{23} , θ_{13} constrained	
1.40 ^{+0.22} _{-0.18}	3	ABE	20F T2K	Normal mass ordering	
1.33 ^{+0.45} _{-0.51}	4	ABE	18B SKAM	Normal mass ordering, θ_{13} constrained	
● ● ● We do not use the following data for averages, fits, limits, etc. ● ● ●					
1.52 ^{+0.30} _{-0.41}	1,5	ACERO	22 NOVA	Inverted mass ordering, octant II for θ_{23} , θ_{13} constrained	
1.08 ^{+0.13} _{-0.12}	6	SALAS	21 FIT	Normal mass ordering, global fit	
1.58 ^{+0.15} _{-0.16}	6	SALAS	21 FIT	Inverted mass ordering, global fit	
1.09 ^{+0.15} _{-0.13}	7	ESTEBAN	20A FIT	Normal mass ordering, global fit	
1.57 ^{+0.14} _{-0.17}	7	ESTEBAN	20A FIT	Inverted mass ordering, global fit	
0.0 ^{+1.3} _{-0.4}	8	ACERO	19 NOVA	Normal mass ordering, octant II for θ_{23}	
1.33 ^{+0.46} _{-0.53}	9	ABE	18B SKAM	3ν osc: normal mass ordering, θ_{13} free	
1.22 ^{+0.76} _{-0.67}	9	ABE	18B SKAM	3ν osc: inverted mass ordering, θ_{13} free	
1.33 ^{+0.48} _{-0.53}	4	ABE	18B SKAM	3ν osc: inverted mass ordering, θ_{13} constrained	
1.40 \pm 0.20	10	ABE	18G T2K	Normal mass ordering, θ_{13} constrained	
1.54 ^{+0.14} _{-0.12}	95	10	ABE	18G T2K	Inverted mass ordering, θ_{13} constrained
1.21 ^{+0.91} _{-0.30}	11	ACERO	18 NOVA	Normal mass ordering, octant II for θ_{23}	
1.46 ^{+0.56} _{-0.42}	11	ACERO	18 NOVA	Normal mass order; octant I for θ_{23}	
1.32 ^{+0.21} _{-0.15}		DE-SALAS	18 FIT	Normal mass ordering, global fit	
1.56 ^{+0.13} _{-0.15}		DE-SALAS	18 FIT	Inverted mass ordering, global fit	
1.45 ^{+0.27} _{-0.26}	12	ABE	17F T2K	Normal mass ordering	
1.54 ^{+0.22} _{-0.23}	12	ABE	17F T2K	Inverted mass ordering	
1.50 ^{+0.53} _{-0.57}	13	ADAMSON	17B NOVA	Inverted mass ordering; θ_{23} in octant II	
0.74 ^{+0.57} _{-0.93}	13	ADAMSON	17B NOVA	Normal mass ordering; θ_{23} in octant II	

$1.48^{+0.69}_{-0.58}$		¹³ ADAMSON	17B	NOVA	Normal mass ordering; θ_{23} in octant I
0.0 to 0.1, 0.5 to 2.0	90	^{13,14} ADAMSON	16	NOVA	Inverted mass ordering
0.0 to 2.0	90	¹⁴ ADAMSON	16	NOVA	Normal mass ordering
0 to 0.15, 0.83 to 2	90	ABE	15D	T2K	Normal mass ordering
1.09 to 1.92	90	ABE	15D	T2K	Inverted mass ordering
0.05 to 1.2	90	¹⁵ ADAMSON	14	MINS	Normal mass ordering
$1.34^{+0.64}_{-0.38}$		FORERO	14	FIT	Normal mass ordering
$1.48^{+0.34}_{-0.32}$		FORERO	14	FIT	Inverted mass ordering
$1.70^{+0.22}_{-0.39}$		¹⁶ GONZALEZ...	14	FIT	Normal mass ordering; global fit
$1.41^{+0.35}_{-0.34}$		¹⁶ GONZALEZ...	14	FIT	Inverted mass ordering; global fit
0 to 1.5 or 1.9 to 2	90	¹⁷ ADAMSON	13A	MINS	Normal mass ordering

¹ ACERO 22 uses data from Jun 29, 2016 to Feb 26, 2019 (12.5×10^{20} POT) and Feb 6, 2014 to Mar 20, 2020 (13.6×10^{20} POT). Results for normal and inverted mass ordering, and θ_{23} octant I and II are presented. Supersedes ACERO 19.

² For the octant I (lower octant), the 68% CL allowed region is discontinuous, and all delta values are allowed at 90% CL.

³ ABE 20F results are based on data collected between 2009 and 2018 in (anti)neutrino mode and include a neutrino beam exposure of 1.49×10^{21} (1.64×10^{21}) protons on target. For inverted mass ordering, the quoted result is $1.56^{+0.15}_{-0.17} \pi$ rad. Supersedes ABE 18G.

⁴ ABE 18B uses 328 kton-years of Super-Kamiokande I-IV atmospheric neutrino data to obtain this result. The fit is performed over the three parameters, Δm_{32}^2 , $\sin^2 \theta_{23}$, and δ , while the solar parameters and $\sin^2 \theta_{23}$ are fixed to $\Delta m_{21}^2 = (7.53 \pm 0.18) \times 10^{-5} \text{ eV}^2$, $\sin^2 \theta_{12} = 0.304 \pm 0.014$, and $\sin^2 \theta_{13} = 0.0219 \pm 0.0012$.

⁵ The inverted mass ordering is rejected at 1.0σ . The quoted error bars are based on the local best-fit point.

⁶ SALAS 21 reports results of a global fit to neutrino oscillation data available at the time of the Neutrino 2020 conference.

⁷ ESTEBAN 20A reports results of a global fit to neutrino oscillation data available at the time of the Neutrino 2020 conference.

⁸ ACERO 19 is based on a sample size of 1.33×10^{20} protons on target with combined antineutrino and neutrino data. Superseded by ACERO 22.

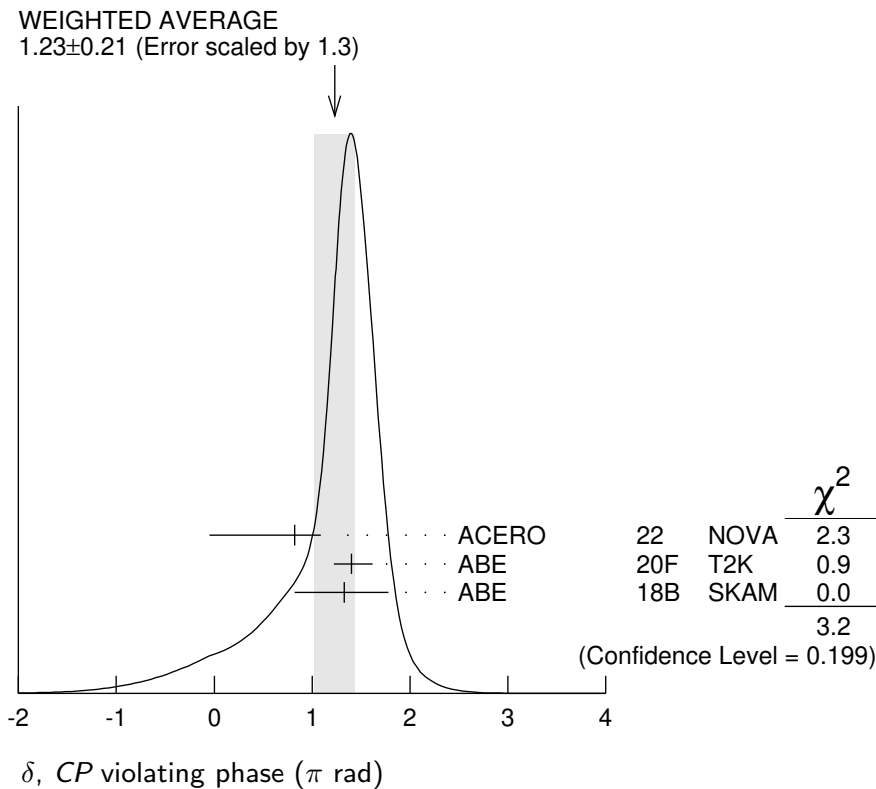
⁹ ABE 18B uses 328 kton-years of Super-Kamiokande I-IV atmospheric neutrino data to obtain this result. The fit is performed over the four parameters, Δm_{32}^2 , $\sin^2 \theta_{23}$, $\sin^2 \theta_{13}$, and δ , while the solar parameters are fixed to $\Delta m_{21}^2 = (7.53 \pm 0.18) \times 10^{-5} \text{ eV}^2$ and $\sin^2 \theta_{12} = 0.304 \pm 0.014$.

¹⁰ ABE 18G confidence intervals are marginalized over both mass orderings. Normal order preferred with a posterior probability of 87%. The 1-sigma result for normal mass ordering used in the average was provided by the experiment via private communications. Supersedes ABE 17F.

¹¹ ACERO 18 performs a joint fit to the data for ν_{μ} disappearance and ν_e appearance. The overall best fit favors normal mass ordering and θ_{23} in octant II. No 1σ confidence intervals are presented for the inverted mass ordering scenarios. Superseded by ACERO 19.

¹² ABE 17F confidence intervals are obtained using a frequentist analysis including θ_{13} constraint from reactor experiments. Bayesian intervals based on Markov Chain Monte Carlo method are also provided by the authors. Superseded by ABE 18G.

- 13 Errors are projections of 68% C.L. curve of δ_{CP} vs. $\sin^2\theta_{23}$.
- 14 ADAMSON 16 result is based on a data sample with 2.74×10^{20} protons on target. The likelihood-based analysis observed 6 ν_e events with an expected background of 0.99 ± 0.11 events.
- 15 ADAMSON 14 result is based on three-flavor formalism and $\theta_{23} > \pi/4$. Likelihood as a function of δ is also shown for the other three combinations of hierarchy and θ_{23} octants; all values of δ are allowed at 90% C.L.
- 16 GONZALEZ-GARCIA 14 result comes from a frequentist global fit. The corresponding Bayesian global fit to the same data results are reported in BERGSTROM 15 as 68% CL intervals of 1.24–1.94 for normal and 1.15–1.77 for inverted mass ordering.
- 17 ADAMSON 13A result is based on ν_e appearance in MINOS and the calculated $\sin^2(2\theta_{23}) = 0.957, \theta_{23} > \pi/4$, and normal mass hierarchy. Likelihood as a function of δ is also shown for the other three combinations of hierarchy and θ_{23} octants; all values of δ are allowed at 90% C.L.



(C) Other neutrino mixing results

The LSND collaboration reported in AGUILAR 01 a signal which is consistent with $\bar{\nu}_\mu \rightarrow \bar{\nu}_e$ oscillations. In a three neutrino framework, this would be a measurement of θ_{12} and Δm_{21}^2 . This does not appear to be consistent with most of the other neutrino data. The following listings include results from $\nu_\mu \rightarrow \nu_e, \bar{\nu}_\mu \rightarrow \bar{\nu}_e$ appearance and $\nu_\mu, \bar{\nu}_\mu, \nu_e,$ and $\bar{\nu}_e$ disappearance experiments, and searches for *CPT* violation.

$\Delta(m^2)$ for $\sin^2(2\theta) = 1$ ($\nu_\mu \rightarrow \nu_e$)

VALUE (eV ²)	CL%	DOCUMENT ID	TECN	COMMENT
--------------------------	-----	-------------	------	---------

• • • We do not use the following data for averages, fits, limits, etc. • • •

0.03 to 0.55	90	¹ AGUILAR-AR...21	MBNE	MiniBooNE	$\nu, \bar{\nu}$ combined
0.03 to 0.05	90	² AGUILAR-AR...18C	MBNE	MiniBooNE	$\nu, \bar{\nu}$ combined
0.015 to 0.050	90	³ AGUILAR-AR...13A	MBNE	MiniBooNE	
<0.34	90	⁴ MAHN	12	MBNE	MiniBooNE/SciBooNE
<0.034	90	AGUILAR-AR...07	MBNE	MiniBooNE	
<0.0008	90	AHN	04	K2K	Water Cherenkov
<0.4	90	ASTIER	03	NOMD	CERN SPS
<2.4	90	AVVAKUMOV	02	NTEV	NUTEV FNAL
		⁵ AGUILAR	01	LSND	$\nu_\mu \rightarrow \nu_e$ osc.prob.
0.03 to 0.3	95	⁶ ATHANASSO...98	LSND		$\nu_\mu \rightarrow \nu_e$
<2.3	90	⁷ LOVERRE	96		CHARM/CDHS
<0.9	90	VILAIN	94C	CHM2	CERN SPS
<0.09	90	ANGELINI	86	HLBC	BEBC CERN PS

¹ AGUILAR-AREVALO 21 result is based on a total of 18.75×10^{20} POT in neutrino mode, and 11.27×10^{20} POT in anti-neutrino mode. Best fit at 0.043 eV^2 . The allowed region does not extend to large Δm^2 . The quoted value is the entire allowed region of Δm^2 at 90% C.L. for all values of $\sin^2(2\theta)$. Supersedes AGUILAR-AREVALO 18C.

² AGUILAR-AREVALO 18C result is based on $\nu_\mu \rightarrow \nu_e$ appearance of 460.5 ± 99.0 events; The best fit value is $\Delta m^2 = 0.041 \text{ eV}^2$. Superseded by AGUILAR-AREVALO 21.

³ AGUILAR-AREVALO 13A result is based on $\nu_\mu \rightarrow \nu_e$ appearance of 162.0 ± 47.8 events; marginally compatible with twoneutrino oscillations. The best fit value is $\Delta m^2 = 3.14 \text{ eV}^2$.

⁴ MAHN 12 is a combined spectral fit of MiniBooNE and SciBooNE neutrino data with the range of Δm^2 up to 25 eV^2 . The best limit is 0.04 at 7 eV^2 .

⁵ AGUILAR 01 is the final analysis of the LSND full data set. Search is made for the $\nu_\mu \rightarrow \nu_e$ oscillations using ν_μ from π^+ decay in flight by observing beam-on electron events from $\nu_e C \rightarrow e^- X$. Present analysis results in $8.1 \pm 12.2 \pm 1.7$ excess events in the $60 < E_e < 200 \text{ MeV}$ energy range, corresponding to oscillation probability of $0.10 \pm 0.16 \pm 0.04\%$. This is consistent, though less significant, with the previous result of ATHANASSOPOULOS 98, which it supersedes. The present analysis uses selection criteria developed for the decay at rest region, and is less effective in removing the background above 60 MeV than ATHANASSOPOULOS 98.

⁶ ATHANASSOPOULOS 98 is a search for the $\nu_\mu \rightarrow \nu_e$ oscillations using ν_μ from π^+ decay in flight. The 40 observed beam-on electron events are consistent with $\nu_e C \rightarrow e^- X$; the expected background is 21.9 ± 2.1 . Authors interpret this excess as evidence for an oscillation signal corresponding to oscillations with probability $(0.26 \pm 0.10 \pm 0.05)\%$. Although the significance is only 2.3σ , this measurement is an important and consistent cross check of ATHANASSOPOULOS 96 who reported evidence for $\bar{\nu}_\mu \rightarrow \bar{\nu}_e$ oscillations from μ^+ decay at rest. See also ATHANASSOPOULOS 98B.

⁷ LOVERRE 96 uses the charged-current to neutral-current ratio from the combined CHARM (ALLABY 86) and CDHS (ABRAMOWICZ 86) data from 1986.

$\sin^2(2\theta)$ for "Large" $\Delta(m^2)$ ($\nu_\mu \rightarrow \nu_e$)

VALUE (units 10^{-3})	CL%	DOCUMENT ID	TECN	COMMENT
● ● ● We do not use the following data for averages, fits, limits, etc. ● ● ●				
6 to 1000	90	¹ AGUILAR-AR...21	MBNE	MiniBooNE; $\nu + \bar{\nu}$
< 5	90	² AGUILAR-AR...18C	MBNE	MiniBooNE; $\nu + \bar{\nu}$
< 7.2	90	AGAFONOVA 13	OPER	$\Delta(m^2) > 0.1 \text{ eV}^2$
0.8 to 3	90	³ AGUILAR-AR...13A	MBNE	MiniBooNE
< 11	90	⁴ ANTONELLO 13	ICAR	$\nu_\mu \rightarrow \nu_e$

< 6.8	90	⁵ ANTONELLO	13A	ICAR	$\nu_\mu \rightarrow \nu_e$
<100	90	⁶ MAHN	12	MBNE	MiniBooNE/SciBooNE
< 1.8	90	⁷ AGUILAR-AR...	07	MBNE	MiniBooNE
<110	90	⁸ AHN	04	K2K	Water Cherenkov
< 1.4	90	ASTIER	03	NOMD	CERN SPS
< 1.6	90	AVVAKUMOV	02	NTEV	NUTEV FNAL
		⁹ AGUILAR	01	LSND	$\nu_\mu \rightarrow \nu_e$ osc.prob.
0.5 to 30	95	¹⁰ ATHANASSO...	98	LSND	$\nu_\mu \rightarrow \nu_e$
< 3.0	90	¹¹ LOVERRE	96		CHARM/CDHS
< 9.4	90	VILAIN	94C	CHM2	CERN SPS
< 5.6	90	¹² VILAIN	94C	CHM2	CERN SPS

¹ AGUILAR-AREVALO 21 result is based on a total of 18.75×10^{20} POT in neutrino mode, and 11.27×10^{20} POT in anti-neutrino mode. The best fit value is $\sin^2(2\theta)=0.807$. The allowed region does not extend to large Δm^2 . The quoted value is the entire allowed region of $\sin^2(2\theta)$ at 90% C.L. for all values of Δm^2 . Supersedes AGUILAR-AREVALO 18C.

² AGUILAR-AREVALO 18C result is based on $\nu_\mu \rightarrow \nu_e$ appearance of 460.5 ± 99.0 events; The best fit value is $\sin^2(2\theta) = 0.92$. The quoted limit for the two-neutrino mixing angle θ is valid above $\Delta m^2 = 0.59 \text{ eV}^2$. Superseded by AGUILAR-AREVALO 21.

³ AGUILAR-AREVALO 13A result is based on $\nu_\mu \rightarrow \nu_e$ appearance of 162.0 ± 47.8 events; marginally compatible with two neutrino oscillations. The best fit value is $\sin^2(2\theta) = 0.002$.

⁴ ANTONELLO 13 use the ICARUS T600 detector at LNGS and ~ 20 GeV beam of ν_μ from CERN 730 km away to search for an excess of ν_e events. Two events are found with 3.7 ± 0.6 expected from conventional sources. This result excludes some parts of the parameter space expected by LSND. Superseded by ANTONELLO 13A.

⁵ Based on four events with a background of 6.4 ± 0.9 from conventional sources with an average energy of 20 GeV and 730 km from the source of ν_μ .

⁶ MAHN 12 is a combined fit of MiniBooNE and SciBooNE neutrino data.

⁷ The limit is $\sin^2 2\theta < 0.9 \times 10^{-3}$ at $\Delta m^2 = 2 \text{ eV}^2$. That value of Δm^2 corresponds to the smallest mixing angle consistent with the reported signal from LSND in AGUILAR 01.

⁸ The limit becomes $\sin^2 2\theta < 0.15$ at $\Delta m^2 = 2.8 \times 10^{-3} \text{ eV}^2$, the best-fit value of the ν_μ disappearance analysis in K2K.

⁹ AGUILAR 01 is the final analysis of the LSND full data set of the search for the $\nu_\mu \rightarrow \nu_e$ oscillations. See footnote in preceding table for further details.

¹⁰ ATHANASSOPOULOS 98 report $(0.26 \pm 0.10 \pm 0.05)\%$ for the oscillation probability; the value of $\sin^2 2\theta$ for large Δm^2 is deduced from this probability. See footnote in preceding table for further details, and see the paper for a plot showing allowed regions. If effect is due to oscillation, it is most likely to be intermediate $\sin^2 2\theta$ and Δm^2 . See also ATHANASSOPOULOS 98B.

¹¹ LOVERRE 96 uses the charged-current to neutral-current ratio from the combined CHARM (ALLABY 86) and CDHS (ABRAMOWICZ 86) data from 1986.

¹² VILAIN 94C limit derived by combining the ν_μ and $\bar{\nu}_\mu$ data assuming CP conservation.

$\Delta(m^2)$ for $\sin^2(2\theta) = 1$ ($\bar{\nu}_\mu \rightarrow \bar{\nu}_e$)

VALUE (eV ²)	CL%	DOCUMENT ID	TECN	COMMENT
● ● ● We do not use the following data for averages, fits, limits, etc. ● ● ●				
0.023 to 0.060	90	¹ AGUILAR-AR... 13A	MBNE	MiniBooNE
<0.16	90	² CHENG 12	MBNE	MiniBooNE/SciBooNE

0.03–0.09	90	³ AGUILAR-AR...10	MBNE	$E_\nu > 475$ MeV
0.03–0.07	90	⁴ AGUILAR-AR...10	MBNE	$E_\nu > 200$ MeV
<0.06	90	AGUILAR-AR...09B	MBNE	MiniBooNE
<0.055	90	⁵ ARMBRUSTER02	KAR2	Liquid Sci. calor.
<2.6	90	AVVAKUMOV 02	NTEV	NUTEV FNAL
0.03–0.05		⁶ AGUILAR 01	LSND	LAMPF
0.05–0.08	90	⁷ ATHANASSO...96	LSND	LAMPF
0.048–0.090	80	⁸ ATHANASSO...95		
<0.07	90	⁹ HILL 95		
<0.9	90	VILAIN 94C	CHM2	CERN SPS
<0.14	90	¹⁰ FREEDMAN 93	CNTR	LAMPF

¹ Based on $\bar{\nu}_\mu \rightarrow \bar{\nu}_e$ appearance of 78.4 ± 28.5 events. The best fit values are $\Delta m^2 = 0.043 \text{ eV}^2$ and $\sin^2 2\theta = 0.88$.

² CHENG 12 is a combined fit of MiniBooNE and SciBooNE antineutrino data.

³ This value is for a two neutrino oscillation analysis for excess antineutrino events with $E_\nu > 475$ MeV. The best fit is at 0.07. The allowed region is consistent with LSND reported by AGUILAR 01. Supersedes AGUILAR-AREVALO 09B.

⁴ This value is for a two neutrino oscillation analysis for excess antineutrino events with $E_\nu > 200$ MeV with subtraction of the expected 12 events low energy excess seen in the neutrino component of the beam. The best fit value is 0.007 for $\Delta(m^2) = 4.4 \text{ eV}^2$.

⁵ ARMBRUSTER 02 is the final analysis of the KARMEN 2 data for 17.7 m distance from the ISIS stopped pion and muon neutrino source. It is a search for $\bar{\nu}_e$, detected by the inverse β -decay reaction on protons and ^{12}C . 15 candidate events are observed, and 15.8 ± 0.5 background events are expected, hence no oscillation signal is detected. The results exclude large regions of the parameter area favored by the LSND experiment.

⁶ AGUILAR 01 is the final analysis of the LSND full data set. It is a search for $\bar{\nu}_e$ 30 m from LAMPF beam stop. Neutrinos originate mainly for π^+ decay at rest. $\bar{\nu}_e$ are detected through $\bar{\nu}_e p \rightarrow e^+ n$ ($20 < E_{e^+} < 60$ MeV) in delayed coincidence with $np \rightarrow d\gamma$. Authors observe $87.9 \pm 22.4 \pm 6.0$ total excess events. The observation is attributed to $\bar{\nu}_\mu \rightarrow \bar{\nu}_e$ oscillations with the oscillation probability of $0.264 \pm 0.067 \pm 0.045\%$, consistent with the previously published result. Taking into account all constraints, the most favored allowed region of oscillation parameters is a band of $\Delta(m^2)$ from $0.2\text{--}2.0 \text{ eV}^2$. Supersedes ATHANASSOPOULOS 95, ATHANASSOPOULOS 96, and ATHANASSOPOULOS 98.

⁷ ATHANASSOPOULOS 96 is a search for $\bar{\nu}_e$ 30 m from LAMPF beam stop. Neutrinos originate mainly from π^+ decay at rest. $\bar{\nu}_e$ could come from either $\bar{\nu}_\mu \rightarrow \bar{\nu}_e$ or $\nu_e \rightarrow \bar{\nu}_e$; our entry assumes the first interpretation. They are detected through $\bar{\nu}_e p \rightarrow e^+ n$ ($20 \text{ MeV} < E_{e^+} < 60 \text{ MeV}$) in delayed coincidence with $np \rightarrow d\gamma$. Authors observe $51 \pm 20 \pm 8$ total excess events over an estimated background 12.5 ± 2.9 . ATHANASSOPOULOS 96B is a shorter version of this paper.

⁸ ATHANASSOPOULOS 95 error corresponds to the 1.6σ band in the plot. The expected background is 2.7 ± 0.4 events. Corresponds to an oscillation probability of $(0.34^{+0.20}_{-0.18} \pm 0.07)\%$. For a different interpretation, see HILL 95. Replaced by ATHANASSOPOULOS 96.

⁹ HILL 95 is a report by one member of the LSND Collaboration, reporting a different conclusion from the analysis of the data of this experiment (see ATHANASSOPOULOS 95). Contrary to the rest of the LSND Collaboration, Hill finds no evidence for the neutrino oscillation $\bar{\nu}_\mu \rightarrow \bar{\nu}_e$ and obtains only upper limits.

¹⁰ FREEDMAN 93 is a search at LAMPF for $\bar{\nu}_e$ generated from any of the three neutrino types ν_μ , $\bar{\nu}_\mu$, and ν_e which come from the beam stop. The $\bar{\nu}_e$'s would be detected by the reaction $\bar{\nu}_e p \rightarrow e^+ n$. FREEDMAN 93 replaces DURKIN 88.

$\sin^2(2\theta)$ for "Large" $\Delta(m^2)$ ($\bar{\nu}_\mu \rightarrow \bar{\nu}_e$)

VALUE (units 10^{-3})	CL%	DOCUMENT ID	TECN	COMMENT
● ● ● We do not use the following data for averages, fits, limits, etc. ● ● ●				
<640	90	1 ANTONELLO 13A	ICAR	$\bar{\nu}_e$ appearance
<150	90	2 CHENG 12	MBNE	MiniBooNE/SciBooNE
0.4–9.0	99	3 AGUILAR-AR...10	MBNE	$E_\nu > 475$ MeV
0.4–9.0	99	4 AGUILAR-AR...10	MBNE	$E_\nu > 200$ MeV
< 3.3	90	5 AGUILAR-AR...09B	MBNE	MiniBooNE
< 1.7	90	6 ARMBRUSTER02	KAR2	Liquid Sci. calor.
< 1.1	90	AVVAKUMOV 02	NTEV	NUTEV FNAL
$5.3 \pm 1.3 \pm 9.0$		7 AGUILAR 01	LSND	LAMPF
$6.2 \pm 2.4 \pm 1.0$		8 ATHANASSO...96	LSND	LAMPF
3–12	80	9 ATHANASSO...95		
< 6	90	10 HILL 95		

¹ ANTONELLO 13A obtained the limit by assuming $\bar{\nu}_\mu \rightarrow \bar{\nu}_e$ oscillation from the $\sim 2\%$ of $\bar{\nu}_\mu$ evnets contamination in the CNGS beam.

² CHENG 12 is a combined fit of MiniBooNE and SciBooNE antineutrino data.

³ This value is for a two neutrino oscillation analysis for excess antineutrino events with $E_\nu > 475$ MeV. At 90% CL there is no solution at high $\Delta(m^2)$. The best fit is at maximal mixing. The allowed region is consistent with LSND reported by AGUILAR 01. Supersedes AGUILAR-AREVALO 09B.

⁴ This value is for a two neutrino oscillation analysis for excess antineutrino events with $E_\nu > 200$ MeV with subtraction of the expected 12 events low energy excess seen in the neutrino component of the beam. At 90% CL there is no solution at high $\Delta(m^2)$. The best fit value is 0.007 for $\Delta(m^2) = 4.4 \text{ eV}^2$.

⁵ This result is inconclusive with respect to small amplitude mixing suggested by LSND.

⁶ ARMBRUSTER 02 is the final analysis of the KARMEN 2 data. See footnote in the preceding table for further details, and the paper for the exclusion plot.

⁷ AGUILAR 01 is the final analysis of the LSND full data set. The deduced oscillation probability is $0.264 \pm 0.067 \pm 0.045\%$; the value of $\sin^2 2\theta$ for large $\Delta(m^2)$ is twice this probability (although these values are excluded by other constraints). See footnote in preceding table for further details, and the paper for a plot showing allowed regions. Supersedes ATHANASSOPOULOS 95, ATHANASSOPOULOS 96, and ATHANASSOPOULOS 98.

⁸ ATHANASSOPOULOS 96 reports $(0.31 \pm 0.12 \pm 0.05)\%$ for the oscillation probability; the value of $\sin^2 2\theta$ for large $\Delta(m^2)$ should be twice this probability. See footnote in preceding table for further details, and see the paper for a plot showing allowed regions.

⁹ ATHANASSOPOULOS 95 error corresponds to the 1.6σ band in the plot. The expected background is 2.7 ± 0.4 events. Corresponds to an oscillation probability of $(0.34^{+0.20}_{-0.18} \pm 0.07)\%$. For a different interpretation, see HILL 95. Replaced by ATHANASSOPOULOS 96.

¹⁰ HILL 95 is a report by one member of the LSND Collaboration, reporting a different conclusion from the analysis of the data of this experiment (see ATHANASSOPOULOS 95). Contrary to the rest of the LSND Collaboration, Hill finds no evidence for the neutrino oscillation $\bar{\nu}_\mu \rightarrow \bar{\nu}_e$ and obtains only upper limits.

———— Sterile neutrino limits ————

$\Delta(m^2)$ for $\sin^2(2\theta) = 1$ ($\nu_\mu \rightarrow \nu_s$)

ν_s means ν_τ or any sterile (noninteracting) ν .

VALUE (10^{-5} eV^2)	CL%	DOCUMENT ID	TECN	COMMENT
----------------------------------	-----	-------------	------	---------

● ● ● We do not use the following data for averages, fits, limits, etc. ● ● ●

<3000 (or <550)	90	¹ OYAMA	89	KAMI	Water Cherenkov
< 4.2 or > 54.	90	BIONTA	88	IMB	Flux has $\nu_\mu, \bar{\nu}_\mu, \nu_e,$ and $\bar{\nu}_e$

¹ OYAMA 89 gives a range of limits, depending on assumptions in their analysis. They argue that the region $\Delta(m^2) = (100-1000) \times 10^{-5} \text{ eV}^2$ is not ruled out by any data for large mixing.

Search for ν_μ or $\nu_e \rightarrow \nu_s$

VALUE	CL%	DOCUMENT ID	TECN	COMMENT
● ● ● We do not use the following data for averages, fits, limits, etc. ● ● ●				
<0.05	95	¹ ALMAZAN	23	STEREO
<0.02	95	² AKER	22A	SPEC T β decay
<0.0035	95	³ ATIF	22	RENO, NEOS
0.42 $\begin{smallmatrix} +0.15 \\ -0.17 \end{smallmatrix}$	68	⁴ BARINOV	22A	BEST
<0.05	95	⁵ ANDRIAMIR...	21	PROSPECT
<0.005	95	⁶ SEREBROV	21	Neutrino-4
<0.008	95	⁷ SKROBOVA	20	DANSS
<0.01	90	⁸ ALEKSEEV	18	DANSS
<0.06	90	⁹ ALMAZAN	18	STEREO
<0.1	95	¹⁰ ASHENFELT...	18	PROSPECT
<0.4	90	¹¹ AARTSEN	17B	ICCB IceCube-DeepCore
<8	×	¹² ABDURASHI...	17	T β decay
10^{-3}				
<1	×	¹³ KO	17	NEOS
10^{-2}				
<2	×	¹⁴ AARTSEN	16	ICCB IceCube
10^{-2}				
<4.5	×	¹⁵ ADAMSON	16B	MINOS, DayaBay
10^{-4}				
<8.6	×	¹⁶ ADAMSON	16C	MINS
10^{-2}				
<1.1	×	¹⁷ AN	16B	DAYA
10^{-2}				
		¹⁸ AMBROSIO	01	MCRO matter effects
		¹⁹ FUKUDA	00	SKAM neutral currents + matter effects

¹ ALMAZAN 23 use inverse beta decay data collected by the STEREO experiment, placed 9 to 11 m from the ILL research reactor, to search for $\bar{\nu}_e \rightarrow \bar{\nu}_s$ oscillations. The ILL research reactor uses highly enriched ^{235}U fuel. No indication of the oscillation to sterile neutrinos is found, the stated limit on $\sin^2(2\theta_{14})$ correspond to $\Delta m_{41}^2 \sim 1 \text{ eV}^2$ where the exclusion is maximal. Supersedes ALMAZAN 18.

² AKER 22A uses the first two science runs of the KATRIN tritium β decay neutrino mass experiment to search for an admixture of sterile neutrinos. No evidence is found for a spectral anomaly, indicating such admixture. The resulting limit is on $\sin^2(2\theta_{14})$ for sterile neutrino masses $m_4 < 40 \text{ eV}$. It is most restrictive at $\Delta m_{41}^2 \sim 400 \text{ eV}^2$. A 3+1 model is assumed.

³ ATIF 22 report results from the combined analysis of the RENO (419 m) and NEOS (24 m) experiments data, collected at the Hanbit Nuclear Power Plant. Results, in terms of $\sin^2(2\theta_{14})$, constrain for $\bar{\nu}_e \rightarrow \bar{\nu}_s$ oscillations. The authors report both excluded and allowed parameter combinations. The exclusion result reported here is based on the Feldman-Cousins method and for $\Delta m_{41}^2 \simeq 0.55 \text{ eV}^2$. Part of the allowed area is excluded by the STEREO and PROSPECT experiments.

- ⁴ BARINOV 22A report an event deficit observed using the segmented Baksan Ga neutrino detector, exposed to a 3.4 MCi ^{51}Cr source. Equal suppression factors are observed for the inner and outer segments. The deficit is interpreted as evidence for oscillations to sterile neutrinos. The result is in terms of $\sin^2(2\theta_{14})$, for a best fit of $\Delta m_{41}^2 = 3.3^{+\infty}_{-2.3} \text{ eV}^2$. Some, but not all, of the allowed neutrino parameter space conflicts with other experiments.
- ⁵ ANDRIAMIRADO 21 reports a search for $\bar{\nu}_e \rightarrow \bar{\nu}_s$ oscillations at the HFIR research reactor, at baselines from 6.7 to 9.2 m. The reactor has a ^{235}U core. 4 tons of ^6Li -doped liquid scintillator are used in a segmented detector. Oscillations into sterile neutrinos are disfavored. The stated limit for $\sin^2(2\theta_{14})$ is for $\Delta m_{41}^2 \sim 2 \text{ eV}^2$ where the sensitivity is maximal.
- ⁶ SEREBROV 21 searches for $\bar{\nu}_e \rightarrow \bar{\nu}_s$ oscillations with a moveable detector with baseline 6–12 m from the SM-3 research reactor with highly enriched ^{235}U fuel. Analyzing the L/E dependence a χ^2 minimum is found at $\Delta m_{41}^2 = 7.3 \pm 0.13 \pm 1.16 \text{ eV}^2$ and $\sin^2(2\theta_{14}) = 0.36 \pm 0.12$. The quoted limit of 0.005 for $\sin^2(2\theta_{14})$ corresponds to $\Delta m_{41}^2 \sim 2 \text{ eV}^2$. This is the result from 720 days of reactor ON and 860 days of reactor OFF measurements. The significance of the χ^2 minimum is 2.9σ . Supersedes SEREBROV 20, SEREBROV 19 and SEREBROV 18A.
- ⁷ SKROBOVA 20 searches for $\bar{\nu}_e - \bar{\nu}_s$ oscillations using the DANSS detector at 10.7, 11.2, and 12.7 m from the 3.1 GW_{th} power reactor. The DANSS detector is highly segmented and moveable; the positions are changed usually 3 times a week. The analysis is based on the ratio of the events at top and bottom position; the middle position is used for checks of consistency. No evidence for sterile neutrinos is found. The quoted limit 0.008, the smallest excluded $\sin^2(2\theta_{14})$, corresponds to $\Delta m_{41}^2 \sim 1.0 \text{ eV}^2$. Supersedes ALEKSEEV 18.
- ⁸ ALEKSEEV 18 searches for $\bar{\nu}_e \rightarrow \bar{\nu}_s$ oscillations using the DANSS detector at 10.7, 11.2, and 12.7 m from the 3.1 GW_{th} power reactor. The DANSS detector is highly segmented and moveable; the positions are changed usually 3 times a week. The analysis is based on the ratio of the events at top and bottom position; the middle position is used for checks of consistency. The best fit point is at $\Delta m_{41}^2 = 1.4 \text{ eV}^2$ and $\sin^2(2\theta_{14}) = 0.05$ with $\Delta\chi^2 = 13.1$ (statistical errors only) compared to the fit with 3 active neutrinos only. The quoted limit of 0.01 for $\sin^2(2\theta_{14})$ corresponds to $\Delta m_{41}^2 \sim 1.0 \text{ eV}^2$. Superseded by SKROBOVA 20.
- ⁹ ALMAZAN 18 searches for the $\bar{\nu}_e \rightarrow \bar{\nu}_s$ oscillations with baseline from 9.4 to 11.1 m from the ILL research reactor with highly enriched ^{235}U fuel. The STEREO detector consists of six separated cells with Gd loaded scintillator, with 15 m water equivalent overburden. The detected rate is $396.3 \pm 4.7 \bar{\nu}_e/\text{day}$ with signal to background ratio of about 0.9. The reported results corresponds to 66 days of reactor-on. The analysis uses the relative rates normalized to the cell number 1. No indication of the oscillation to the sterile neutrinos is found, the stated limit on $\sin^2(2\theta_{14})$ correspond to $\Delta m_{41}^2 \sim 3.5 \text{ eV}^2$ where the exclusion is maximal. Superseded by ALMAZAN 23.
- ¹⁰ ASHENFELTER 18 searches for the $\bar{\nu}_e \rightarrow \bar{\nu}_s$ oscillations at baseline from 6.7 to 9.2 m from the 85 MW research reactor with pure ^{235}U core. The segmented 4 ton ^6Li -doped liquid scintillator is operated with about 1 m water equivalent overburden and recorded 25461 ± 283 IBD events. No indication of oscillations into sterile neutrinos was observed. The stated limit for $\sin^2(2\theta_{14})$ is for $\Delta m_{41}^2 \sim 2 \text{ eV}^2$ where the sensitivity is maximal.
- ¹¹ AARTSEN 17B uses three years of upward-going atmospheric neutrino data in the energy range of 10-60 GeV to constrain their disappearance into light sterile neutrinos. The reported limit $\sin^2\theta_{24} < 0.11$ at 90% C.L. is for $\Delta m_{41}^2 = 1.0 \text{ eV}^2$. We convert the result to $\sin^2 2\theta_{24}$ for the listing. AARTSEN 17B also reports $\cos^2\theta_{24} \cdot \sin^2\theta_{34} < 0.15$ at 90% C.L. for $\Delta m_{41}^2 = 1.0 \text{ eV}^2$.

- ¹² ABDURASHITOV 17 use the Troitsk nu-mass experiment to search for sterile neutrinos with mass 0.1 - 2 keV. We convert the reported limit from $U_{e4}^2 < 0.002$ to $\sin^2 2\theta_{14} < 0.008$ assume $U_{e4} \sim \sin\theta_{14}$. The stated limit corresponds to the smallest U_{e4}^2 . The exclusion curve begins at U_{e4}^2 of 0.02 for $m_4 = 0.1$ keV.
- ¹³ KO 17 reports on short baseline reactor oscillation search ($\bar{\nu}_e \rightarrow \bar{\nu}_s$), motivated by the so-called "reactor antineutrino anomaly". The experiment is conducted at 23.7 m from the core of unit 5 of the Hanbit Nuclear Power Complex in Korea. The reported limit on $\sin^2(2\theta_{41})$ for sterile neutrinos was determined using the reactor antineutrino spectrum determined by the Daya Bay experiment for Δm_{14}^2 around 0.55 eV² where the sensitivity is maximal. A fraction of the parameter space derived from the "reactor antineutrino anomaly" is excluded by this work. Compared to reactor models an event excess is observed at about 5 MeV, in agreement with other experiments.
- ¹⁴ AARTSEN 16 use one year of upward-going atmospheric muon neutrino data in the energy range of 320 GeV to 20 TeV to constrain their disappearance into light sterile neutrinos. Sterile neutrinos are expected to produce distinctive zenith distribution for these energies for $0.01 \leq \Delta m^2 \leq 10$ eV². The stated limit is for $\sin^2 2\theta_{24}$ at Δm^2 around 0.3 eV².
- ¹⁵ ADAMSON 16B combine the results of AN 16B, ADAMSON 16C, and Bugey-3 reactor experiments to constrain ν_μ to ν_e mixing through oscillations into light sterile neutrinos. The stated limit for $\sin^2 2\theta_{\mu e}$ is at $|\Delta m_{41}^2| = 1.2$ eV².
- ¹⁶ ADAMSON 16C use the NuMI beam and exposure of 10.56×10^{20} protons on target to search for the oscillation of ν_μ dominated beam into light sterile neutrinos with detectors at 1.04 and 735 km. The reported limit $\sin^2(\theta_{24}) < 0.022$ at 95% C.L. is for $|\Delta m_{41}^2| = 0.5$ eV². We convert the result to $\sin^2(2\theta_{24})$ for the listing.
- ¹⁷ AN 16B utilize 621 days of data to place limits on the $\bar{\nu}_e$ disappearance into a light sterile neutrino. The stated limit corresponds to the smallest $\sin^2(2\theta_{14})$ at $|\Delta m_{41}^2| \sim 3 \times 10^{-2}$ eV² (obtained from Figure 3 in AN 16B). The exclusion curve begins at $|\Delta m_{41}^2| \sim 1.5 \times 10^{-4}$ eV² and extends to ~ 0.25 eV². The analysis assumes $\sin^2(2\theta_{12}) = 0.846 \pm 0.021$, $\Delta m_{21}^2 = (7.53 \pm 0.18) \times 10^{-5}$ eV², and $|\Delta m_{32}^2| = (2.44 \pm 0.06) \times 10^{-3}$ eV².
- ¹⁸ AMBROSIO 01 tested the pure 2-flavor $\nu_\mu \rightarrow \nu_s$ hypothesis using matter effects which change the shape of the zenith-angle distribution of upward through-going muons. With maximum mixing and Δm^2 around 0.0024 eV², the $\nu_\mu \rightarrow \nu_s$ oscillation is disfavored with 99% confidence level with respect to the $\nu_\mu \rightarrow \nu_\tau$ hypothesis.
- ¹⁹ FUKUDA 00 tested the pure 2-flavor $\nu_\mu \rightarrow \nu_s$ hypothesis using three complementary atmospheric-neutrino data samples. With this hypothesis, zenith-angle distributions are expected to show characteristic behavior due to neutral currents and matter effects. In the Δm^2 and $\sin^2 2\theta$ region preferred by the Super-Kamiokande data, the $\nu_\mu \rightarrow \nu_s$ hypothesis is rejected at the 99% confidence level, while the $\nu_\mu \rightarrow \nu_\tau$ hypothesis consistently fits all of the data sample.

————— **CPT tests** —————

$\langle \Delta m_{21}^2 - \Delta \bar{m}_{21}^2 \rangle$

<u>VALUE (10⁻⁴ eV²)</u>	<u>CL%</u>	<u>DOCUMENT ID</u>	<u>TECN</u>	<u>COMMENT</u>
<1.1	99.7	¹ DEGOUVEA 05	FIT	solar vs. reactor

¹ DEGOUVEA 05 obtained this bound at the 3 σ CL from the KamLAND (ARAKI 05) and solar neutrino data.

$$\langle \Delta m_{32}^2 - \Delta \bar{m}_{32}^2 \rangle$$

VALUE (10^{-3} eV^2)	CL%	DOCUMENT ID	TECN	COMMENT
$-0.12^{+0.26}_{-0.24}$		¹ ADAMSON	13B	MINS beam and atmospheric

• • • We do not use the following data for averages, fits, limits, etc. • • •

$0.6^{+2.4}_{-0.8}$	90	² ADAMSON	12B	MINS MINOS atmospheric
---------------------	----	----------------------	-----	------------------------

¹ ADAMSON 13B quotes this difference as a negative of our convention.

² The quoted result is the single-parameter 90% C.L. interval determined from the 90% C.L. contour in the $(\Delta m^2, \Delta \bar{m}^2)$ plane, which is obtained by minimizing the four parameter log-likelihood function with respect to the other oscillation parameters.

REFERENCES FOR Neutrino Mixing

ALMAZAN	23	NAT 613 257	H. Almazan <i>et al.</i>	(STEREO Collab.)
ACERO	22	PR D106 032004	M.A. Acero <i>et al.</i>	(NOvA Collab.)
AKER	22A	PR D105 072004	M. Aker <i>et al.</i>	(KATRIN Collab.)
APPEL	22	PRL 129 252701	S. Appel <i>et al.</i>	(Borexino Collab.)
ATIF	22	PR D105 L111101	Z. Atif <i>et al.</i>	(RENO and NEOS Collab.)
BARINOV	22A	PR C105 065502	V.V. Barinov <i>et al.</i>	(BEST Collab.)
Also		PRL 128 232501	V.V. Barinov <i>et al.</i>	(BEST Collab.)
ABE	21A	PR D103 L011101	K. Abe <i>et al.</i>	(T2K Collab.)
ABRAHAO	21	JHEP 2101 190	T. Abrahao <i>et al.</i>	(Double Chooz Collab.)
AGOSTINI	21	ASP 125 102509	M. Agostini <i>et al.</i>	(Borexino Collab.)
AGUILAR-AR...	21	PR D103 052002	A.A. Aguilar-Arevalo <i>et al.</i>	(MiniBooNE Collab.)
ANDRIAMIR...	21	PR D103 032001	M. Andriamirado <i>et al.</i>	(PROSPECT Collab.)
SALAS	21	JHEP 2102 071	P.F. de Salas <i>et al.</i>	(STOH, VALE, INFN+)
SEREBROV	21	PR D104 032003	A.P. Serebrov <i>et al.</i>	(Neutrino-4 Collab.)
AARTSEN	20	EPJ C80 9	M.G. Aartsen <i>et al.</i>	(IceCube Collab.)
ABE	20F	NAT 580 339	K. Abe <i>et al.</i>	(T2K Collab.)
Also		PR D103 112008	K. Abe <i>et al.</i>	(T2K Collab.)
ADAMSON	20A	PRL 125 131802	P. Adamson <i>et al.</i>	(MINOS+ Collab.)
AGOSTINI	20A	PR D101 062001	M. Agostini <i>et al.</i>	(Borexino Collab.)
AGOSTINI	20D	NAT 587 577	M. Agostini <i>et al.</i>	(Borexino Collab.)
AHARMIM	20	PR D102 062006	B. Aharmim <i>et al.</i>	(SNO Collab.)
ALMAZAN	20	PRL 125 201801	H. Almazan <i>et al.</i>	(STEREO Collab.)
DE-KERRET	20	NATP 16 558	H. de Karret <i>et al.</i>	(Double Chooz Collab.)
ESTEBAN	20A	JHEP 2009 178	I. Esteban <i>et al.</i>	(NuFIT Collab.)
PDG	20	PTEP 2020 083C01	P.A. Zyla <i>et al.</i>	(PDG Collab.)
SEREBROV	20	JETPL 112 199	A.P. Serebrov, R.M. Samoilov	(PNPI)
		Translated from ZETFP 112 211.		
SHIN	20	JHEP 2004 029	C.D. Shin <i>et al.</i>	(RENO Collab.)
SKROBOVA	20	IJMP A35 2044015	N. Skrobova	(DANSS Collab.)
AARTSEN	19C	PR D99 032007	M.G. Aartsen <i>et al.</i>	(IceCube Collab.)
ACERO	19	PRL 123 151803	M.A. Acero <i>et al.</i>	(NOvA Collab.)
ADEY	19	PR D100 052004	D. Adey <i>et al.</i>	(Daya Bay Collab.)
AGAFONOVA	19	PR D100 051301	N. Agafonova <i>et al.</i>	(OPERA Collab.)
ALBERT	19	JHEP 1906 113	A. Albert <i>et al.</i>	(ANTARES Collab.)
ANDERSON	19	PR D99 012012	M. Anderson <i>et al.</i>	(SNO+ Collab.)
SEREBROV	19	JETPL 109 213	A.P. Serebrov <i>et al.</i>	(Neutrino-4 Collab.)
AARTSEN	18A	PRL 120 071801	M.G. Aartsen <i>et al.</i>	(IceCube Collab.)
ABE	18B	PR D97 072001	K. Abe <i>et al.</i>	(Super-Kamiokande Collab.)
ABE	18G	PRL 121 171802	K. Abe <i>et al.</i>	(T2K Collab.)
ACERO	18	PR D98 032012	M.A. Acero <i>et al.</i>	(NOvA Collab.)
ADEY	18A	PRL 121 241805	D. Adey <i>et al.</i>	(Daya Bay Collab.)
AGAFONOVA	18	PRL 120 211801	N. Agafonova <i>et al.</i>	(OPERA Collab.)
AGAFONOVA	18A	JHEP 1806 151	N. Agafonova <i>et al.</i>	(OPERA Collab.)
AGOSTINI	18B	NAT 562 505	M. Agostini <i>et al.</i>	(Borexino Collab.)
AGUILAR-AR...	18C	PRL 121 221801	A.A. Aguilar-Arevalo <i>et al.</i>	(MiniBooNE Collab.)
ALEKSEEV	18	PL B787 56	I. Alekseev <i>et al.</i>	(DANSS Collab.)
ALMAZAN	18	PRL 121 161801	H. Almazan <i>et al.</i>	(STEREO Collab.)
ASHENFELT...	18	PRL 121 251802	J. Ashenfelter <i>et al.</i>	(PROSPECT Collab.)
BAK	18	PRL 121 201801	G. Bak <i>et al.</i>	(RENO Collab.)
CAPOZZI	18	PPNP 102 48	F. Capozzi <i>et al.</i>	
DE-SALAS	18	PL B782 633	P.F. de Salas <i>et al.</i>	

PDG	18	PR D98 030001	M. Tanabashi <i>et al.</i>	(PDG Collab.)
SEO	18	PR D98 012002	S.H. Seo <i>et al.</i>	(RENO Collab.)
SEREBROV	18A	PPN 49 701	A.P. Serebrov <i>et al.</i>	(Neutrino-4 Collab.)
AARTSEN	17B	PR D95 112002	M.G. Aartsen <i>et al.</i>	(IceCube Collab.)
ABDURASHI...	17	JETPL 105 753	J.N. Abdurashitov <i>et al.</i>	(Troitsk nu-mass Collab.)
ABE	17A	PRL 118 151801	K. Abe <i>et al.</i>	(T2K Collab.)
ABE	17C	PR D96 011102	K. Abe <i>et al.</i>	(T2K Collab.)
ABE	17F	PR D96 092006	K. Abe <i>et al.</i>	(T2K Collab.)
Also		PR D98 019902 (errat.)	K. Abe <i>et al.</i>	(T2K Collab.)
ADAMSON	17A	PRL 118 151802	P. Adamson <i>et al.</i>	(NOvA Collab.)
ADAMSON	17B	PRL 118 231801	P. Adamson <i>et al.</i>	(NOvA Collab.)
AN	17A	PR D95 072006	F.P. An <i>et al.</i>	(Daya Bay Collab.)
ESTEBAN	17	JHEP 1701 087	I. Esteban <i>et al.</i>	
KO	17	PRL 118 121802	Y.J. Ko <i>et al.</i>	(NEOS Collab.)
VINYOLES	17	APJ 835 202	N. Vinyoles <i>et al.</i>	
AARTSEN	16	PRL 117 071801	M.G. Aartsen <i>et al.</i>	(IceCube Collab.)
ABE	16B	JHEP 1601 163	Y. Abe <i>et al.</i>	(Double Chooz Collab.)
ABE	16C	PR D94 052010	K. Abe <i>et al.</i>	(Super-Kamiokande Collab.)
ABE	16D	PRL 116 181801	K. Abe <i>et al.</i>	(T2K Collab.)
ADAMSON	16	PRL 116 151806	P. Adamson <i>et al.</i>	(NOvA Collab.)
ADAMSON	16A	PR D93 051104	P. Adamson <i>et al.</i>	(NOvA Collab.)
ADAMSON	16B	PRL 117 151801	P. Adamson <i>et al.</i>	(Daya Bay and MINOS Collab.)
ADAMSON	16C	PRL 117 151803	P. Adamson <i>et al.</i>	(MINOS Collab.)
AN	16	PRL 116 061801	F.P. An <i>et al.</i>	(Daya Bay Collab.)
AN	16A	PR D93 072011	F.P. An <i>et al.</i>	(Daya Bay Collab.)
AN	16B	PRL 117 151802	F.P. An <i>et al.</i>	(Daya Bay Collab.)
CHOI	16	PRL 116 211801	J.H. Choi <i>et al.</i>	(RENO Collab.)
PDG	16	CP C40 100001	C. Patrignani <i>et al.</i>	(PDG Collab.)
AARTSEN	15A	PR D91 072004	M.G. Aartsen	(IceCube Collab.)
ABE	15D	PR D91 072010	K. Abe <i>et al.</i>	(T2K Collab.)
AGAFONOVA	15A	PRL 115 121802	N. Agafonova <i>et al.</i>	(OPERA Collab.)
AN	15	PRL 115 111802	F.P. An <i>et al.</i>	(Daya Bay Collab.)
BERGSTROM	15	JHEP 1509 200	J. Bergstrom <i>et al.</i>	(BARC, STON, MADU+)
GANDO	15	PR C92 055808	A. Gando <i>et al.</i>	(KamLAND Collab.)
ABE	14	PRL 112 181801	K. Abe <i>et al.</i>	(T2K Collab.)
Also		PR D91 072010	K. Abe <i>et al.</i>	(T2K Collab.)
ABE	14A	PL B735 51	Y. Abe <i>et al.</i>	(Double Chooz Collab.)
ABE	14B	PR D89 092003	K. Abe <i>et al.</i>	(T2K Collab.)
ABE	14C	PRL 112 061802	K. Abe <i>et al.</i>	(T2K Collab.)
ABE	14H	JHEP 1410 086	Y. Abe <i>et al.</i>	(Double Chooz Collab.)
Also		JHEP 1502 074 (errat.)	Y. Abe <i>et al.</i>	(Double Chooz Collab.)
ADAMSON	14	PRL 112 191801	P. Adamson <i>et al.</i>	(MINOS Collab.)
AN	14	PRL 112 061801	F.P. An <i>et al.</i>	(Daya Bay Collab.)
AN	14B	PR D90 071101	F.P. An <i>et al.</i>	(Daya Bay Collab.)
BELLINI	14A	NAT 512 383	G. Bellini <i>et al.</i>	(Borexino Collab.)
FORERO	14	PR D90 093006	D.V. Forero, M. Tortola, J.W.F. Valle	
GONZALEZ...	14	JHEP 1411 052	M.C. Gonzalez-Garcia, M. Maltoni, T. Schwetz	
PDG	14	CP C38 070001	K. Olive <i>et al.</i>	(PDG Collab.)
RENSHAW	14	PRL 112 091805	A. Renshaw <i>et al.</i>	(Super-Kamiokande Collab.)
AARTSEN	13B	PRL 111 081801	M.G. Aartsen <i>et al.</i>	(IceCube Collab.)
ABE	13C	PL B723 66	Y. Abe <i>et al.</i>	(Double Chooz Collab.)
ABE	13E	PR D88 032002	K. Abe <i>et al.</i>	(T2K Collab.)
ABE	13G	PRL 111 211803	K. Abe <i>et al.</i>	(T2K Collab.)
ADAMSON	13A	PRL 110 171801	P. Adamson <i>et al.</i>	(MINOS Collab.)
ADAMSON	13B	PRL 110 251801	P. Adamson <i>et al.</i>	(MINOS Collab.)
AGAFONOVA	13	JHEP 1307 004	N. Agafonova <i>et al.</i>	(OPERA Collab.)
AGUILAR-AR...	13A	PRL 110 161801	A.A. Aguilar-Arevalo <i>et al.</i>	(MiniBooNE Collab.)
AHARMIM	13	PR C88 025501	B. Aharmim <i>et al.</i>	(SNO Collab.)
AN	13	CP C37 011001	F.P. An <i>et al.</i>	(Daya Bay Collab.)
ANTONELLO	13	EPJ C73 2345	M. Antonello <i>et al.</i>	(ICARUS Collab.)
ANTONELLO	13A	EPJ C73 2599	M. Antonello <i>et al.</i>	(ICARUS Collab.)
GANDO	13	PR D88 033001	A. Gando <i>et al.</i>	(KamLAND Collab.)
ABE	12	PRL 108 131801	Y. Abe <i>et al.</i>	(Double Chooz Collab.)
ABE	12A	PR D85 031103	K. Abe <i>et al.</i>	(T2K Collab.)
ABE	12B	PR D86 052008	Y. Abe <i>et al.</i>	(Double Chooz Collab.)
ADAMSON	12	PRL 108 191801	P. Adamson <i>et al.</i>	(MINOS Collab.)
ADAMSON	12B	PR D86 052007	P. Adamson <i>et al.</i>	(MINOS Collab.)
ADRIAN-MAR...	12	PL B714 224	S. Adrian-Martinez <i>et al.</i>	(ANTARES Collab.)
AHN	12	PRL 108 191802	J.K. Ahn <i>et al.</i>	(RENO Collab.)
AN	12	PRL 108 171803	F.P. An <i>et al.</i>	(Daya Bay Collab.)
BELLINI	12A	PRL 108 051302	G. Bellini <i>et al.</i>	(Borexino Collab.)

CHENG	12	PR D86 052009	G. Cheng <i>et al.</i>	(MiniBooNE/SciBooNE Collab.)
MAHN	12	PR D85 032007	K.B.M. Mahn <i>et al.</i>	(MiniBooNE/SciBooNE Collab.)
ABE	11	PR D83 052010	K. Abe <i>et al.</i>	(Super-Kamiokande Collab.)
ABE	11A	PRL 107 041801	K. Abe <i>et al.</i>	(T2K Collab.)
ABE	11B	PR C84 035804	S. Abe <i>et al.</i>	(KamLAND Collab.)
ABE	11C	PRL 107 241801	K. Abe <i>et al.</i>	(Super-Kamiokande Collab.)
ADAMSON	11	PRL 106 181801	P. Adamson <i>et al.</i>	(MINOS Collab.)
ADAMSON	11B	PRL 107 021801	P. Adamson <i>et al.</i>	(MINOS Collab.)
ADAMSON	11C	PR D84 071103	P. Adamson <i>et al.</i>	(MINOS Collab.)
ADAMSON	11D	PRL 107 181802	P. Adamson <i>et al.</i>	(MINOS Collab.)
BELLINI	11	PL B696 191	G. Bellini <i>et al.</i>	(Borexino Collab.)
BELLINI	11A	PRL 107 141302	G. Bellini <i>et al.</i>	(Borexino Collab.)
FOGLI	11	PR D84 053007	G.L. Fogli <i>et al.</i>	
GANDO	11	PR D83 052002	A. Gando <i>et al.</i>	(KamLAND Collab.)
HUBER	11	PR C84 024617	P. Huber	(VPI)
Also		PR C85 029901 (errat.)	P. Huber	(VPI)
MUELLER	11	PR C83 054615	Th.A. Mueller <i>et al.</i>	
SERENELLI	11	APJ 743 24	A.M. Serenelli, W.C. Haxton, C. Pena-Garay	
ADAMSON	10A	PR D82 051102	P. Adamson <i>et al.</i>	(MINOS Collab.)
AGUILAR-AR...	10	PRL 105 181801	A.A. Aguilar-Arevalo <i>et al.</i>	(MiniBooNE Collab.)
AHARMIM	10	PR C81 055504	B. Aharmim <i>et al.</i>	(SNO Collab.)
BELLINI	10A	PR D82 033006	G. Bellini <i>et al.</i>	(Borexino Collab.)
DENIZ	10	PR D81 072001	M. Deniz <i>et al.</i>	(TEXONO Collab.)
KAETHER	10	PL B685 47	F. Kaether <i>et al.</i>	
WENDELL	10	PR D81 092004	R. Wendell <i>et al.</i>	(Super-Kamiokande Collab.)
ABDURASHI...	09	PR C80 015807	J.N. Abdurashitov <i>et al.</i>	(SAGE Collab.)
ADAMSON	09B	PRL 103 261802	P. Adamson <i>et al.</i>	(MINOS Collab.)
AGUILAR-AR...	09B	PRL 103 111801	A.A. Aguilar-Arevalo <i>et al.</i>	(MiniBooNE Collab.)
ABE	08A	PRL 100 221803	S. Abe <i>et al.</i>	(KamLAND Collab.)
Also		PRL 101 119904E	S. Abe <i>et al.</i>	(KamLAND Collab.)
ADAMSON	08	PR D77 072002	P. Adamson <i>et al.</i>	(MINOS Collab.)
ADAMSON	08A	PRL 101 131802	P. Adamson <i>et al.</i>	(MINOS Collab.)
AHARMIM	08	PRL 101 111301	B. Aharmim <i>et al.</i>	(SNO Collab.)
Also		PR C87 015502	B. Aharmim <i>et al.</i>	(SNO Collab.)
ARPESELLA	08A	PRL 101 091302	C. Arpesella <i>et al.</i>	(Borexino Collab.)
CRAVENS	08	PR D78 032002	J.P. Cravens <i>et al.</i>	(Super-Kamiokande Collab.)
FOGLI	08	PRL 101 141801	G.L. Fogli	
ADAMSON	07	PR D75 092003	P. Adamson <i>et al.</i>	(MINOS Collab.)
AGUILAR-AR...	07	PRL 98 231801	A.A. Aguilar-Arevalo <i>et al.</i>	(MiniBooNE Collab.)
AHARMIM	07	PR C75 045502	B. Aharmim <i>et al.</i>	(SNO Collab.)
ADAMSON	06	PR D73 072002	P. Adamson <i>et al.</i>	(MINOS Collab.)
AHN	06A	PR D74 072003	M.H. Ahn <i>et al.</i>	(K2K Collab.)
BALATA	06	EPJ C47 21	M. Balata <i>et al.</i>	(Borexino Collab.)
HOSAKA	06	PR D73 112001	J. Hosaka <i>et al.</i>	(Super-Kamiokande Collab.)
HOSAKA	06A	PR D74 032002	J. Hosaka <i>et al.</i>	(Super-Kamiokande Collab.)
MICHAEL	06	PRL 97 191801	D. Michael <i>et al.</i>	(MINOS Collab.)
WINTER	06A	PR C73 025503	W.T. Winter <i>et al.</i>	
YAMAMOTO	06	PRL 96 181801	S. Yamamoto <i>et al.</i>	(K2K Collab.)
AHARMIM	05A	PR C72 055502	B. Aharmim <i>et al.</i>	(SNO Collab.)
ALIU	05	PRL 94 081802	E. Aliu <i>et al.</i>	(K2K Collab.)
ALLISON	05	PR D72 052005	W.W.M. Allison <i>et al.</i>	(SOUDAN-2 Collab.)
ALTMANN	05	PL B616 174	M. Altmann <i>et al.</i>	(GNO Collab.)
ARAKI	05	PRL 94 081801	T. Araki <i>et al.</i>	(KamLAND Collab.)
ASHIE	05	PR D71 112005	Y. Ashie <i>et al.</i>	(Super-Kamiokande Collab.)
BAHCALL	05	APJ 621 L85	J.N. Bahcall, A.M. Serenelli, S. Basu	(IAS+)
DEGOUVEA	05	PR D71 093002	A. de Gouvea, C. Pena-Garay	
AHARMIM	04	PR D70 093014	B. Aharmim <i>et al.</i>	(SNO Collab.)
AHMED	04A	PRL 92 181301	S.N. Ahmed <i>et al.</i>	(SNO Collab.)
AHN	04	PRL 93 051801	M.H. Ahn <i>et al.</i>	(K2K Collab.)
AMBROSIO	04	EPJ C36 323	M. Ambrosio <i>et al.</i>	(MACRO Collab.)
ASHIE	04	PRL 93 101801	Y. Ashie <i>et al.</i>	(Super-Kamiokande Collab.)
EGUCHI	04	PRL 92 071301	K. Eguchi <i>et al.</i>	(KamLAND Collab.)
SMY	04	PR D69 011104	M.B. Smy <i>et al.</i>	(Super-Kamiokande Collab.)
AHN	03	PRL 90 041801	M.H. Ahn <i>et al.</i>	(K2K Collab.)
AMBROSIO	03	PL B566 35	M. Ambrosio <i>et al.</i>	(MACRO Collab.)
APOLLONIO	03	EPJ C27 331	M. Apollonio <i>et al.</i>	(CHOOZ Collab.)
ASTIER	03	PL B570 19	P. Astier <i>et al.</i>	(NOMAD Collab.)
EGUCHI	03	PRL 90 021802	K. Eguchi <i>et al.</i>	(KamLAND Collab.)
GANDO	03	PRL 90 171302	Y. Gando <i>et al.</i>	(Super-Kamiokande Collab.)
IANNI	03	JP G29 2107	A. Ianni	(INFN Gran Sasso)
SANCHEZ	03	PR D68 113004	M. Sanchez <i>et al.</i>	(Soudan 2 Collab.)

ABDURASHI...	02	JETP 95 181 Translated from ZETF 122 211.	J.N. Abdurashitov <i>et al.</i>	(SAGE Collab.)
AHMAD	02	PRL 89 011301	Q.R. Ahmad <i>et al.</i>	(SNO Collab.)
AHMAD	02B	PRL 89 011302	Q.R. Ahmad <i>et al.</i>	(SNO Collab.)
ARMBRUSTER	02	PR D65 112001	B. Armbruster <i>et al.</i>	(KARMEN 2 Collab.)
AVVAKUMOV	02	PRL 89 011804	S. Avvakumov <i>et al.</i>	(NuTeV Collab.)
FUKUDA	02	PL B539 179	S. Fukuda <i>et al.</i>	(Super-Kamiokande Collab.)
AGUILAR	01	PR D64 112007	A. Aguilar <i>et al.</i>	(LSND Collab.)
AHMAD	01	PRL 87 071301	Q.R. Ahmad <i>et al.</i>	(SNO Collab.)
AMBROSIO	01	PL B517 59	M. Ambrosio <i>et al.</i>	(MACRO Collab.)
BOEHM	01	PR D64 112001	F. Boehm <i>et al.</i>	
FUKUDA	01	PRL 86 5651	S. Fukuda <i>et al.</i>	(Super-Kamiokande Collab.)
AMBROSIO	00	PL B478 5	M. Ambrosio <i>et al.</i>	(MACRO Collab.)
BOEHM	00	PRL 84 3764	F. Boehm <i>et al.</i>	
FUKUDA	00	PRL 85 3999	S. Fukuda <i>et al.</i>	(Super-Kamiokande Collab.)
ALLISON	99	PL B449 137	W.W.M. Allison <i>et al.</i>	(Soudan 2 Collab.)
APOLLONIO	99	PL B466 415	M. Apollonio <i>et al.</i>	(CHOOZ Collab.)
Also		PL B472 434 (errat.)	M. Apollonio <i>et al.</i>	(CHOOZ Collab.)
FUKUDA	99C	PRL 82 2644	Y. Fukuda <i>et al.</i>	(Super-Kamiokande Collab.)
FUKUDA	99D	PL B467 185	Y. Fukuda <i>et al.</i>	(Super-Kamiokande Collab.)
HAMPEL	99	PL B447 127	W. Hampel <i>et al.</i>	(GALLEX Collab.)
AMBROSIO	98	PL B434 451	M. Ambrosio <i>et al.</i>	(MACRO Collab.)
APOLLONIO	98	PL B420 397	M. Apollonio <i>et al.</i>	(CHOOZ Collab.)
ATHANASSO...	98	PRL 81 1774	C. Athanassopoulos <i>et al.</i>	(LSND Collab.)
ATHANASSO...	98B	PR C58 2489	C. Athanassopoulos <i>et al.</i>	(LSND Collab.)
CLEVELAND	98	APJ 496 505	B.T. Cleveland <i>et al.</i>	(Homestake Collab.)
FELDMAN	98	PR D57 3873	G.J. Feldman, R.D. Cousins	
FUKUDA	98C	PRL 81 1562	Y. Fukuda <i>et al.</i>	(Super-Kamiokande Collab.)
HATAKEYAMA	98	PRL 81 2016	S. Hatakeyama <i>et al.</i>	(Kamiokande Collab.)
CLARK	97	PRL 79 345	R. Clark <i>et al.</i>	(IMB Collab.)
AGLIETTA	96	JETPL 63 791 Translated from ZETFP 63 753.	M. Aglietta <i>et al.</i>	(LSD Collab.)
ATHANASSO...	96	PR C54 2685	C. Athanassopoulos <i>et al.</i>	(LSND Collab.)
ATHANASSO...	96B	PRL 77 3082	C. Athanassopoulos <i>et al.</i>	(LSND Collab.)
FUKUDA	96	PRL 77 1683	Y. Fukuda <i>et al.</i>	(Kamiokande Collab.)
FUKUDA	96B	PL B388 397	Y. Fukuda <i>et al.</i>	(Kamiokande Collab.)
GREENWOOD	96	PR D53 6054	Z.D. Greenwood <i>et al.</i>	(UCI, SVR, SCUC)
HAMPEL	96	PL B388 384	W. Hampel <i>et al.</i>	(GALLEX Collab.)
LOVERRE	96	PL B370 156	P.F. Loverre	
ACHKAR	95	NP B434 503	B. Achkar <i>et al.</i>	(SING, SACL D, CPPM, CDEF+)
AHLEN	95	PL B357 481	S.P. Ahlen <i>et al.</i>	(MACRO Collab.)
ATHANASSO...	95	PRL 75 2650	C. Athanassopoulos <i>et al.</i>	(LSND Collab.)
DAUM	95	ZPHY C66 417	K. Daum <i>et al.</i>	(FREJUS Collab.)
HILL	95	PRL 75 2654	J.E. Hill	(PENN)
DECLAIS	94	PL B338 383	Y. Declais <i>et al.</i>	
FUKUDA	94	PL B335 237	Y. Fukuda <i>et al.</i>	(Kamiokande Collab.)
VILAIN	94C	ZPHY C64 539	P. Vilain <i>et al.</i>	(CHARM II Collab.)
FREEDMAN	93	PR D47 811	S.J. Freedman <i>et al.</i>	(LAMPF E645 Collab.)
BECKER-SZ...	92B	PR D46 3720	R.A. Becker-Szendy <i>et al.</i>	(IMB Collab.)
BEIER	92	PL B283 446	E.W. Beier <i>et al.</i>	(KAM2 Collab.)
Also		PTRSL A346 63	E.W. Beier, E.D. Frank	(PENN)
HIRATA	92	PL B280 146	K.S. Hirata <i>et al.</i>	(Kamiokande II Collab.)
CASPER	91	PRL 66 2561	D. Casper <i>et al.</i>	(IMB Collab.)
HIRATA	91	PRL 66 9	K.S. Hirata <i>et al.</i>	(Kamiokande II Collab.)
KUVSHINN...	91	JETPL 54 253	A.A. Kuvshinnikov <i>et al.</i>	(KIAE)
BERGER	90B	PL B245 305	C. Berger <i>et al.</i>	(FREJUS Collab.)
HIRATA	90	PRL 65 1297	K.S. Hirata <i>et al.</i>	(Kamiokande II Collab.)
AGLIETTA	89	EPL 8 611	M. Aglietta <i>et al.</i>	(FREJUS Collab.)
DAVIS	89	ARNPS 39 467	R. Davis, A.K. Mann, L. Wolfenstein	(BNL, PENN+)
OYAMA	89	PR D39 1481	Y. Oyama <i>et al.</i>	(Kamiokande II Collab.)
BIONTA	88	PR D38 768	R.M. Bionta <i>et al.</i>	(IMB Collab.)
DURKIN	88	PRL 61 1811	L.S. Durkin <i>et al.</i>	(OSU, ANL, CIT+)
ABRAMOWICZ	86	PRL 57 298	H. Abramowicz <i>et al.</i>	(CDHS Collab.)
ALLABY	86	PL B177 446	J.V. Allaby <i>et al.</i>	(CHARM Collab.)
ANGELINI	86	PL B179 307	C. Angelini <i>et al.</i>	(PISA, ATHU, PADO+)
VUILLEUMIER	82	PL 114B 298	J.L. Vuilleumier <i>et al.</i>	(CIT, SIN, MUNI)
BOLIEV	81	SJNP 34 787 Translated from YAF 34 1418.	M.M. Boliev <i>et al.</i>	(INRM)
KWON	81	PR D24 1097	H. Kwon <i>et al.</i>	(CIT, ISNG, MUNI)
BOEHM	80	PL 97B 310	F. Boehm <i>et al.</i>	(ILLG, CIT, ISNG, MUNI)
CROUCH	78	PR D18 2239	M.F. Crouch <i>et al.</i>	(CASE, UCI, WITW)